VIBRATION PROBLEMS OF SKIPS IN MINE SHAFTS

THE EFFECT OF COMPRESSIVE FORCES IN THE GUIDES

by

T S Pretorius

A thesis submitted in partial fulfilment of the requirements for the degree of Master of Science in Engineering

Department of Civil Engineering
University of Cape Town
7700 Rondebosch, South Africa

October 1989

Declaration

This is to certify that the results, calculations and other work presented in this thesis are essentially my own work, and that no part of it has been submitted for a degree at this or any other university.

T S Pretorius Signature Removed

October 1989

Dedication

I would like to dedicate this thesis to my wife Patricia, for her consistant encouragement and patience.

Acknowledgements

I hereby acknowledge, and greatly appreciate, the help of the following people and organisations:

Professor John Martin *, for providing me with opportunity and the theoretical guidance to do this work.

Dr Colin Mercer **, for assisting me with the day to day problems encountered, and for proofreading this document.

Dr Malcolm Greenway ***, for introducing me to the problem.

My colleagues in the FRD/UCT Centre for Research in Computational and Applied Mechanics for their willing assistance.

The Chamber of Mines Research Organisation (COMRO) for their financial assistance.

The Foundation for Research and Development (FRD) for their financial assistance.

$\star$ Dean of Engineering

$\star\star$ Senior Research Officer
FRD/UCT Centre for Research in
Computational and Applied Mechanics

$\star\star\star$ Consulting Mechanical Engineer
Mechanical Engineering Department
Anglo American Corporation of South Africa

Abstract

Investigations into problems involving the vibration of conveyances in deep mining shafts have led to the identification of 'slamming' as a significant event in the initiation of large perturbations in the motion of the skip. Slamming occurs when the flexible rollers on the skip which normally act on the guides are inoperative. The primary concern is that this slamming event can give rise to large lateral loads on the shaft steelwork and is therefore a factor which limits the speed at which the skip can be drawn up the shaft. This study extends previous work to investigate the influence of compressive forces in the guides on the response of the skip and the steelwork. These forces are induced as a result of mining operations and lead to a decrease in the transverse stiffness of the guides. A mathematical model of the slamming event is formulated and a numerical solution for a specific case is performed. An alternative simplified solution is discussed and compared to the initial formulation, with the aim of facilitating the use of previous research results. A model to simulate the response of the skip when the skip rollers are functional is formulated, and numerical solutions of different examples are given. An important conclusion is that the compressive forces can significantly reduce the transverse stiffness of the guides, and should be taken into account in future designs.

Contents

List of Figures

List of Tables

1 Introduction to the Problem

Organisations:

AAC	Anglo American Corporation of South Africa Limited, Johannesburg, South Africa.
AMRU	UCT/CSIR Applied Mechanics Research Unit, University of Cape Town, South Africa.
CERECAM	FRD/UCT Centre for Research in Computational and Applied Mechanics, University of Cape Town, South Africa.
COM	Chamber of Mines, Johannesburg, South Africa.
COMRO	Chamber of Mines Research Organisation, Johannesburg, South Africa.
SDRC	Structural Dynamics Research Corporation, Milford, Ohio, United States of America.

Glossary:

Bunton	This is an elastic translational and rotational support for the guide.
Damping	This is friction or resistance encountered by a system during its vibratory motion, e.g. air damping, fluid friction, internal damping, etc., which causes the eventual dying out of the oscillation. The system is said to be *over-damped* if no oscillation occurs; while if oscillation does occur, the system is said to be *under-damped*, and has the least damping. A *critically-damped* system is one where the mass will simply return to its static equilibrium position, without overshooting it, upon being released. A *dashpot* is the element used to model viscous damping.
Dashpot	The element used to model *viscous damping*, e.g. a shock absorber in a motor vehicle. The internal force in a dashpot is proportional to the velocity across the dashpot.
Guide	A continuous prismatic beam supporting the skip laterally while it is being hoisted or lowered in the shaft.

Roller	This is the connection between the *skip* and its supporting *guide* and it consists of a nonlinear *spring* and *dashpot.*
Skip	This is the conveyance used to transport material up and down the mine shaft.
Spring	The element used to model *stiffness.* The internal force in a spring is proportional to the displacement across the spring.

1.1 Introduction

Over the years, South African gold mines have become larger and deeper with the emphasis placed on productivity. This has resulted in higher hoisting speeds, heavier payloads in the skips, and so on. The steelwork in the shaft is a lattice structure supporting the various conveyances and pipes along the length of the shaft. The steelwork consists of horizontal bunton sets occurring at intervals in the shaft, and vertical members between the bunton sets, called guides, restraining the conveyances horizontally in the shaft. Until recently, designers used a percentage of vertical loads (usually 10%) for the design of the lateral strength of the steelwork, thus ignoring dynamic effects.

In the the early 1960's, the lack of dynamic considerations was identified, but studies conducted at the time by CSIR for COM did not influence design or operating procedures in the mining houses. Various failures of shaft steelwork have been noted over the years and at least one shaft required a bunton and guide realignment process. Although such severe failures are rare, loosening of bolts, minor cracking of components, etc., do occur on a more regular basis, and require time consuming and expensive repair and maintenance.

These failures led to an increased interest in the design and analysis of shaft steelwork, and since 1982, COMRO has funded research work on the investigation of the dynamic behaviour of shaft steelwork and conveyances. SDRC [25,26,27,28,29] carried out work for COMRO; this research program consisted of test, analysis and design guidelines phases. The test phase was intended to develop a physical understanding of the problem by collecting modal and operating data. The modal data was used to characterise the system and the operating data was used as a comparison for the results of the analytical phase. The analytical phase consisted of the development of a computer model to simulate the response of the skip when excited by the misalignment of the guides. The third phase was to develop a set of design guidelines for the design of shaft steelwork. A fourth phase was later added to the program to calibrate the design guidelines.

An important parameter in the dynamic analyses was omitted in previous studies, namely the inclusion of the effects of axial compressive forces on the lateral stiffness of the guides. These compressive forces are induced by deformation of the rock surrounding the shaft as a result of mining operations. Excavations take place away from the mine shaft, leaving a pillar or core surrounding the actual shaft. This pillar has to support the weight of the rock above the excavations, hence vertical stresses in the pillar region increase. This leads to an increase in vertical compressive strains in the walls of the shaft, and consequently the distance between the buntons, to which the the guides are fixed, decreases. The transverse stiffness of the guides, i.e. the property of the guides to resist transverse deflections, are affected by these axial compressive strains. The compressive forces induced in the guides as a result lead to a decrease in

the transverse stiffness of the guides, with the potential of increased amplification of the responses of the skip and steelwork.

Due to the compressive forces in the guides and the motions of the skip, the guides can deform, so that the guides become misaligned. The inertial forces generated in the skip in response to the guide misalignment are transmitted to the guides by means of impacts. The energy may either be transferred via a rigid body impact, where a term 'slamming' has been identified by previous researchers, or through flexible rollers on the skip. Since it is difficult to develop an understanding of the two mechanisms acting simultaneously, each event is investigated separately. The two cases provide an upper and a lower bound to the response of the skip to the guide misalignment.

The study of the sensitivity of these two events to axial compressive forces in the guides is in essence the objective of this thesis. The problem is introduced in Chapter 1, and work by previous researchers is outlined. In Chapter 2, the slamming event is analysed, where a mathematical model is implemented in a computer program. The case when the rollers are active is investigated in Chapter 3, where again a mathematical model is implemented in a computer program. Finally, in Chapter 4, conclusions and recommendations are made, along with suggestions for further study.

1.2 Review of Previous Work

Various authors have addressed the problems of mine shaft vibrations, and a brief discussion of the essential points of a few of the authors follows.

Redpath and Shaver [23] discussed various aspects of guide design and included calculations for the forces on the guides for various types of misalignment. They stated that smooth and flexible joints are the most important characteristic of a good guide system. A discussion of a paper by Bentley, and a subsequent comment by Backeberg is also included. Bentley stated that the 10% of the skip weight acting laterally was too conservative, while Backeberg disagrees, and states that loads of up to 17% of the skip weight have been measured on the guides. A suggestion by Hoischen that a lateral force of 8.33% should be used is also discussed.

Galloway and Tiley [6] presented a numerical model to predict the velocities at which the skip rebounds from the guide. They stated that lateral loads on the guides of up to 2 times the skip weight have been measured on an occasion. A major observation is that the skip is largely ignored when the shaft system is designed. They also stated that the easiest way to alleviate high forces in the guides is to have stiff rollers with sufficient room for them to work. A number of applications were investigated to test their model.

Schmidt and Tondl [24] presented the analysis of vibrations of a mine cage as an example of the analyses of excited systems. An energy approach was adopted to perform a parametric vibration analysis. They suggest that stiffer rollers should be used with a slight prestress to counter sub-harmonic resonances.

Hutton, James and Schwartz [14] identify the problem of axial compressive strains in the guides in a paper which investigates the feasability of mining out of the column of rock around the shaft (called the pillar). They discuss the various pillar types in use at present, as well as various shaft steelwork configurations. The effects of the ground movements on the steelwork are discussed, as well as possible ways to alleviate the compressive stresses in the steelwork when the pillars are mined out.

SDRC were commissioned by COMRO to research the design philosophies of shaft steelwork. A test phase [25] to study the interaction between the skip and the shaft steelwork system in a problematic shaft was used to obtain a physical understanding of the problems. A computer model was developed in the analytical phase [26] to parametrically study various shaft configurations.

The main conclusions of the analytical phase include the statement that the misalignment of the guides are the main excitation mechanisms, and the response of the skip is more sensitive to local misalignment of the guides than overall plumbness of the guides

in the shaft. Two dominant modes of vibration, namely translation and rotation were identified, and a tendency towards resonance when the frequency of a mode of vibration nears half the bunton passing frequency was noted. The roller and guide stiffnesses are recognised as important parameters which could be used to 'detune' the system. Other parameters affecting the bunton passing frequency and hence fulfil the resonance criteria should be considered. It is recommended that future shaft steelwork designs take the skip into consideration.

A design guideline phase [27] to establish a design procedure for future designs was also included. The design guidelines were calibrated [28] with respect to extensive test data, and the effects of the skip flexibility [29] on the analyses were investigated.

Greenway [7] extended the SDRC [26] analytical phase by non-dimensionalising the single slamming event, and produced contour plots to simplify the solution, i.e. repeated computer analyses will not have to be performed. He extended these ideas [8] even further and enhanced the contour plots to include shaded areas representing actual mine shafts. Experimental data [10] was reported for several mine shafts, and he summarised previous research work as well as outlining future trends in shaft steelwork design [11].

1.3 Objectives of this Thesis

The specific aim of this thesis is to illustrate the effects that axial compressive loads have on the dynamic response of the skip, and hence on shaft steelwork. This objective will be achieved by developing an understanding of the mechanisms involved, and then formulating mathematical models to determine the equations which govern the motions and the response of the skip. These models will then be numerically implemented into a computer program, in order to solve the equations of motion determined mathematically. The models will be verified using previous research results, and once confidence is attained with the models, the results obtained will be used to show the influence of the axial compressive loads on the shaft.

2 System Behaviour without Rollers

2.1 Introduction to Slamming Analysis

Investigations into problems involving the vibration of conveyances or skips in deep mining shafts in South Africa have led to the identification of 'slamming' as a significant event in initiating large perturbances of the skip motion and hence causing large lateral forces to be exerted on the shaft steelwork. Slamming occurs when the flexible rollers guiding the skip along the vertical shaft steelwork (guides) are inoperative.

During a slamming event, one corner of the skip impacts the guide with some transverse velocity, and results in transverse deflections of the guide. As the skip approaches a bunton where the guide is supported, the transverse stiffness of the guide increases sharply, and the skip may leave the guide with an amplified velocity. Consequently, this may lead to a succession of further slamming events which can damage the guides. Accurate modelling of successive slamming events is difficult to achieve due to the sensitivity of the system to random effects such as guide misalignment, guide gauge variation and other geometric effects. Hence, this thesis will be confined to the analysis of a single slamming event. This slamming behaviour is of concern in that it is a factor which may cause large lateral forces on the guides, hence limiting the speed at which the skip can move up and down the shaft.

A detailed numerical simulation of slamming has been carried out by SDRC [26] and by Greenway [7,8]. In this thesis, the previous work is extended in order to investigate the influence of axial compressive forces in the guides. These forces are induced by vertical deformation of the rock surrounding the shaft, termed the pillar. As a result of mining operations, the pillar has to carry the selfweight of the rock above the mined out area, and hence increased vertical compressive strains arise in the walls of the shaft.

The approach in this thesis is conservative, in that it is assumed that the compressive forces induced in the guides are constant, and independent of the transverse deflection of the guides. In reality, the compressive forces vary with depth and increase sharply near the mining area. They are large with respect to the forces away from the stope, and may be taken as being constant. It is assumed that the total axial compressive force acts even after the guide has deflected. In the numerical study, the worst scenario is modelled, hence the conservative approach is justified.

In Chapter 2.2 a mathematical model is formulated which extends previous work by including the reduced transverse flexibility of the guides due to a fixed axial compressive force. In Chapter 2.3 the numerical solution of the governing equation of motion of the system is discussed, as well as the implementation of the model in a computer program. Results of a parametric study are given in Chapter 2.4, in which the effects of the axial

compressive forces are compared to the case where the compressive force is zero.

A simplified analysis is investigated in Chapter 2.5, in which the reduction of the transverse stiffness of the guide due to inclusion of the axial compressive loads is accounted for only in the evaluation of the midspan stiffness of the guide. It is shown that this approach leads to errors which do not exceed approximately 20% when compared to the formulation discussed in Chapter 2.2. If such errors are acceptable in the design procedure, a simple modification of the midspan stiffness permits results for the zero compressive force analysis to be used when compressive forces are present.

One of the primary assumptions in the formulation of the lateral stiffness of the guide described in Chapter 2.2 is that the guide undergoes only small displacements and is modelled as a simply-supported beam. As a result, the effects of finite or second order deformations that cause stiffening have been ignored. A study of these stiffening effects has been included in Chapter 2.6.

2.2 Analytical Model for the Slamming Analysis

2.2.1 Introduction

In the analytical model for the slamming analysis, the skip is modelled as a rigid body with mass m and mass moment of inertia I_G. The centre of gravity is located a distance l_1 below the top of the skip. The skip moves vertically in the shaft at a constant hoisting velocity of v_s. Therefore, the motion of the skip can be described by two degrees of freedom, the translation d and the rotation θ, acting at the centre of gravity. Since only one slamming event is considered, the system can be reduced to a single degree of freedom system, with the top left corner of the skip chosen as the point of impact. In order to simplify the mathematics, the motion of this corner can be described in terms of a degree of freedom y. The components are illustrated in Figure 2.1.

The guide is modelled as a prismatic beam of negligible mass, which is either pinned or rotationally fixed at the buntons. The case of pinned joints was used in this study as this closely models the configuration generally used in practice. A bunton set at a specific level of the shaft is modelled as a translational spring resisting lateral motion. The above description summarises the essential constituents of the SDRC [26] model. For the present study, a constant axial compressive force was assumed to be acting in the guides.

2.2.2 Determination of the Governing Equations

The derivation of the equations of motion is now discussed below using the notation defined in Figure 2.2.

The two equations of motion in terms of d and θ are:

$$m\ddot{d} + T = 0 \tag{2.1}$$

and

$$I_G\ddot{\theta} + Tl_1 = 0 \tag{2.2}$$

where T is the force that the skip exerts on the guide, and the dots above the variables indicate differentiation with respect to time, i.e. $\ddot{\theta} = \frac{d^2\theta}{dt^2}$. This force can be expressed in terms of an effective stiffness of the guide $k_e(\xi)$ and the beam deflection $y(\xi)$, both evaluated at a position ξl along the guide ($0 \leq \xi \leq 1$). Thus:

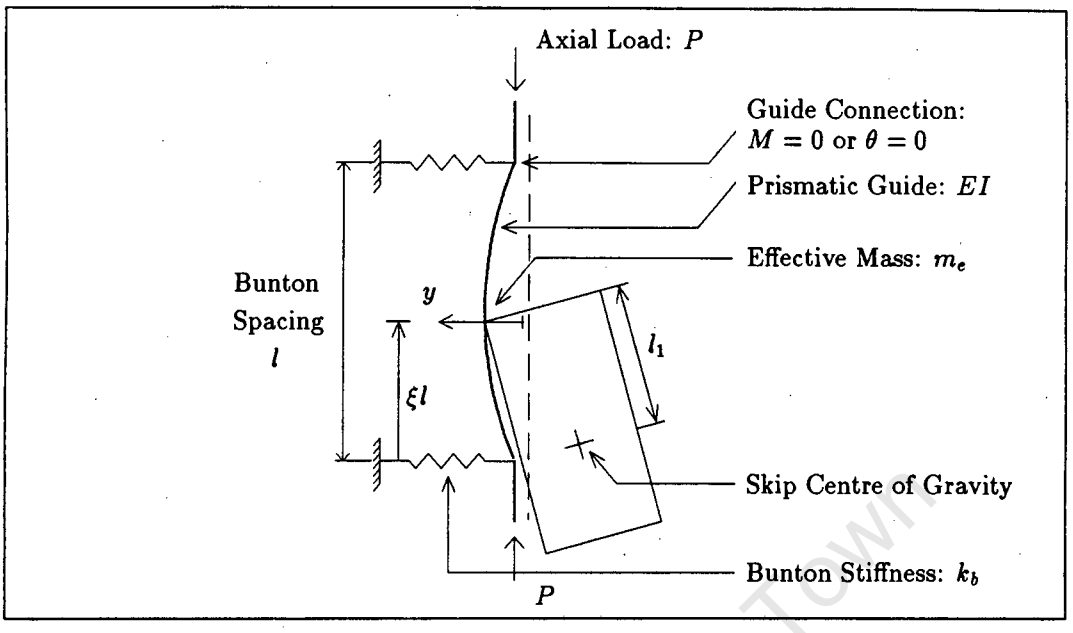

Figure 2.1: Slamming Model Including Axial Compressive Loads

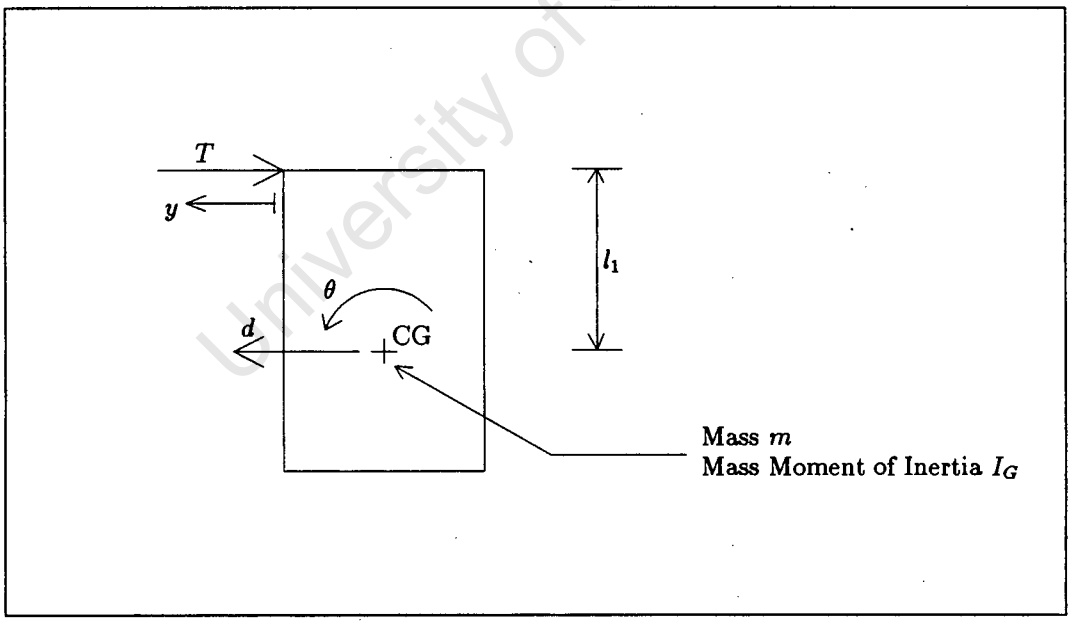

Figure 2.2: Model Showing Notation

$$T = k_e(\xi)\, y \tag{2.3}$$

From the geometry of the system, and assuming that θ is small, the following relationships between y, d and θ can be obtained:

$$y = d + \theta l_1$$

and

$$\ddot{y} = \ddot{d} + \ddot{\theta} l_1 \tag{2.4}$$

Substituting equations (2.1), (2.2) and (2.3) into equation (2.4), gives the following equation describing the motion of the skip:

$$\left(\frac{mI_G}{I_G + ml_1^2} \right) \ddot{y} + k_e\, y = 0 \tag{2.5}$$

A term called the effective mass is defined:

$$m_e = \frac{mI_G}{I_G + ml_1^2} \tag{2.6}$$

The equation of motion can be written in terms of the displacement of the corner of the skip $y(\xi)$ (i.e. the beam deflection) as:

$$m_e \ddot{y}(\xi) + k_e(\xi) y(\xi) = 0\,, \quad \xi = \xi(t) \tag{2.7}$$

2.2.3 Calculation of the Effective Stiffness

The procedure to obtain the relationship between the skip force T and the beam deflection y is now described. Firstly, an isolated simply supported prismatic beam is considered, with cross sectional properties EI, length l, an axial compressive force P, and a transverse force T (which is the force that the skip exerts on the guide), applied at a distance ξl along the beam. The displacement under the load is $y(\xi)$, as shown in Figure 2.3.

The bending moment in the beam, at a distance x along the beam, is given as:

$$M(x) = M_s(x) + Py(x) \tag{2.8}$$

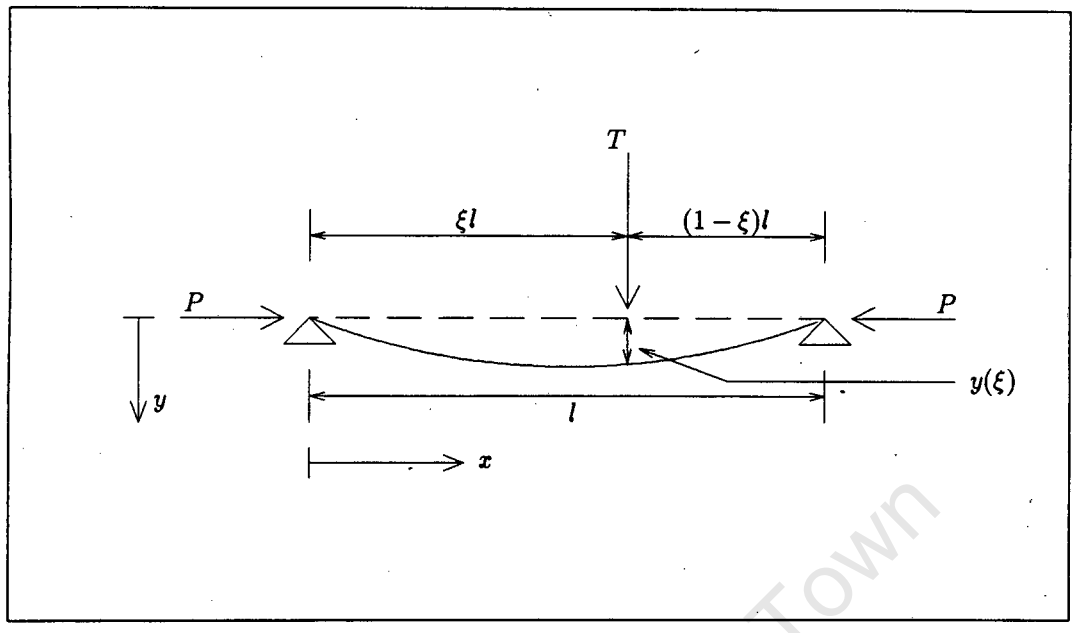

Figure 2.3: An Isolated, Simply-Supported Beam with Axial Load P

where $M_s(x)$ is the bending moment due to the transverse load T, and $Py(x)$ is the bending moment that develops in the beam due to the deflection $y(x)$ and the axial compressive force P.

Since the ratio between the length and the depth of the guide is large, the guide is assumed to act in pure flexure. From this simple beam theory, in which the transverse shear strains are ignored, a relationship between the bending moments M and the guide deflections y can be obtained:

$$M = EI\frac{d^2y(x)}{dx^2} = EIy''(x)$$

Substituting this relationship into equation (2.8) gives the following differential equation describing the displacements at a distance x along the beam:

$$y''(x) + \frac{P}{EI}\,y(x) = \frac{1}{EI}\,M_s(x) \tag{2.9}$$

Since the bending moments appear to have a periodic nature (this is more apparent for multi-span or continuous beams), and the only periodic polynomials are constant

functions, one has to use other function classes for the effective approximation of periodic functions. The trigonometric polynomials offer themselves as an appropriate alternative. Fourier series [16] are the most popular trigonometric polynomial approximations and are of the form:

$$g(x) \approx a_0 + \sum_{n=1}^{\infty} (a_n \sin nx + b_n \cos nx)$$

where the Fourier coefficients are (for period $2c$):

$$\begin{aligned} a_0 &= \tfrac{1}{2c} \int_{-c}^{c} g(x)\,dx \\ a_n &= \tfrac{1}{c} \int_{-c}^{c} g(x) \sin nx\,dx \\ b_n &= \tfrac{1}{c} \int_{-c}^{c} g(x) \cos nx\,dx \qquad n = 1, 2, \cdots \end{aligned}$$

The series converges uniformly if $g(x)$ is continuous with a piecewise-continuous first derivative. The bending moment $M_s(x)$ is continuous with a piecewise-continuous first derivative, and can therefore be expressed as a Fourier series consisting of n terms. Note that the b_n terms are zero because $M_s(x)$ is an odd function, i.e. $M_s(-x) = -M_s(x)$ for all x. The expression for $M_s(x)$ is therefore:

$$M_s(x) = \sum_{m=1}^{n} a_m \sin\left(\frac{m\pi x}{l}\right) \tag{2.10}$$

where a_m are the Fourier coefficients.

Using this expansion, the solution for equation (2.9) is of the form:

$$y(x) = \sum_{m=1}^{n} a_m^{*} \sin\left(\frac{m\pi x}{l}\right) \tag{2.11}$$

where $a_m^{*} = \frac{a_m}{m^2 P_{cr} - P}$

and $P_{cr} = \frac{\pi^2 EI}{l^2}$.

At this stage it is expedient to consider the transverse displacement $y(x)$ as the sum of two contributions: the displacement resulting from the transverse load T, $y_T(x)$; and the displacement that is due to the axial force P, $y_P(x)$. Thus:

$$y(x) = y_T(x) + y_P(x) \tag{2.12}$$

In terms of a Fourier series expansion, the displacement due to the transverse load, can be obtained by setting $P = 0$ in equation (2.11):

$$y_T(x) = \sum_{m=1}^{n} \frac{a_m}{m^2 P_{cr}} \sin\left(\frac{m\pi x}{l}\right) \tag{2.13}$$

$y_P(x)$ is now written in terms of a Fourier series expansion by substituting equation (2.13) into equation (2.12) to give:

$$y_P(x) = \sum_{m=1}^{n} \frac{a_m}{m^2 P_{cr}} \frac{P/P_{cr}}{m^2 - P/P_{cr}} \sin\left(\frac{m\pi x}{l}\right) \tag{2.14}$$

Using elementary beam theory, the displacement due to the transverse load T alone, can also be written as a function of the position of the load, i.e. when $x = \xi l$, as follows:

$$y_T(\xi) = \frac{\xi^2 (1-\xi)^2 l^3}{3\,EI} T \tag{2.15}$$

By evaluating equation (2.14) at $x = \xi l$, an expression for the total displacement under the load can be obtained:

$$y(\xi) = \frac{\xi^2 (1-\xi)^2 l^3}{3\,EI} T + \sum_{m=1}^{n} \frac{a_m}{m^2 P_{cr}} \frac{P/P_{cr}}{m^2 - P/P_{cr}} \sin(m\pi\xi) \tag{2.16}$$

To determine the coefficients for the Fourier approximation, a_m, the following functions are used to describe the bending moment diagram for the case of the transverse load T, as shown in Figure 2.4:

$$M_s(x) = \begin{cases} (1-\xi)\,T\,x & 0 \le x \le \xi l \\ \xi\,T\,x' & 0 \le x' \le (1-\xi)l \end{cases}$$

The Fourier coefficients are given by:

$$a_m = \frac{2}{l} \int_0^l M_s(x) \sin\left(\frac{m\pi x}{l}\right) dx$$

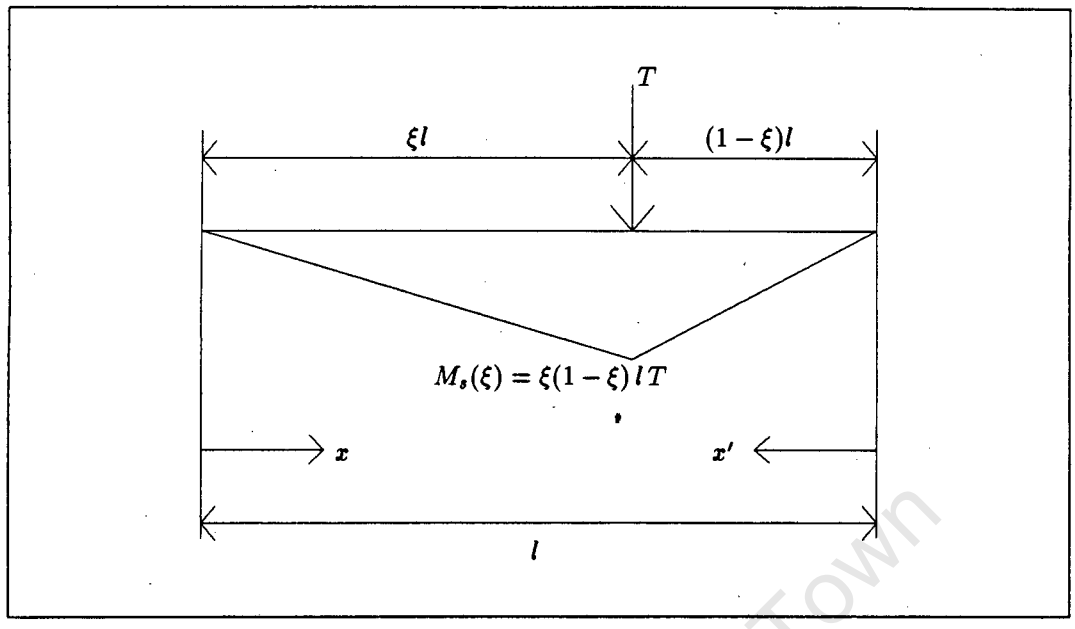

Figure 2.4: Bending Moment Diagram for Transverse Load T Only

Integrating this expression and substituting for $M_s(x)$, the first five coefficients are (letting $x = \xi l$):

$$a_1 = \frac{2T\,l}{\pi^2} \sin(\pi\xi)$$

$$a_2 = \frac{T\,l\,(1-2\xi)}{2\pi^2} \sin(2\pi\xi) - \frac{2T\,l\,\xi\,(1-\xi)}{\pi} \cos(2\pi\xi)$$

$$a_3 = \frac{2T\,l}{9\pi^2} \sin(3\pi\xi)$$

$$a_4 = \frac{T\,l\,(1-2\xi)}{8\pi^2} \sin(4\pi\xi) - \frac{T\,l\,\xi\,(1-\xi)}{\pi} \cos(4\pi\xi)$$

$$a_5 = \frac{2T\,l}{25\pi^2} \sin(5\pi\xi)$$

A sensivity study was conducted to determine how many coefficients are required to approximate the bending moments with reasonable accuracy. The results showed that

the first two coefficients would provide sufficient accuracy. Details of the sensitivity study are given in Appendix A. Substituting these terms into equation (2.16), the following relationship for the displacement under the load is obtained:

$$\begin{aligned} y(\xi) &= \xi^2 (1-\xi)^2 \frac{Tl^3}{3\,EI} + \frac{2Tl^3}{\pi^4\,EI} \sin^2(\pi\xi) \frac{p}{1-p} \\ &+ \left\{ \frac{Tl^3\,(1-2\xi)}{8\pi^4\,EI} \sin^2(2\pi\xi) \right. \\ &\left. - \frac{Tl^3\,\xi\,(1-\xi)}{2\pi^3\,EI} \cos(2\pi\xi)\,\sin(2\pi\xi) \right\} \frac{p}{4-p} \end{aligned} \tag{2.17}$$

where $p = \frac{P}{P_{cr}}$.

Setting $k_g = \frac{48EI}{l^3}$ (the midspan stiffness of a simply supported beam), equation (2.17) can be written as:

$$\begin{aligned} y(\xi) &= \frac{T}{k_g} \left[16\xi^2(1-\xi)^2 + \frac{96}{\pi^4} \sin^2(\pi\xi) \frac{p}{1-p} \right. \\ &\left. - \left\{ \frac{6}{\pi^4}(2\xi-1)\sin^2(2\pi\xi) + \frac{12}{\pi^3}\xi(1-\xi)\sin(4\pi\xi) \right\} \frac{p}{4-p} \right] \end{aligned} \tag{2.18}$$

This relationship assumes that the bunton supports do not displace. To include this displacement, the displacement for a rigid beam is superimposed with the relationship in equation (2.18). The deflection y_b at $x = \xi l$ of the rigid beam (as illustrated in Figure 2.5) is:

$$y_b(\xi) = \frac{T}{k_b} \left[\xi^2 + (1-\xi)^2 \right] \tag{2.19}$$

The assumption was made that the displacements of the buntons do not cause bending moments due to the axial compressive loads. The justification of this assumption is given in Appendix B. Therefore, adding this displacement to the displacement calculated in equation (2.18), the total displacement of the guide is:

$$\begin{aligned} y(\xi) &= \frac{T}{k_b} \left[\xi^2 + (1-\xi)^2 + 16r\xi^2(1-\xi)^2 + \frac{96\,r}{\pi^4} \sin^2(\pi\xi) \frac{p}{1-p} \right. \\ &\left. - \left\{ \frac{6\,r}{\pi^4}(2\xi-1)\sin^2(2\pi\xi) + \frac{12\,r}{\pi^3}\xi(1-\xi)\sin(4\pi\xi) \right\} \frac{p}{4-p} \right] \end{aligned} \tag{2.20}$$

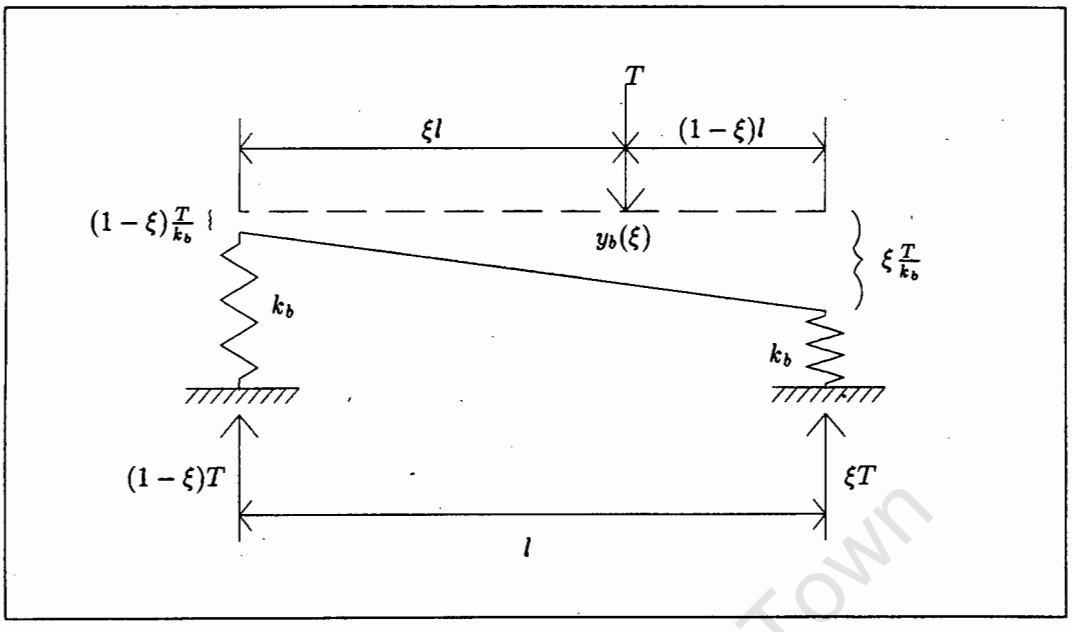

Figure 2.5: Displacements of the Buntons

where $r = \frac{k_b}{k_g}$.

This relationship can be expressed in the form of equation (2.3). Defining $k_e\,(\xi\, l) = k_b\, f(\xi\, l)$, the following relationship for the dimensionless multiplier $f(\xi)$ can be obtained:

$$f(\xi) = \left[\xi^2 + (1-\xi)^2 + 16r\xi^2(1-\xi)^2 + \frac{96\,r}{\pi^4}\sin^2(\pi\xi)\,\frac{p}{1-p} - \left\{ \frac{6\,r}{\pi^4}(2\xi-1)\sin^2(2\pi\xi) + \frac{12\,r}{\pi^3}\xi(1-\xi)\sin(4\pi\xi) \right\} \frac{p}{4-p} \right]^{-1} \qquad (2.21)$$

2.2.4 Dimensionless Formulation of the Equation of Motion

It is desirable to write the equation of motion in a dimensionless form so that parametric studies can be performed for a general class of problems rather than for specific cases.

Substituting $k_e(\xi) = k_b f(\xi)$ into the equation of motion (equation (2.7)) gives:

$$m_e\ddot{y}(\xi) + k_b f(\xi) y(\xi) = 0\,, \quad \xi = \xi(t) \qquad (2.22)$$

with initial conditions: $y(\xi(0)) = 0$ and $\dot{y}(\xi(0)) = \dot{u}_0$. The following dimensionless parameters are adopted:

$$Y(\xi) = \omega_0 \frac{y(\xi)}{\dot{u}_0} \quad \omega_0 = \sqrt{\frac{k_b}{m_e}} \quad \text{and} \quad \tau = \omega_0 t$$

The equation of motion (equation (2.22)) can then be rewritten as:

$$\ddot{Y}(\xi) + f(\xi)Y(\xi) = 0 \tag{2.23}$$

where $\ddot{Y}(\xi) = \frac{d^2Y(\xi)}{d\tau^2}$, with the initial conditions: $Y(\xi(0)) = 0$ and $\dot{Y}(\xi(0)) = 1$.
The parameter ξ is a function of time, defined through the relationship:

$$\xi(t) = \xi_0 + \frac{v_s}{l} t$$

where v_s is the constant vertical velocity of the skip and ξ_0 is the initial point of impact of the skip. The following dimensionless parameter for the skip velocity is introduced:

$$V_s = \frac{v_s}{l}\sqrt{\frac{m_e}{k_b}} = \frac{v_s}{\omega_0 l} \tag{2.24}$$

and the dimensionless relationship between ξ and τ is therefore:

$$\xi(\tau) = \xi_0 + V_s\tau$$

2.2.5 System Parameters

The solution of the equation of motion (equation (2.23)) depends on the following four dimensionless parameters:

$r = \frac{k_b}{k_g}$ being the ratio of the bunton stiffness to the guide midspan stiffness,

$p = \frac{P}{P_{cr}}$ being the ratio of the applied axial compressive load to the critical (buckling) load of the guide,

$V_s = \frac{v_s}{\omega_0 l}$ being the dimensionless form of the vertical velocity of the skip,

$\xi_0 = \frac{x_0}{l}$ being the initial point of impact between the skip and the guide.

2.2.6 Calculation of the Forces in the System

The internal forces in the system may be evaluated as follows.

Equation (2.3) can be written as:

$$T(\xi) = k_b f(\xi) y(\xi)$$

where $k_e(\xi) = k_b f(\xi)$.

The skip force $T(\xi)$ is written in a dimensionless form as:

$$\overline{T}(\xi) = f(\xi) Y(\xi) \tag{2.25}$$

where $\overline{T}(\xi) = \frac{\omega_0}{k_b \dot{u}_0} T(\xi)$.

Similarly, the forces in the buntons as defined in Figure 2.5, are:

$$\overline{B}_1(\xi) = (1-\xi) f(\xi) Y(\xi) \quad \text{and} \quad \overline{B}_2(\xi) = \xi f(\xi) Y(\xi) \tag{2.26}$$

The maximum bunton force at any instant is the maximum of $\overline{B}_1(\xi)$ and $\overline{B}_2(\xi)$.

The maximum bending moment due to the transverse load T will always occur at the position of the load, while the maximum bending moment due to the axial loads P will always occur at the position of maximum beam deflection. Since the positions of these two maxima are invariably not the same, and the value of the beam deflection is only known at the position of the load, the assumption is made that the maximum bending moment always occurs at the position of the transverse load T, i.e. at position ξl. The bending moment due to the skip force $T(\xi)$ (for a simply supported beam, as illustrated in Figure 2.4) is:

$$M_s(\xi) = \xi(1-\xi)\, l\, T(\xi)$$

and the bending moment due to the axial compressive forces P is:

$$M_a(\xi) = P y(\xi)$$

Therefore, the total bending moment at position ξl (in dimensionless form) is:

$$\overline{M}(\xi) = \xi(1-\xi) f(\xi) Y(\xi) + \frac{\pi^2}{48} \frac{p}{r} Y(\xi) \tag{2.27}$$

where $\overline{M}(\xi) = \frac{\omega_0}{k_b l \dot{u}_0} M(\xi)$.

2.3 Numerical Implementation of the Model

In this section, the numerical implementation of the model is discussed. An integration algorithm (average acceleration method) is used for the time-stepping, and the selection of a suitable time-step is discussed, along with a scheme to terminate the solution.

2.3.1 The Average Acceleration Method

The average acceleration method is a member of the Newmark family of time integration methods. It was chosen as it is unconditionally stable and simple to implement.

Expressing the differential equation describing the motion of the system, equation (2.23), at time $\tau + \Delta\tau$, yields the following equation:

$$\ddot{Y}_{\tau+\Delta\tau} + f(\xi_{\tau+\Delta\tau})\, Y_{\tau+\Delta\tau} = 0 \tag{2.28}$$

where ξ is a function of τ since:

$$\xi_{\tau+\Delta\tau} = \xi_0 + (\tau + \Delta\tau)\, V_s$$

The method assumes that the acceleration over a specific time interval is constant. In this thesis, all the time intervals are taken to be of equal duration. The relationship between acceleration and time in shown in Figure 2.6.

The acceleration at any arbitrary time $\bar{\tau}$ ($\tau \leq \bar{\tau} \leq \tau + \Delta\tau$) is taken as the average of the accelerations at the preceeding and the following time-steps:

$$\ddot{Y}(\bar{\tau}) \approx \frac{1}{2}(\ddot{Y}_\tau + \ddot{Y}_{\tau+\Delta\tau})$$

Expressions for the velocity and displacement are obtained by integrating this approximation for the acceleration as follows:

$$\dot{Y}_{\tau+\Delta\tau} = \dot{Y}_\tau + \frac{\Delta\tau}{2}(\ddot{Y}_\tau + \ddot{Y}_{\tau+\Delta\tau}) \tag{2.29}$$

and

$$Y_{\tau+\Delta\tau} = Y_\tau + \Delta\tau\, \dot{Y}_\tau + \frac{\Delta\tau^2}{4}(\ddot{Y}_\tau + \ddot{Y}_{\tau+\Delta\tau}) \tag{2.30}$$

Solving for $\ddot{Y}_{\tau+\Delta\tau}$ and substituting into equation (2.28), yields the following expression for the displacement:

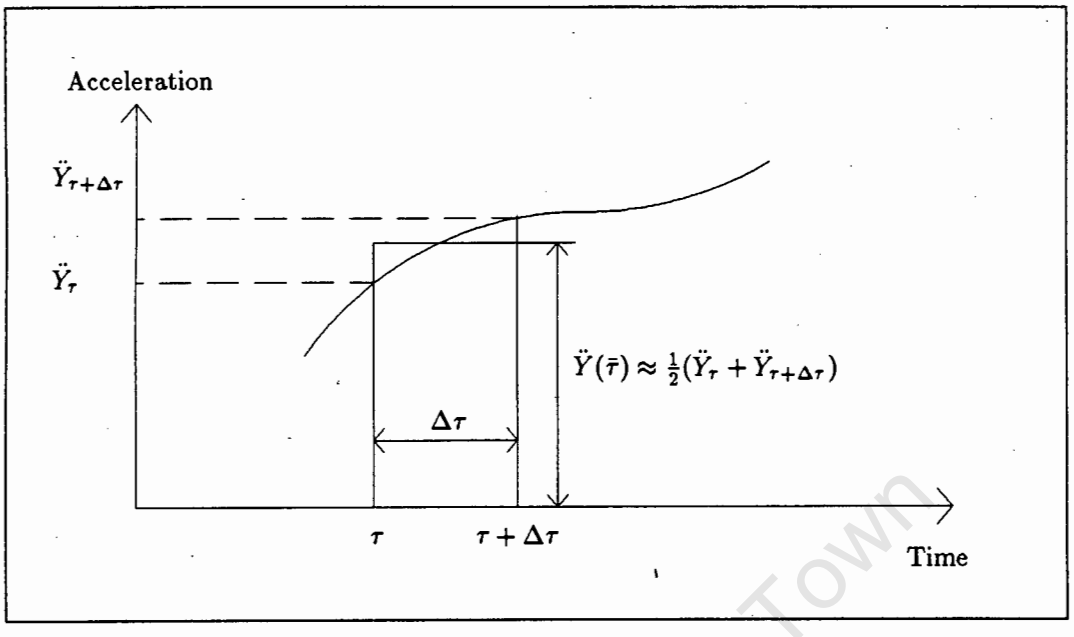

Figure 2.6: Plot of Acceleration versus Time

$$Y_{\tau+\Delta\tau} = \frac{\frac{\Delta\tau^2}{4}\ddot{Y}_{\tau} + \Delta\tau\,\dot{Y}_{\tau} + Y_{\tau}}{1 + \frac{\Delta\tau^2}{4} f(\xi_{\tau+\Delta\tau})} \tag{2.31}$$

To solve for the velocities and accelerations at time $\tau + \Delta\tau$, $Y_{\tau+\Delta\tau}$ is substituted into equations (2.29) and (2.30), to give:

$$\dot{Y}_{\tau+\Delta\tau} = \frac{2}{\Delta\tau}(Y_{\tau+\Delta\tau} - Y_{\tau}) - \dot{Y}_{\tau} \tag{2.32}$$

and

$$\ddot{Y}_{\tau+\Delta\tau} = \frac{2}{\Delta\tau}(\dot{Y}_{\tau+\Delta\tau} - \dot{Y}_{\tau}) - \ddot{Y}_{\tau} \tag{2.33}$$

2.3.2 Program UCTSLAM

A computer program called **UCTSLAM** [21] was developed in order to perform the slamming analysis described in Chapter 2.2. The program was written in FORTRAN 77, and implemented on a DEC MicroVAX II.

2.3.3 Termination of the Solution

The solution is terminated when the skip leaves the guide, i.e. when $Y_{\tau>0} = 0$. The time at which the skip leaves the guide will not fall precisely at the end of a time-step. A linear interpolation is performed to obtain a better approximation of the time when the skip leaves the guide. This new final time-increment is used to calculate the values of the velocity and acceleration when the skip leaves the guide, as well as the position at which the skip left the guide.

2.3.4 Selection of a Suitable Time-Step

To select a suitable timestep, the equation of motion, equation (2.28), is considered at time τ:

$$\ddot{Y}_\tau + f(\xi_\tau)\, Y_\tau = 0$$

The maximum value that $f(\xi_\tau)$ could attain is $f(\xi_\tau) = 2$, occurring when the guide is rigid. Therefore the 'stiffest' form of the equation of motion is:

$$\ddot{Y}_\tau + 2Y_\tau = 0 \tag{2.34}$$

with boundary conditions:

$$Y_{\tau=0} = 0 \quad \text{and} \quad \dot{Y}_{\tau=0} = 1 \tag{2.35}$$

Solving the above boundary value problem and noting that the solution procedure must be terminated when $Y_{\tau>0} = 0$, i.e. when the skip leaves the guide, the time elapsed while the skip is in contact with the guide is:

$$\tau = \frac{\pi}{\sqrt{2}} \approx 2.221 \ldots$$

This suggests that a time interval of not greater than $\Delta\tau = 0.1$ should be used, which would give approximately 20 time-steps. The total time taken for the skip to leave the guide for the above case is a minimum, as the stiffest possible value of $f(\xi_\tau l)$ was used. Therefore, for more flexible cases, the contact time will be longer, and hence more than 20 time-steps will be required for a complete solution.

A sensitivity analysis of the size of the time-step was performed using the following data. This choice allows a direct comparison to be made with the results obtained by the SDRC [26]:

$r = \frac{k_b}{k_g}$ was kept constant at a value of $r = \frac{26330}{810} = 32.506$.

$p = \frac{P}{P_{cr}}$ was set to $p = 0.0$.

$V_s = \frac{v_s}{\omega_0 l}$ was kept constant at a value of $V_s = \frac{15.24}{\sqrt{\frac{26330}{6.95}}\,6.096} = 0.041$.

$\xi_0 = \frac{x_0}{l}$ was set to $\xi_0 = 0.1$.

The results that were obtained are presented in Table 2.1.

	UCTSLAM					SDRC
Time-step ($\Delta\tau$)	0.0001	0.001	0.01	0.1	1.0	0.001
Skip Left Guide (x/l)	0.7579	0.7578	0.7571	0.7498	0.6565	0.76
Skip Left Guide (τ)	16.1967	16.1950	16.1774	15.9980	13.7003	n/a
Rebound Velocity	-0.7174	-0.7172	-0.7155	-0.6985	-0.5543	-0.71
Max. Skip Force	0.1581	0.1582	0.1584	0.1611	0.2105	0.1579
Max. Bunton Force	0.0535	0.0534	0.0533	0.0515	0.0395	0.0531
Max. Bending Moment	0.0315	0.0315	0.0315	0.0312	0.0296	n/a
No. of Iterations	161969	16196	1619	161	15	n/a

Table 2.1: Time-Step Sensitivity Analysis

A time-step of $\Delta\tau = 0.01$ was chosen as it provides accurate solutions without requiring too much computational time.

2.4 Results of Numerical Modelling

2.4.1 Introduction

The influence of the axial load P on the system is now shown. A set of datum results was required to make a direct comparison with the results obtained by SDRC [26]. For this purpose, the following set of data was chosen:

$r = \frac{k_h}{k_g}$ was kept constant at a value of $r = \frac{26330}{810} = 32.506$.

$p = \frac{P}{P_{cr}}$ was varied from $p = 0.0$ to $p = 0.9$.

$V_s = \frac{v_s}{\omega_0 l}$ was kept constant at a value of $V_s = \frac{15.24}{\sqrt{\frac{26330}{6.95}}\,6.096} = 0.041$.

$\xi_0 = \frac{x_0}{l}$ was varied from $\xi_0 = 0.0$ to $\xi_0 = 1.0$.

2.4.2 Presentation of Results

The results are presented graphically showing the output component versus the initial point of impact between the skip and the guide. The results show the maxima over the whole time that the skip is in contact with the guide for a specific initial impact position. These plots are presented for different values of $p = \frac{P}{P_{cr}}$, the ratio of the axial load to the critical (Euler buckling) load of the guide. Therefore, for each output parameter, we have a plot of the parameter versus the initial impact position, for various values of p.

The general trends of the results are discussed, and amplification factors are given to show the effect of the axial compressive load P. These amplification factors are calculated with respect to the values for $p = 0.0$, and are presented in tables for different values of p .

The following results were calculated by the program **UCTSLAM**:

(a) the maximum displacement of the skip corner

(b) the position (vertically) when the skip leaves the guide, called the rebound position

(c) the time when the skip leaves the guide, called the contact time

(d) the maximum velocity at which the skip leaves the guide, called the rebound velocity

(e) the maximum force in the slipper plate of the skip, called the skip force

(f) the maximum force that the buntons experience due to the impact of the skip with the guide

(g) the maximum bending moment that the guide experiences due to the impact of the skip with the guide.

2.4.3 Discussion of Results

Maximum Deflection of the Guide

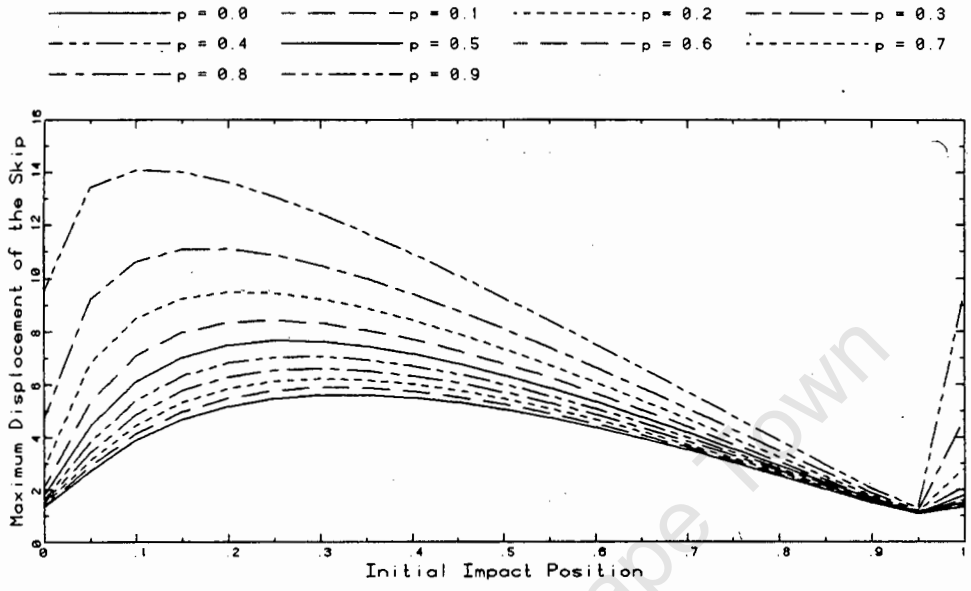

Figure 2.7: Maximum Deflection of the Guide

When the skip impacts the guide near the first bunton (i.e. when $0.0 < \xi_0 < 0.3$), the displacements of the skip corner are relatively large, as illustrated in Figure 2.7. The converse is true when the skip impact point approaches the next bunton, i.e. when $\xi_0 \approx 0.95$; the displacements of the skip corner are small. For values of ξ_0 between 0.95 and 1.0, the displacements increase dramatically. This occurs because the skip does not rebound at the second bunton (see Figure 2.8), and the skip enters the more flexible region of the guide. The effects of the axial loads are illustrated by means of amplification factors based on the results for $p = 0.0$. These factors are presented in Table 2.2.

p	Amplification Factor
0.3	1.2
0.5	1.4
0.7	1.7
0.9	2.5

Table 2.2: Amplification Factors for Guide Deflection

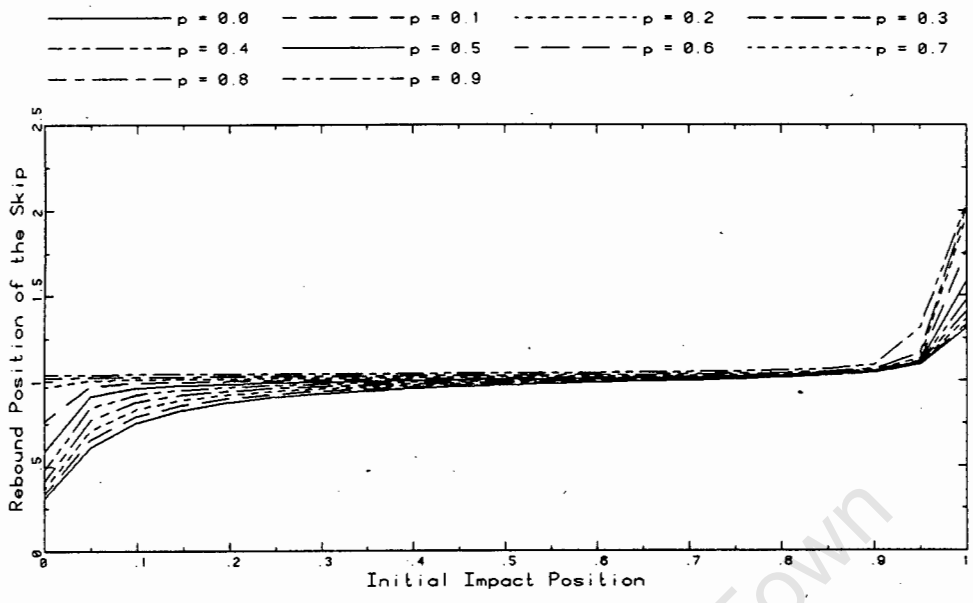

Figure 2.8: Position at which the Skip leaves the Guide

Rebound Position

From Figure 2.8 it can be seen that the skip generally rebounds when it reaches the following bunton, i.e. when $\xi \approx 1.0$. An exception occurs when the skip initially impacts the guide near $\xi_0 = 0.1$, where the skip rebounds before the next bunton is reached. Here a trend towards a rebound position near the next bunton, i.e. $\xi \approx 1.0$, occurs as p increases. For impacts near the next bunton, i.e. $\xi_0 = 0.95$, and for higher values of p, the rebound position tends to occur near the following bunton, i.e. when $\xi_0 \approx 2.0$.

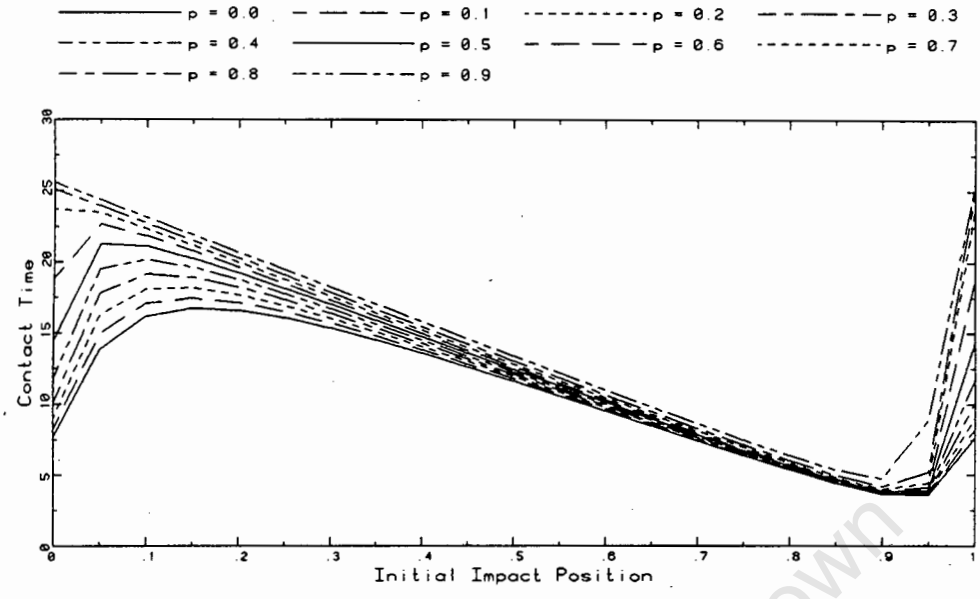

Figure 2.9: Time of Contact between the Skip and the Guide

Contact Time

From Figure 2.9, it is apparent that the contact time decreases almost linearly from $\tau \approx 25.0$ at $\xi_0 = 0.0$ to $\tau \approx 4.0$ at $\xi_0 = 0.9$. For impact positions between $\xi_0 = 0.9$ and $\xi_0 = 1.0$, the skip does not rebound at the bunton at $\xi = 1.0$ (see Figure 2.8); hence the longer contact time. For impact positions ξ_0 from 0.0 to about 0.4, the relationship is not linear for low values of p, but as p increases, so the trend becomes increasingly linear. This phenomenon can be linked to the rebound position, i.e. the skip did not rebound at the next bunton for the cases of low ξ and p.

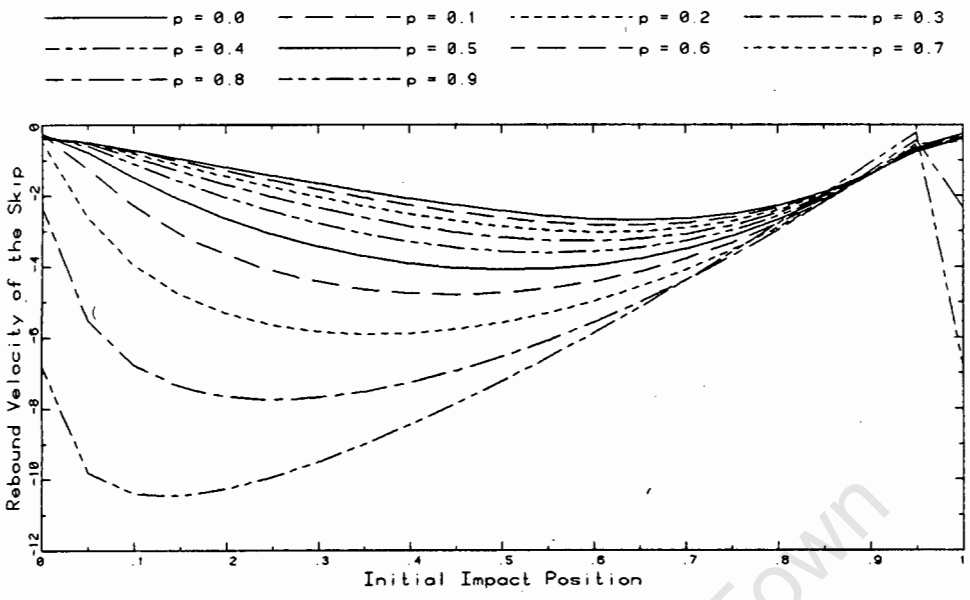

Figure 2.10: Velocity at which the Skip leaves the Guide

Rebound Velocity

The velocity at which the skip rebounds from the guide varies from about 0.5 for impacts near the buntons, to about 2.5 for impacts near the midspan of the guide for $p = 0.0$, shown in Figure 2.10. Here the influence of the axial compressive force ratio p can be clearly seen. Amplification factors for various values of p are tabulated in Table 2.3. Note that, as p increases, the maximum velocity occurs at an initial impact position approaching $\xi_0 = 0.0$. This is due to the kinetic energy of the skip being converted to strain energy in the guide, and since this strain energy is a maximum at midspan, the response of the skip will be greater for skip impacts before the guide midspan.

p	Amplification Factor
0.3	1.2
0.5	1.6
0.7	2.4
0.9	3.8

Table 2.3: Amplification Factors for Rebound Velocities

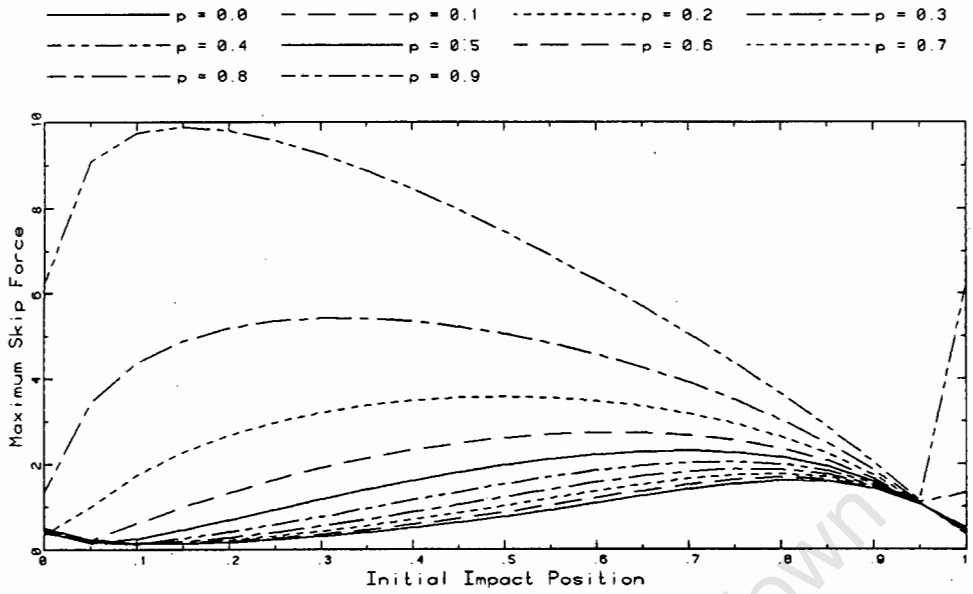

Figure 2.11: Maximum Force acting on the Skip

Maximum Skip Force

In Figure 2.11, the amplification of the maximum skip force is apparent when the ratio of the axial compressive load to the critical load, p, is increased. Amplification factors for different values of p are given in Table 2.4. The maximum skip force for higher values of p occurs when the skip impacts the guide nearer the first bunton (i.e. when $\xi_0 = 0.0$) than for lower values of p. This is due to the kinetic energy of the skip being converted to strain energy in the guide, and since this strain energy as well as the dependence of the skip force on axial compressive loads are maxima at midspan, the response of the skip will be greater for the skip impacting the guide before the midspan of the guide.

p	Amplification Factor
0.3	1.1
0.5	1.4
0.7	2.3
0.9	6.5

Table 2.4: Amplification Factors for Maximum Skip Forces

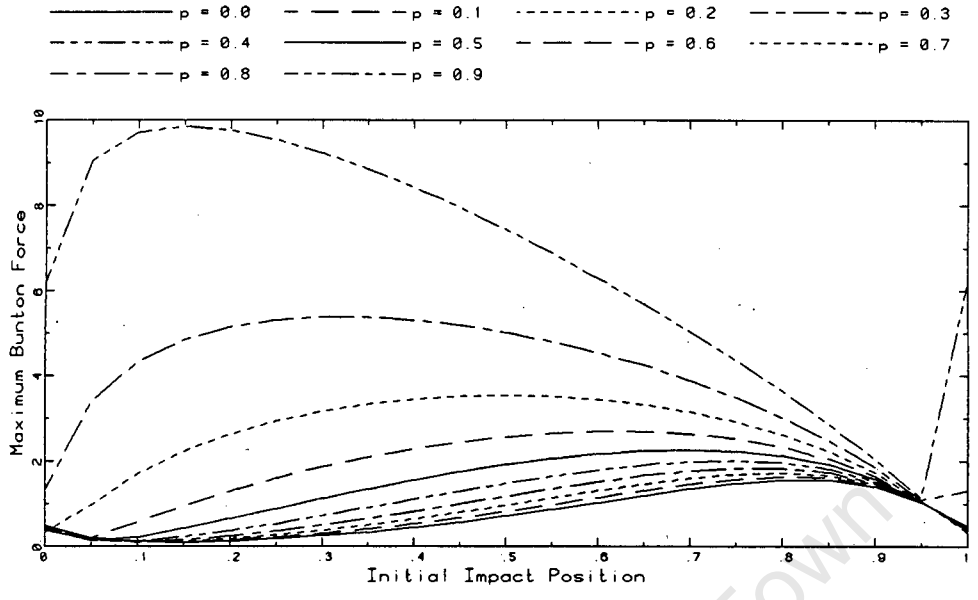

Figure 2.12: Maximum Force in the Bunton

Maximum Bunton Force

As expected, the curves for the maximum bunton forces, illustrated in Figure 2.12, are the similar to those of the maximum skip force, which are illustrated in Figure 2.11. This similarity occurs because the bunton force depends on the skip force and the position of the skip, and since the maximum skip forces occur when the lateral motion of the skip is arrested, which is generally close to a bunton (where the effective stiffness of the guide is relatively large), the results are similar. Amplification factors for increasing values of p are presented in Table 2.5.

p	Amplification Factor
0.3	1.1
0.5	1.4
0.7	2.3
0.9	6.5

Table 2.5: Amplification Factors for Maximum Bunton Forces

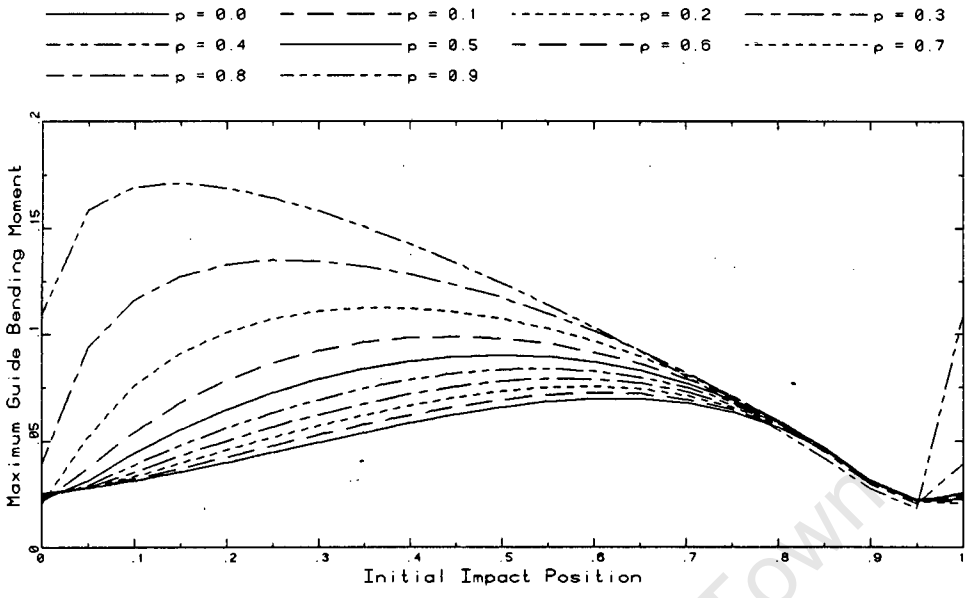

Figure 2.13: Maximum Bending Moment in the Guide

Maximum Guide Bending Moment

The increase of the guide bending moments with respect to the ratio of the axial compressive force to critical buckling load p is illustrated in Figure 2.13. The bending moments in the guide depend on a combination of the magnitude and the position of the skip force, and the maximum deflection of the guide and the magnitude of the axial compressive load. An assumption is made that the maximum bending moment occurs at the position of the skip force, see Chapter 2.2.6. The amplification factors of the guide bending moments are presented in Table 2.6.

p	Amplification Factor
0.3	1.1
0.5	1.3
0.7	1.7
0.9	2.5

Table 2.6: Amplification Factors for Maximum Guide Bending Moments

2.5 Simplified Solution for Slamming Analyses

2.5.1 Introduction

An alternative, simplified formulation to the problem was suggested by Greenway [9], based on the assumption that the guide midspan stiffness k_g and bunton stiffness k_b are important, while the stiffness distributions between the guide midspan and bunton are not. The guide midspan stiffness k_g can be expressed in the form $k_g\ (1 - P/P_{cr})$. This assumption allows previously obtained results in the form of contour plots [8] to be utilised by simply modifying the bunton to guide midspan stiffness ratio r, as well as providing a more simplified method of determining the effective guide stiffness.

2.5.2 Errors in the Simplified Solution

In order to make any recommendations or conclusions regarding the simplified solution, an idea of the errors has to be known. The errors are presented in a manner showing distribution of the error in displacement along a simply supported beam for various values of the ratio of the axial compressive force to the critical buckling force of the beam, i.e. $p = P/P_{cr}$. The calculation of the errors is now shown.

Considering only the displacements due to the flexibility of the guide (the displacements due to the bunton supports displacing are the same for both formulations), the formulation presented in Chapter 2.2 yields the following relationship describing the guide displacements (see equation (2.18)):

$$\begin{aligned} y &= \frac{T}{k_g}\left[16\xi^2(1-\xi)^2 + \frac{96}{\pi^4}\sin^2(\pi\xi)\frac{p}{1-p}\right] \\ &= \frac{T}{k_g(1-p)}\left[16\xi^2(1-\xi)^2\right] \\ &\quad -\frac{Tp}{k_g(1-p)}\left[16\xi^2(1-\xi)^2 - \frac{96}{\pi^4}\sin^2(\pi\xi)\right] \end{aligned} \tag{2.36}$$

Omitting the bunton deflection contribution, the equation to be used in the simplified solution for the guide displacements is:

$$y^* = \frac{T}{k_g(1-p)}\left[16\xi^2(1-\xi)^2\right] \tag{2.37}$$

The error in the simplified solution is the difference between equations (2.36) and (2.37), and is the following:

$$\begin{aligned} \Delta y_E &= y^* - y \\ &= \frac{Tp}{k_g(1-p)}\left[16\xi^2(1-\xi)^2 - \frac{96}{\pi^4}\sin^2(\pi\xi)\right] \end{aligned} \tag{2.38}$$

To obtain a meaningful representation of the error, it is expressed as the percentage error with respect to the original formulation presented in Chapter 2.2.

$$\begin{aligned} \%\ \text{Error} &= \frac{100\Delta y_E}{y} \\ &\approx \frac{1}{\frac{0.69}{p} - 0.01} \end{aligned} \tag{2.39}$$

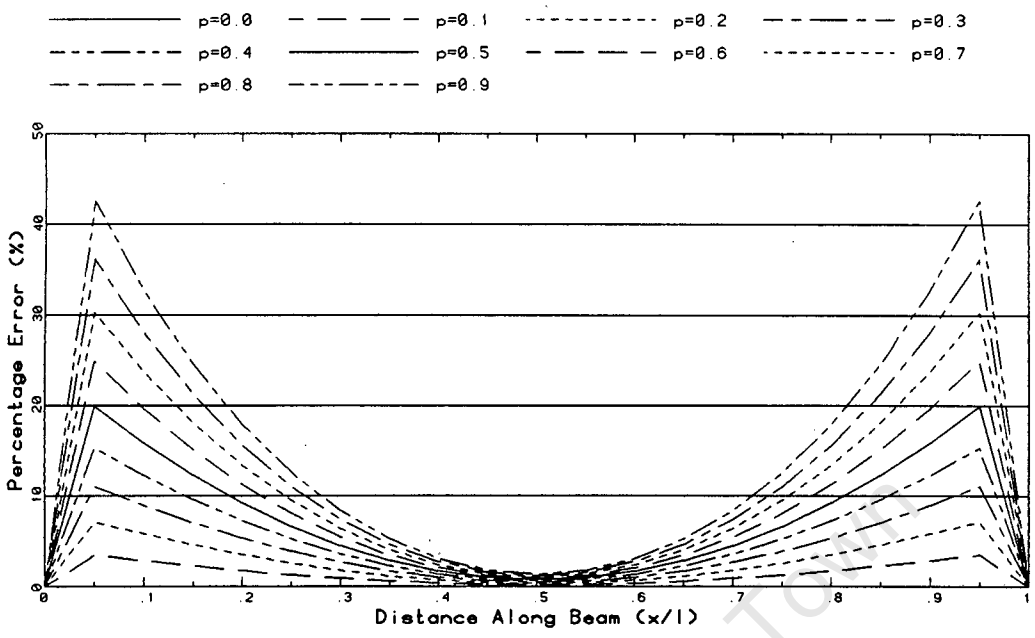

Figure 2.14: Percentage Error Distribution along a Guide

The results presented in Figure 2.14 show the error distribution along a beam for various values of p. Figure 2.14 shows that the errors exceed 40% when the skip is in the regions of $\xi = 0.1$ and $\xi = 0.9$. These errors, however, must be put into perspective. A plot of the absolute error distribution versus guide position for a specific case (the President Steyn No. 4 Shaft will be used again) shows that the maximum errors occur near $\xi = 0.2$, and when compared to the absolute maximum displacement along the guide, they are only 6%. As the buntons are approached, the displacements are very small, so any change in displacement will yield a high percentage error. This absolute error distribution is presented in Figure 2.15.

From the above presentation of the results, it can be seen that the errors in the results compared with those for the initial formulation, are less than 20%. If these errors are acceptable, then this simplified solution provides a method in which results obtained from previous analyses and presented in the form of contour plots [8], can be used. The ratio of the bunton to guide midspan stiffnesses needs to be modified, as discussed in Chapter 2.5.3, in order to utilise these earlier results. The errors are all conservative, i.e. the results for the forces, displacements and velocities are larger than those obtained for the initial formulation.

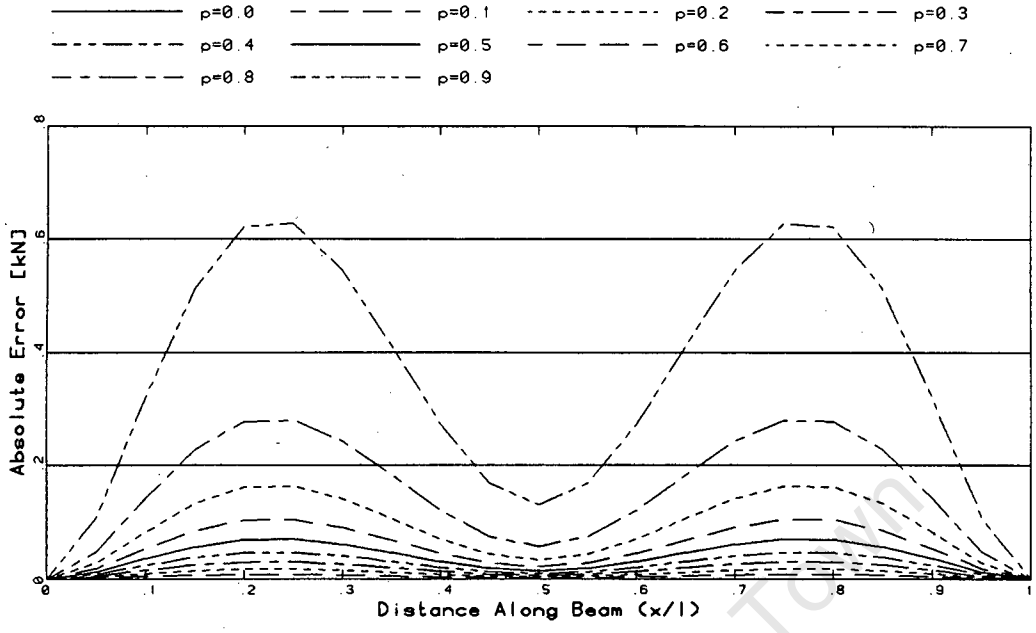

Figure 2.15: Absolute Error Distribution along a Guide

2.5.3 General Results of the Alternate Solution

The results for the alternate proposal are now presented in plots for all values of the input parameters. The input parameters are:

(a) $r = \frac{k_b}{k_g(1-p)}$

(b) $V_s = \frac{v_s}{\omega_0 l}$

The initial impact point ξ_0, was originally an input parameter, but since only the maxima of the output parameters are of interest, irrespective of the position of the skip, this parameter is effectively condensed out.

Previously, the results were presented for specific cases. Since the ratio of the axial compressive force to the critical buckling force can be included in the ratio of the bunton to guide midspan stiffnesses, a generalised set of results can be obtained. Contour plots [8] are used to determine the required output parameters, where the two axes are:

x axis dimensionless bunton stiffness K_b

y axis stiffness ratio r^*

Since:

$$K_b = \frac{k_b l^2}{m_e {v_s}^2}$$

and using equation (2.24), Chapter 2.2.4, the dimensionless bunton stiffness is:

$$K_b = \frac{1}{{V_s}^2}$$

The axial force ratio p is included in the contour plot using the following relationship:

$$r^\star = \frac{k_b}{(1-p)k_g}$$

Therefore, the two axes (constituting the input parameters) are defined, and the user can read off the contour value of the dimensionless bunton force $\bar{b}$, or the impact energy magnification factor $\bar{e}_i$. The impact energy magnification factor is a measure of the rebound velocity:

$$\bar{e}_i = (\text{Rebound Velocity Ratio})^2 - 1$$

The contour plots are presented on the following two pages.

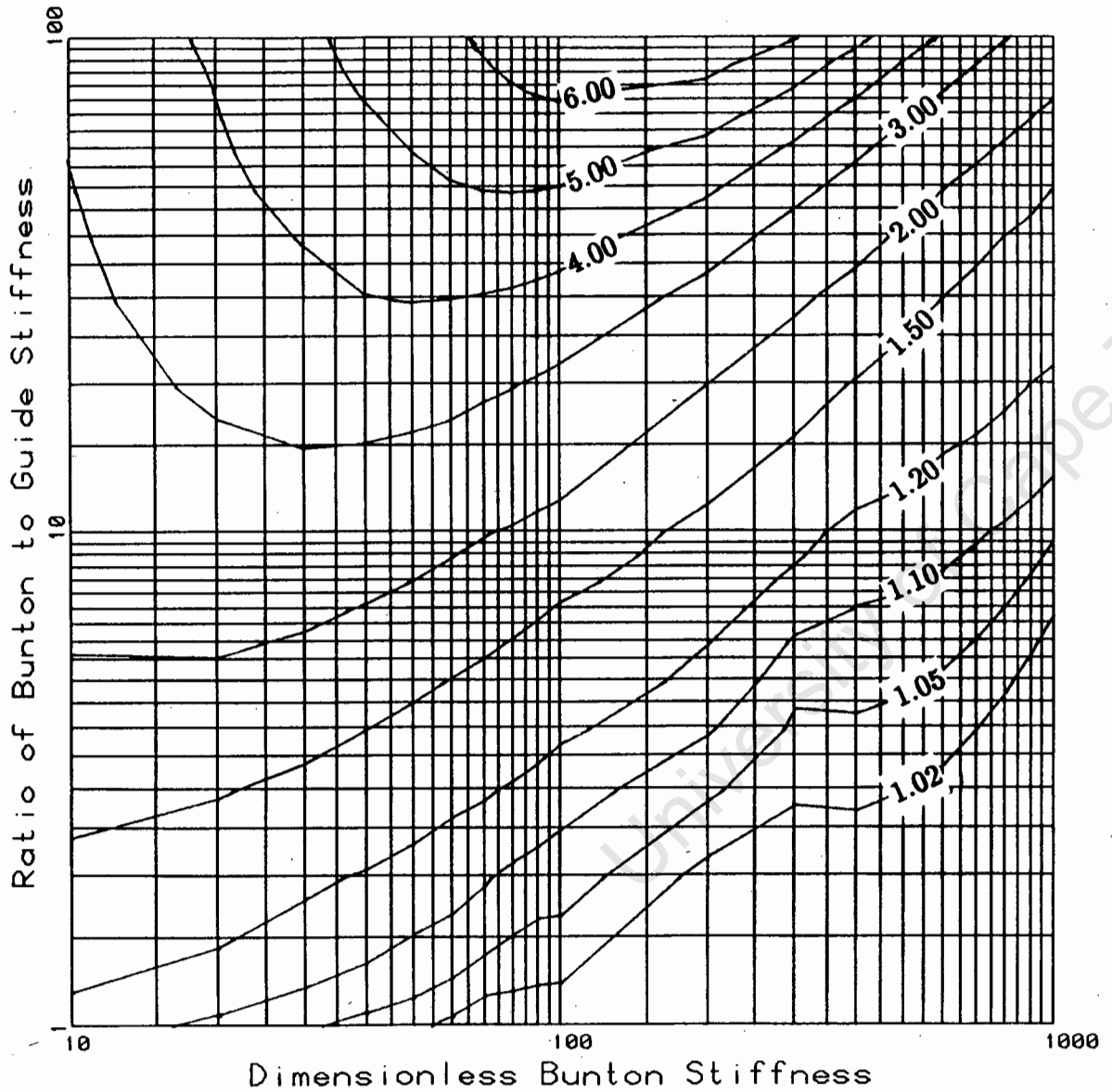

BUNTON IMPACT FORCE

Magnification Contours for Single Event Slamming

Applies to all values of $\frac{u}{v}$ and p.

The guide stiffness is modified for the axial load using the relationship :

$$k_g^\star = (1 - p)\, k_g$$

where $p = \frac{P}{P_{cr}}$.

The ratio of the bunton to guide stiffness r, is given as :

$$r = \frac{k_b}{k_g}$$

To include any value of p, modify the value of k_g in the above relationship.

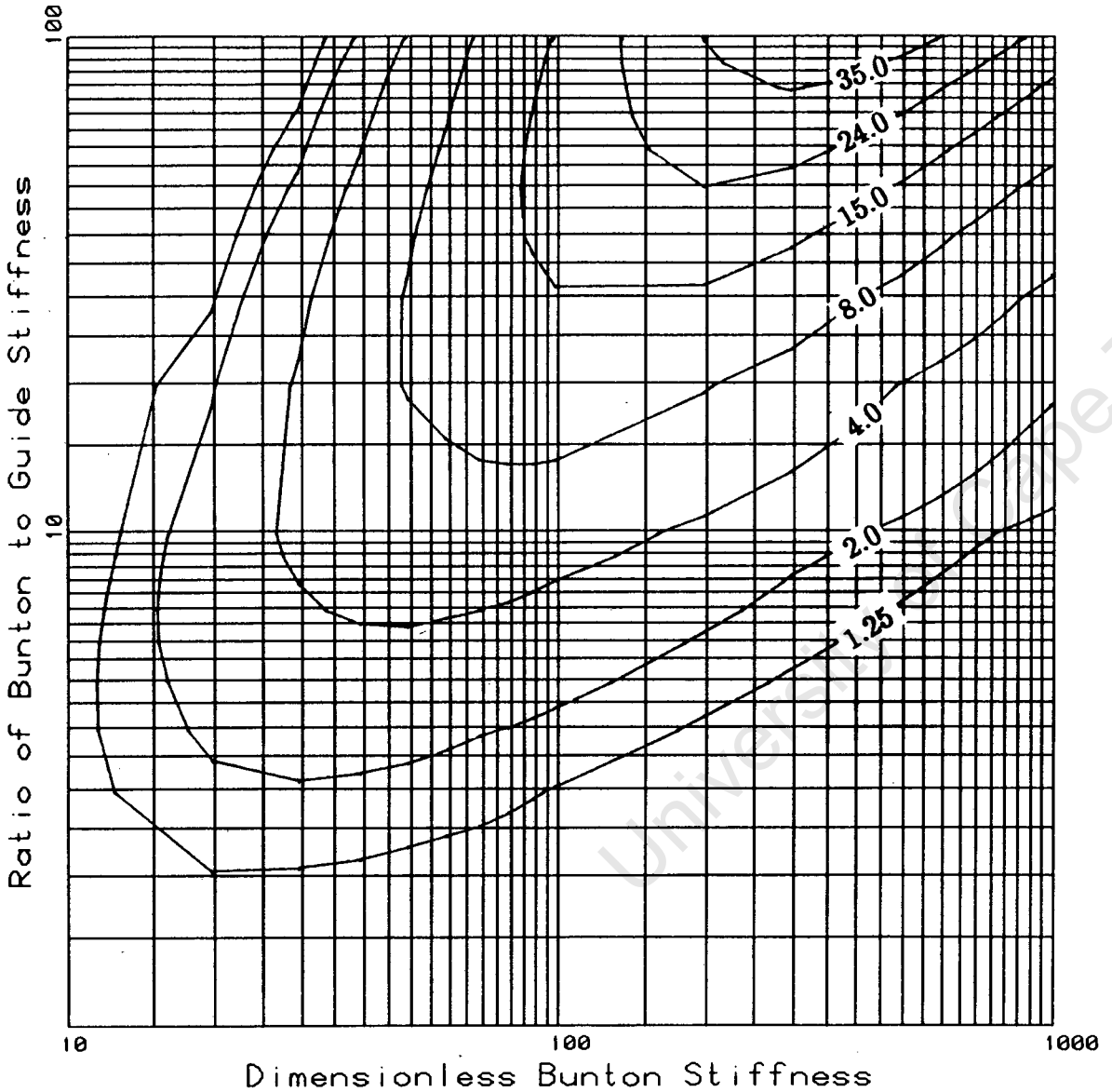

IMPACT ENERGY

Magnification Contours for Single Event Slamming

Applies to all values of $\frac{u}{v}$ and p.

The guide stiffness is modified for the axial load using the relationship :

$$k_g^\star = (1 - p)\, k_g$$

where $p = \frac{P}{P_{cr}}$.

The ratio of the bunton to guide stiffness r, is given as :

$$r = \frac{k_b}{k_g}$$

To include any value of p, modify the value of k_g in the above relationship.

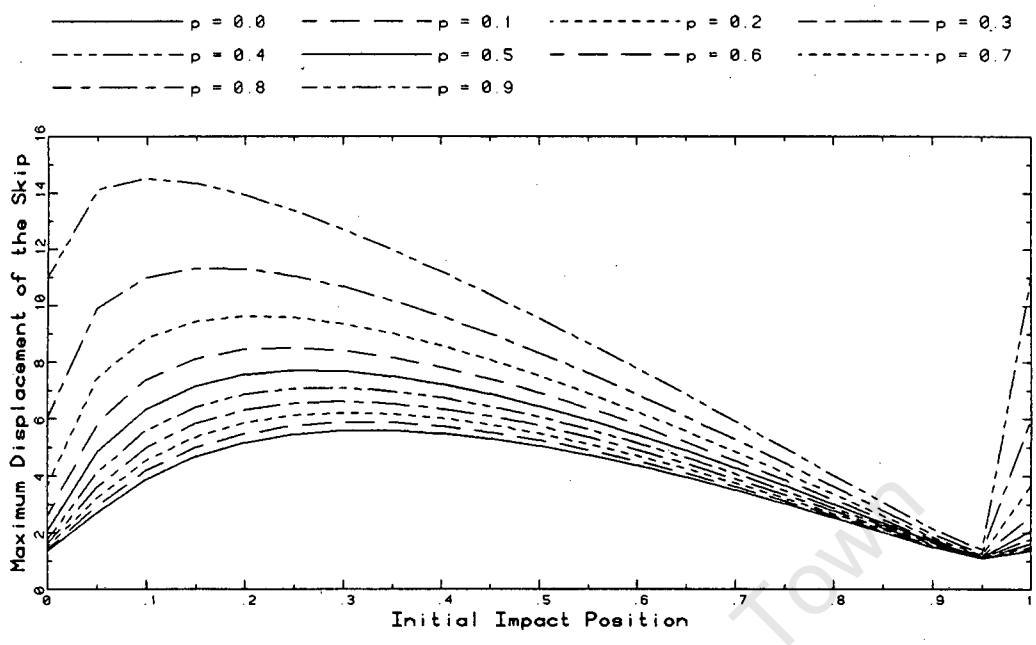

Figure 2.16: Maximum Displacement of the Skip Corner

2.5.4 Presentation of the Results

A few of the results for the alternative, simplified solution are presented here to illustrate the similarities to the results of the original formulation, again using the specific set of data studied in Chapter 2.4. All of the results are presented in Appendix C for completeness.

Maximum Displacement of the Skip Corner

Comparing the maximum displacements, illustrated in Figure 2.16, to those in Chapter 2.4, it can be seen that for $p = 0.9$, the maximum is approximately 14.5, while for the initial formulation, it is 14.2. This represents a 2.0% increase. The results differ by a maximum of 1.8% for $p = 0.7$, and for axial force ratios less than $p = 0.5$, the results are in even better agreement with the original formulation. The results do vary more when the initial impact position occurs at or close to a bunton, since the skip rebounds before it reaches the midspan of the guide and the simplified solution is only accurate at the midspan of the guide.

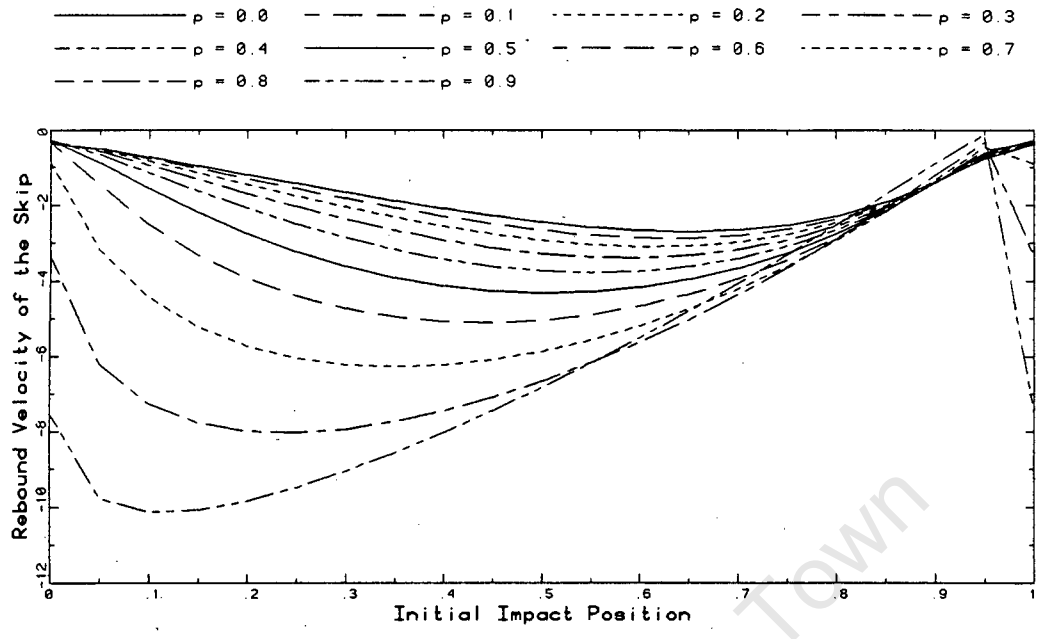

Figure 2.17: Velocity at which the Skip leaves the Guide

Rebound Velocity

When the rebound velocities for the simplified analysis, refer to Figure 2.17, are compared to those in Chapter 2.4, maximum values of -10.2 and -10.5 are obtained respectively. This is a decrease of 3.0%. For $p = 0.7$, values of -6.3 and -5.9 are obtained respectively, which is an increase of 8.5%, and for $p = 0.5$, an increase of 4.0%. For values less than $p = 0.5$, the results differ less, e.g. for $p = 0.4$, an increase of 2.8%. The results also differ from those of the original formulation for an impact at or close to a bunton, for the same reasons given for the maximum displacement of the skip corner.

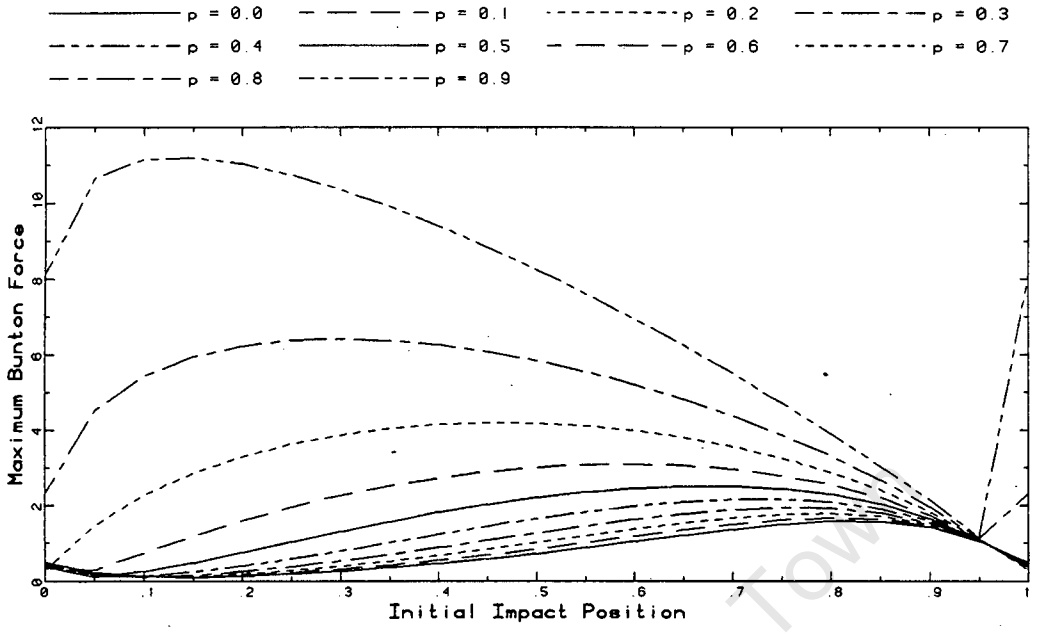

Figure 2.18: Maximum Force in the Bunton

Maximum Bunton Force

Comparing the maximum bunton forces, illustrated in Figure 2.18, to those in Chapter 2.4, values of 11.2 and 9.8 are obtained for $p = 0.9$, for the simplified solution and the original formulation respectively; about a 14.3% increase. The results for $p = 0.8$ show an 18% increase, while those for $p = 0.5$ an increase of 13%. The results for axial force ratios less than $p = 0.4$, are about the same as those for the original formulation. Again, for higher values of the axial force ratio p, the results differ when there is an impact at or close to a bunton.

2.6 Study of Second Order Effects

One of the primary assumptions in the formulation of the lateral stiffness of the guide was that the guide undergoes small displacements and is modelled as a simply-supported beam. As a result, the effects of finite or second order deformations that cause stiffening, have been ignored along with any effects due to the continuity of the beam. It is possible that these stiffening effects could reduce the overall forces in the system, and thus the severity of the slamming event could be reduced. These second order effects are addresed in this section.

2.6.1 Numerical Sensitivity Study

The effects of secondary stiffening are illustrated using the following examples. Six simply-supported beams are studied (**A, B, C, D, E, F**), with three types of end conditions and two different axial compressive loads. The end conditions for the various beams are:

A, D simply-supported, on rollers, with springs to simulate the axial effects of the rest of the structure,

B, E simply-supported, on rollers,

C, F pinned with no axial displacements allowed.

The loading conditions (in addition to a transverse point load applied at midspan) are:

A, B, C no axial compressive loads,

D, E, F axial compressive loads equal to half of the critical buckling load of the beam are applied at the ends of the beam.

Since the purposes of this study are to determine whether the secondary stiffening effects are significant, only two load cases were investigated, in order to illustrate any effects that the axial compressive force effects may have on response. An axial compressive load equal to half the critical buckling load of the beam is a representative value, from which tentative conclusions may be drawn. The other case is for zero axial loads. The inclusion of the pinned cases (**C, F**) is to show the upper bounds of the ranges of the secondary stiffening effects for the different values of the axial compressive load. Similarly, the purely simply-supported cases (**B, E**) are included to show the lower bounds of these ranges. These lower bounds are in fact the simply-supported midspan stiffnesses used

in the formulation described in Chapter 2.5. The simply-supported cases with springs to simulate the axial effects of the rest of the structure (**A, D**), illustrate the secondary stiffening effects, and do fall within the ranges specified by the upper and lower bounds.

2.6.2 Material and Cross-Section Data

A guide from President Steyn Shaft #4 Compartment #5 was used for this study. The cross-section is a top-hat section with the following material and section properties:

Young's Modulus	E = 200 GPa
Poisson's Ratio	$\nu = 0.3$
Length	$\ell = 6.096$ m
Cross-sectional Area	A = 7.313×10^{-3} m^2
Second Moment of Area	I = 10.135×10^{-6} m^4.

The stiffness of the springs used to simulate the continuous structure was obtained from a frame analysis [15] involving several layers of the shaft steelwork which are linked together by the guides. A spring stiffness of k_s = 49145 kN/m was used.

Large displacement analyses of the various beam configurations were performed, using the commercial nonlinear finite element program ABAQUS [12], to obtain the relationships between lateral forces applied at midspan and the corresponding displacements. The gradients of the resulting force-displacement curves are simply the midspan stiffnesses of the various beam configurations.

2.6.3 Results of the Sensitivity Study

The force-displacement curves obtained from the large displacement analyses are now discussed. Initially, a global view of these force-displacement curves is presented to show the overall trends of the various beam configurations. The beams were allowed to deflect to one tenth of their original length, which are unrealistically large deflections. The reason for this is to clearly show the global trends. Secondly, the results in the region of interest are discussed. The results for a displacement value of 0.122 m have been chosen for discussion as this corresponds with the maximum lateral displacement that the guide undergoes according to the original formulation for $p = 0.5$, see Chapter 2.4.

Global Perspective of Results

The secondary stiffening effects are clearly evident in Figure 2.19. The two curves for the pinned cases (**C** for $p = 0.0$ and **F** for $p = 0.5$) are upper bounds of the secondary

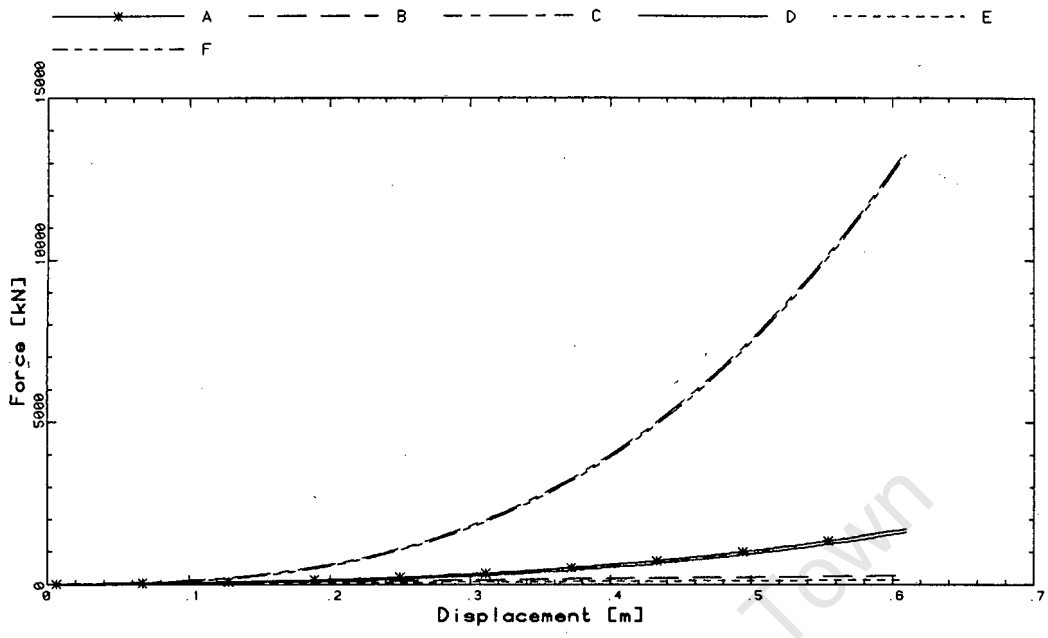

Figure 2.19: Force-Displacement Curve Exhibiting Secondary Stiffening

stiffening effects for the respective axial compressive forces. The lower bounds are given by the straight lines for the simply-supported cases (**B** for $p = 0.0$ and **E** for $p = 0.5$). These curves are the midspan stiffnesses of the guide in the simplified formulation discussed in Chapter 2.6, and are linear relationships between the midspan applied forces and resultant displacements. The actual stiffnesses of the guides lie between these two sets of curves. The two curves with the axial springs included to simulate the continuity of the structure (**A** for $p = 0.0$ and **D** for $p = 0.5$) fall within the upper and lower bounds, and are initially asymptotic to the linear curves. This result was expected since the secondary effects only influence the response of the structure when the deflections of the beam are finite.

Results in Relevant Range

At a displacement of 0.122 m, the force in the guide (at midspan) is 52 kN for the formulation used by SDRC [26], 26 kN for the solution discussed in Chapter 2.5 of this thesis, and 41 kN when the secondary stiffening effects are included. The corresponding stiffnesses are 430 kN/m, 215 kN/m and 336 kN/m respectively when the beam has displaced by 0.122 m. Curve **D** originally starts off asymptotic to the simply-supported case while the displacements are still small, but when the displacements become larger, it diverges exhibiting the nonlinear secondary stiffening effects.

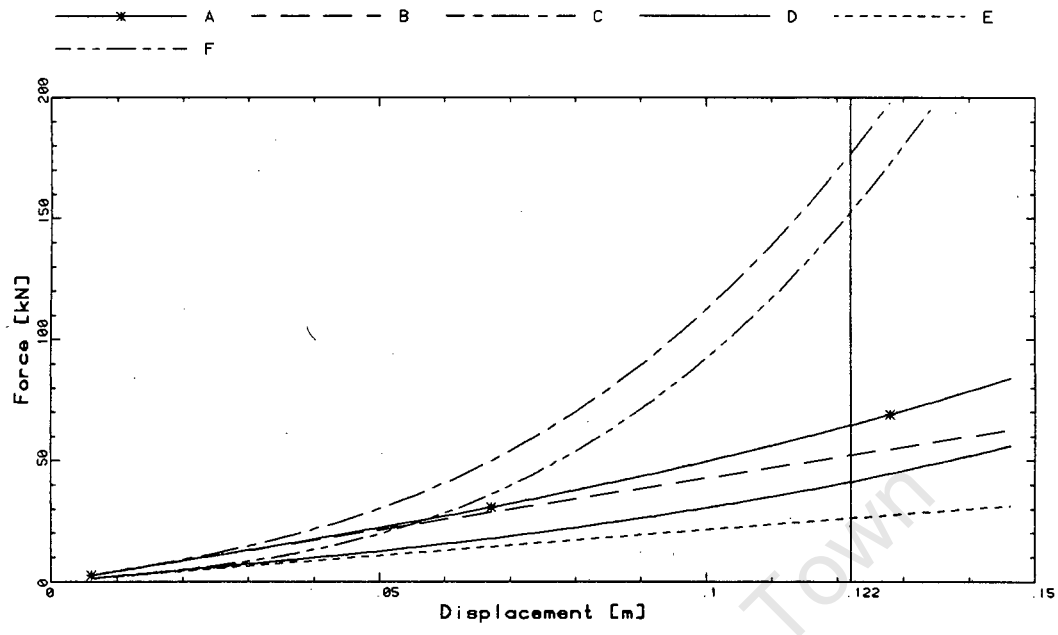

Figure 2.20: Force-Displacement Curve Exhibiting Secondary Stiffening

This thesis includes the effects of axial compressive forces in the guide, in effect the formulation now uses the stiffness of curve **E**, shown in Figure 2.20, instead of curve **B** for $p = 0.5$ for the guide midspan stiffness. The inclusion of secondary stiffening (curve **D**) shows that the formulation in this thesis appears to be too conservative. Therefore the inclusion of secondary stiffening is less conservative than the formulation discussed in Chapter 2.5.

2.6.4 Numerical Example of an Actual Case

A numerical example is presented to illustrate the effects of the nonlinear secondary stiffening on slamming. The same data (President Steyn No. 4 Shaft) was used as for the previous numerical studies to facilitate comparisons. The dimensionless guide stiffness (using the simplified formulation of Chapter 2.5) is:

$$f^*(\xi l) = \left[\xi^2 + (1-\xi)^2 + 16r^*\xi^2(1-\xi)^2 \right]^{-1}$$

where $r^\star = \frac{k_b}{(1-p)k_g}$, and k_g is the midspan stiffness of the simply supported guide. Therefore, to include the effects of secondary stiffening, the value of k_g must be modified. Since the relationship between the midspan force and the corresponding displacement is

nonlinear and is a function of the displacement, an iterative process is used to determine the response of the skip. A predictor-corrector type of solution strategy is employed, where a prediction of the skip force is made using a linear force-displacement relationship for a simply-supported beam. This force is added to that due to the bunton stiffness. This force is used to determine an improved estimate of the stiffness, based on the nonlinear force-displacement relationship obtained from ABAQUS, which in turn is used to calculate a new skip force. The two values of the skip force are compared and if the difference is not less than a specified tolerance, the new force is used to determine an even better estimate of the stiffness, and so on, until convergence is achieved. Approximately three to four iterations were required at each timestep to converge.

2.6.5 Comparison of Results

The results are presented in the same manner as those presented in Chapter 2.4, where only the maximum guide deflections and skip forces versus initial impact position ξ_0 are used to illustrate these second order effects. The effects of secondary stiffening are clearly illustrated, which is what the intention of this study is.

The inclusion of secondary stiffening is justified for the cases of high p-ratios, where there is a marked difference between the results using a linear midspan stiffness versus those using the nonlinear relationship. The results for several cases are presented in Table 2.7. The maximum values of the results are given along with the initial impact position which causes the maximum value.

	Linear			Non-Linear		
	$p = 0.0$	$p = 0.5$	$p = 0.9$	$p = 0.0$	$p = 0.5$	$p = 0.9$
Guide Deflection	5.59	7.70	14.51	5.57	6.73	8.67
@ ξ_0	0.35	0.25	0.10	0.30	0.30	0.20
Skip Force	1.60	2.53	11.22	1.53	1.70	1.92
@ ξ_0	0.80	0.65	0.15	0.80	0.75	0.70

Table 2.7: Secondary Stiffening Sensitivity Analysis

2.6.6 Conclusions

A study of secondary stiffening effects has been presented and it has been shown that these secondary stiffening effects could make the solution less conservative. As this aspect was not included in the objectives of this thesis, no mathematical model to include these effects has been presented, but the results for the specific example above

do indicate the need for second order effects to be investigated more thoroughly in future.

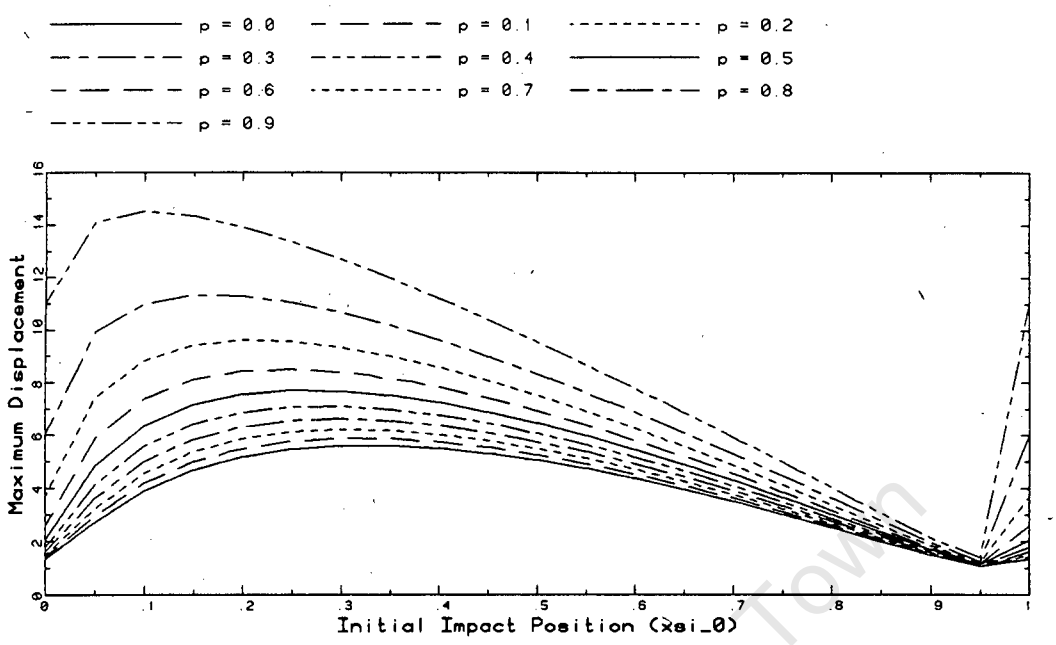

Figure 2.21: Maximum Displacement of the Skip Corner – Linear Case

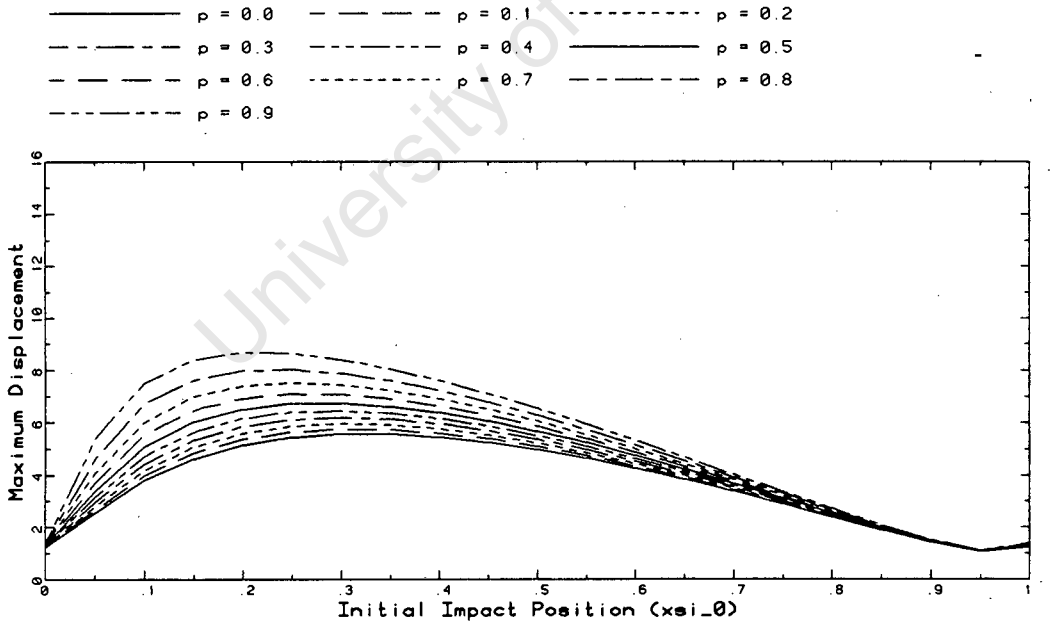

Figure 2.22: Maximum Displacement of the Skip Corner – Non-Linear Case

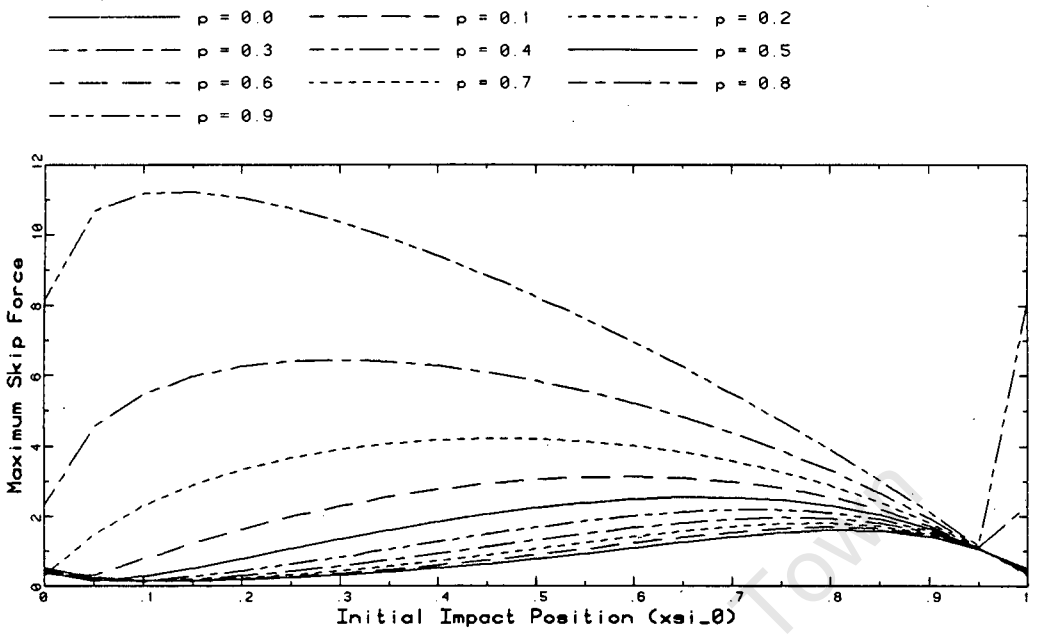

Figure 2.23: Maximum Force acting on the Skip – Linear Case

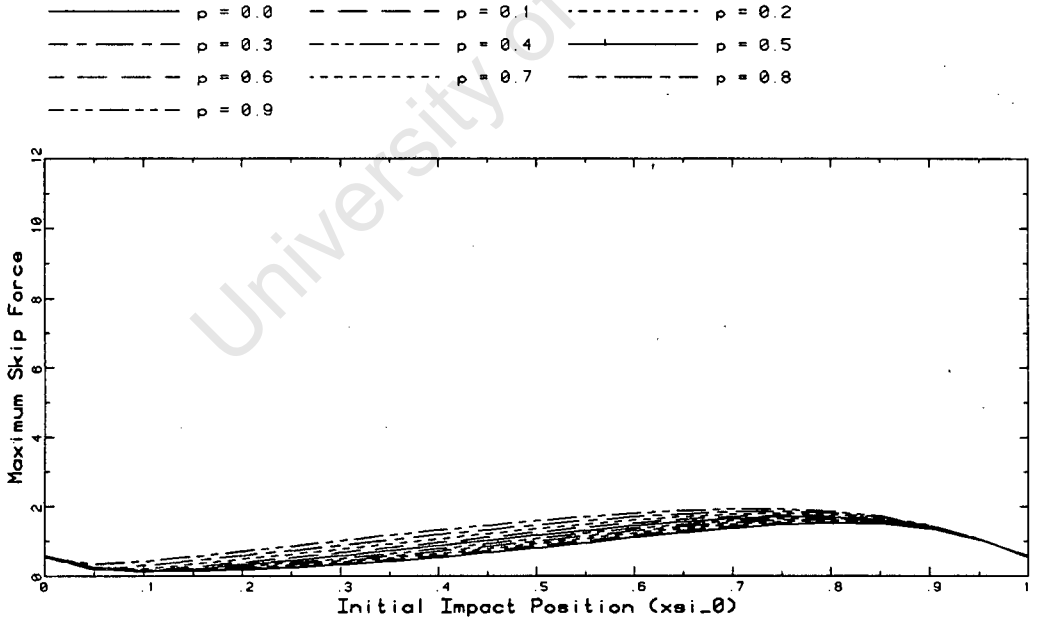

Figure 2.24: Maximum Force acting on the Skip – Non-Linear Case

2.7 Conclusions

From the results of the formulation of a model to describe the slamming event, discussed in Chapter 2.4, it is evident that the axial compressive forces in the guides, induced by the shaft wall strains, do reduce the lateral stiffness of these guides. The results for the maximum forces, bending moments, displacements and velocities (all for a particular case) are amplified when this axial compressive force is present. A simplified analysis, suggested by Greenway [9], is described and the results when compared to the previous set of results (for the same case), exhibit errors of up to 20%. If these errors are acceptable, bearing in mind that the results obtained are all conservative, this simplified formulation can be used in further calculations. Contour plots are included for calculations of the maximum bunton forces and the impact energy magnification factors; or Greenway's [8] contour plots can be used with the modification discussed in Chapter 2.5.3.

One of the primary assumptions in the analysis was that the guide undergoes only small displacements. As a result, the effects of second order deformations causing stiffening, which arise when the structure is allowed to undergo finite deformations, have been ignored. It has been shown that these stiffening effects could reduce the overall forces in the system, and therefore the severity of the slamming that the skip experiences could be reduced. Studies of these second order deformations have been done by Martin [18], and it is an aspect which should be investigated in the future.

3 System Behaviour with Guide Rollers

3.1 Introduction

During hoisting or lowering of the skip in the shaft, transverse motions of the skip due to the guide misalignments are resisted by guides running the length of the shaft. The inertial forces of the skip are transmitted to the guides by means of impacts. The energy may either be transferred via a rigid body impact, i.e. slamming as discussed in Chapter 2, or through flexible rollers on the skip. Previous research treated the two mechanisms as two separate events, providing an upper and a lower bound to the response of the skip to the guide misalignment. In this section, the system behaviour while the guide rollers are active is discussed, with the capability of rigid body impacts included.

A mathematical model is formulated in Chapter 3.2 to describe the dynamic behaviour of the skip when the skip rollers are active. The effects of axial compressive forces on the guides are included by adding geometric stiffness terms to the bending stiffnesses of the guides. The displacement method is employed to evaluate the forces in the rollers, and hence the response of the skip. In Chapter 3.3, the numerical solution of the governing equations of motion of the model are discussed where a predictor-corrector solution strategy [20] is used. The numerical implementation of the model in a computer program is also discussed. Results for various situations are presented in Chapter 3.4, where simple bump tests are performed to verify the model. Results are also presented using actual mine shaft data.

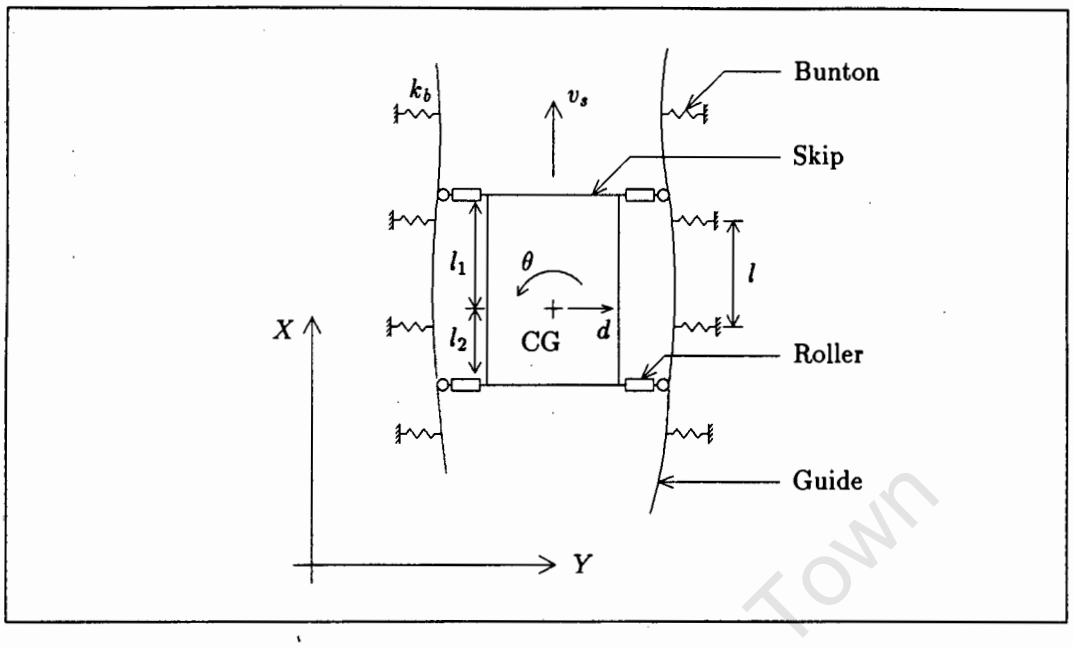

Figure 3.1: System to be Modelled

3.2 Analytical Model

3.2.1 Components to be Modelled

The system chosen to model the response of the skip numerically is shown in Figure 3.1.

A global Cartesian coordinate system is used to describe the motions of the skip, where the X-axis is in the vertical direction of the shaft and the Y-axis is in the horizontal direction. There are four fundamental components in this system which need to be modelled:

(a) The **skip** is modelled as a rigid body with mass m and mass moment of inertia I_G.

(b) The **guides** are modelled as massless beams with properties E, I, A, where E is Young's Modulus, I is the second moment of area of the cross-section and A is the cross-sectional area. In reality, the guides are continuous, but in this thesis they are modelled as repetitive sections of a five-span beam, supported periodically by buntons at intervals of l. The guides are constituted of several lengths spliced by means of a fish plate in every second span, but for the purposes of this thesis, they are modelled as being prismatic. The guide misalignments

are quadratically interpolated between known misalignments at the buntons, and any discontinuities due to the interpolations will be limited to the midspan of the guide. The reason is that since the guide stiffness is lowest at midpsan, any effects due to the discontinuities will be minimised.

(c) The **buntons** are modelled as linear springs giving a lateral support to the guide periodically at intervals of l.

(d) The **rollers** are modelled as piecewise non-linear, damped springs. The rollers may be offset to allow for an initial preload.

Certain assumptions are made in the development of the mathematical model of the response of the skip. As stated previously, the skip is modelled as a rigid body, where this assumption was discussed by earlier researchers [29]. No out of plane motions are considered in this thesis, so only the response in the global X- and Y-axes is analysed. The skip travels with a constant vertical speed v_s, i.e. in the global X-direction, and this fact is utilised in the analysis by having a moving local reference frame based on the vertical position of the skip.

3.2.2 Elements of the Model

The centre of gravity of the skip is a distance l_1 from the top of the skip in the global X-direction, where l_1 is generally taken to be equal to $0.6h$ (h = height of the skip), and half the width of the skip in the global Y-direction. Since only motions in the $X-Y$ plane are considered in the thesis, only two degrees of freedom are used to describe the motion of the skip. They are defined at the centre of gravity of the skip, and are the translation d and rotation θ. The positive sign convention that has been used is shown in Figure 3.1.

The continuous guide is modelled as repetitive sections of a five-span beam, rather than considering the complete guide in the model, as illustrated in Figure 3.2. Since the guides are continuous, the possibility of the two rollers on the same side of the skip being in contact with the same guide exists, and therefore the forces in these two rollers are coupled. The choice of five spans allows all possible combinations of position of the coupled forces acting on the guide to be modelled at any instant in time as well as the future inclusion of splices in the guides in alternate spans. The misalignment of the guides is quadratically interpolated between the misalignment of the buntons, where any discontinuities due to the interpolation are limited to the midspan of the guides.

The presence of axial compressive forces in the guides causes the guides to soften, i.e. the lateral stiffness of the guides is decreased. This reduction in stiffness is accounted for

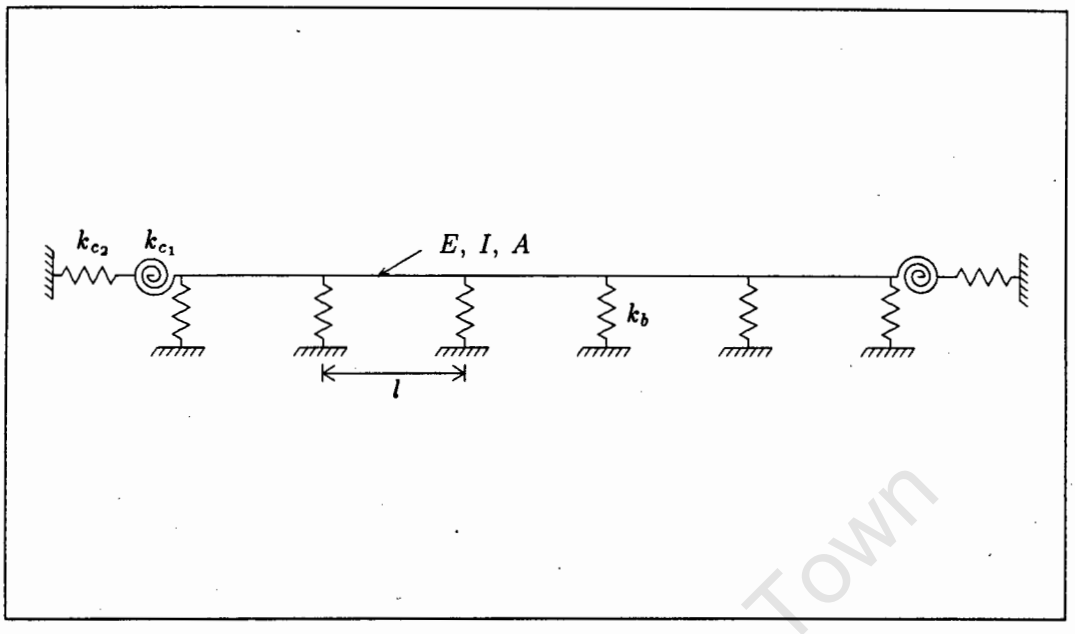

Figure 3.2: Repetitive Five-Span Beam Model

by including the geometric element stiffness matrix when the forces due to imposed displacements are to be calculated, where this geometric stiffness matrix is a function of the axial compressive loads and the length of the guide spans. Because of the continuity of the guide, boundary conditions have to be applied to simulate the effect of the rest of the structure at the ends of the five span beam. These are included as axial and rotational springs, with stiffnesses k_{c_2} and k_{c_1} respectively, as illustrated in Figure 3.3.

The bunton to guide connection is modelled as a pin joint; with no rotational stiffness provided by the buntons. This assumption is valid since this closely models configurations which are found in practice. In addition, it is assumed that the buntons provide no longitudinal stiffness to the guide. The buntons supporting the guide at intervals of l are therefore modelled as springs with lateral stiffnesses of k_b, as shown in Figure 3.3.

The rollers have non-linear force-displacement and force-velocity relationships, where these non-linear relationships are assumed to be piecewise linear, as illustrated in Figure 3.4. The spring, which is used to model the force-displacement relationship, has zero stiffness when there is no contact between the roller and the guide, or it is of infinite stiffness (very large as an infinite value is difficult to include numerically) for the case of the roller bottoming out, i.e. when the roller spring reaches the end of its travel. Two intermediate stiffness values are permitted in the model, allowing for a non-linear

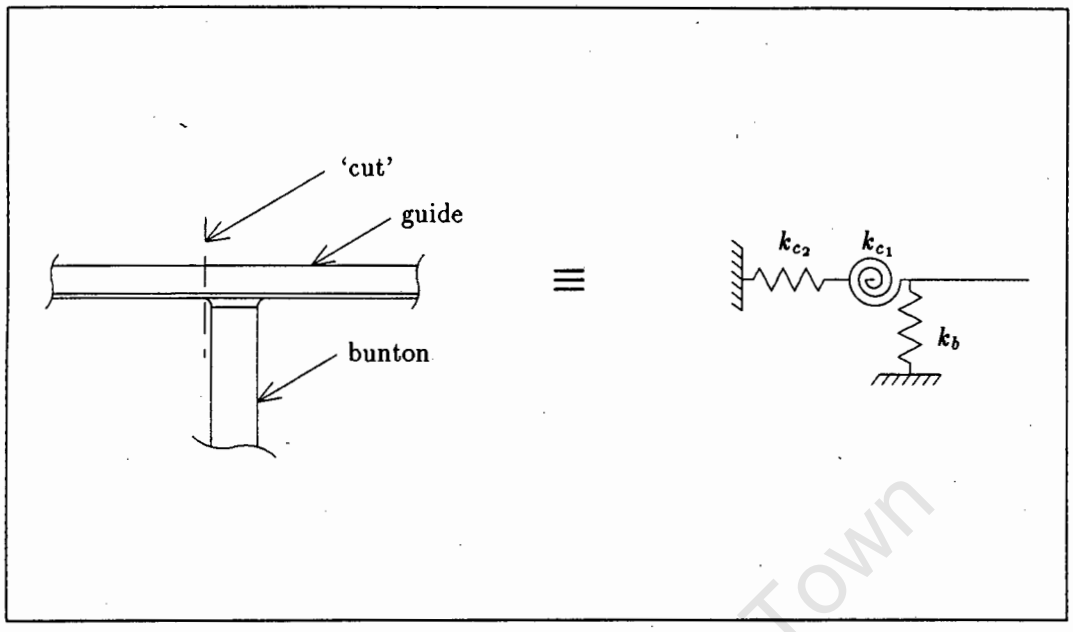

Figure 3.3: Boundary Conditions and Supports for the Continuous Beam

stiffness while the roller is in contact with the guide. The dashpot, which is used to model the force-velocity relationship, either has a constant damping coefficient c_r when the relative velocity across the roller is positive, else the damping coefficient is zero for a non-positive relative velocity across the roller.

3.2.3 Formulation of the Problem

In order to model the system illustrated in Figure 3.1, the various elements of the model have to be included. The translational stiffnesses of the guide and the buntons are combined to give an 'effective' stiffness for the guide, at the point where the roller is acting, which is represented by a translational spring with a stiffness coefficient of k_e. Therefore at each corner i of the skip there is a translational spring, with a stiffness coefficient of $k_{e,i}$ $(i = 1,2,3,4)$. The roller is modelled using a translational spring representing the non-linear roller stiffness $k_{r,i}$, and a dashpot representing the non-linear roller damping coefficient $c_{r,i}$. Since these two components are modelling the same element, i.e. the skip roller, they may be envisaged as acting in parallel with one another. Finally, this parallel combination is modelled as acting is series with the translational spring representing the guide and buntons. The combinations of these elements are illustrated in Figure 3.5 for clarity.

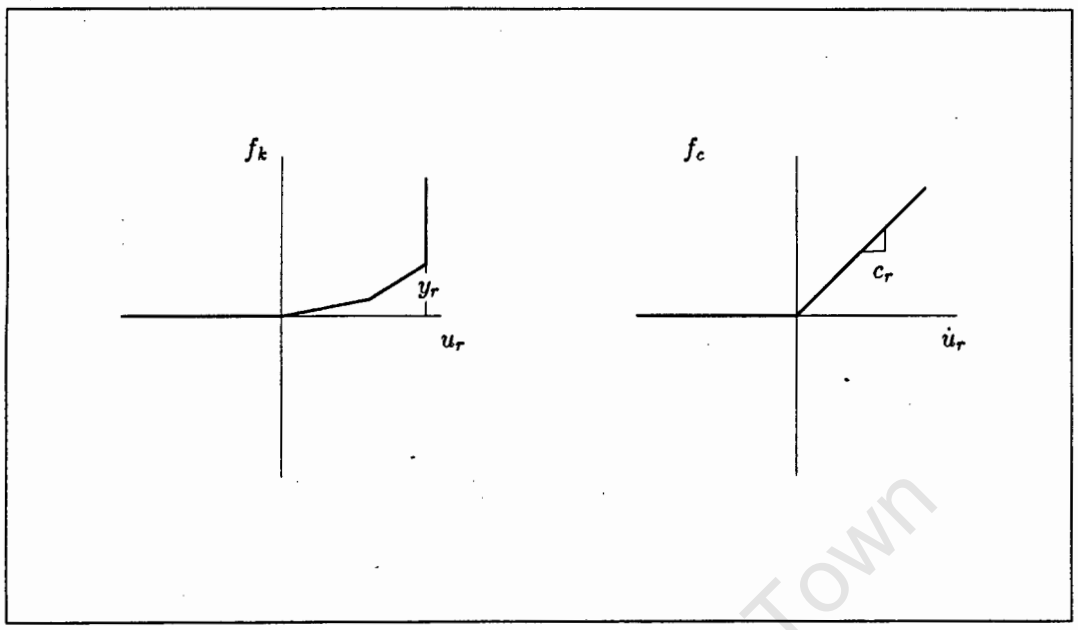

Figure 3.4: Piecewise Non-Linear Roller Relationships

The internal forces of the components of the rollers introduced above may be seen as forces acting on the skip. The skip therefore experiences a force at each of its corners, where a local y-axis is now employed at each corner. The forces are taken as being positive when acting towards the skip, see Figure 3.6, and due to the continuity of the guide, the forces on the same side of the skip are coupled when they are both in contact with the guide.

The equations of motion for the system are as follows:

$$m\ddot{d} + F_1 = 0 \tag{3.1}$$

and

$$I_G\ddot{\theta} + F_2 = 0 \tag{3.2}$$

where $F_1 = -f_1 + f_2 - f_3 + f_4$
and $F_2 = (f_1 - f_2)l_1 - (f_3 - f_4)l_2$.

and are non-linear because of the force-displacement relationships for the rollers.

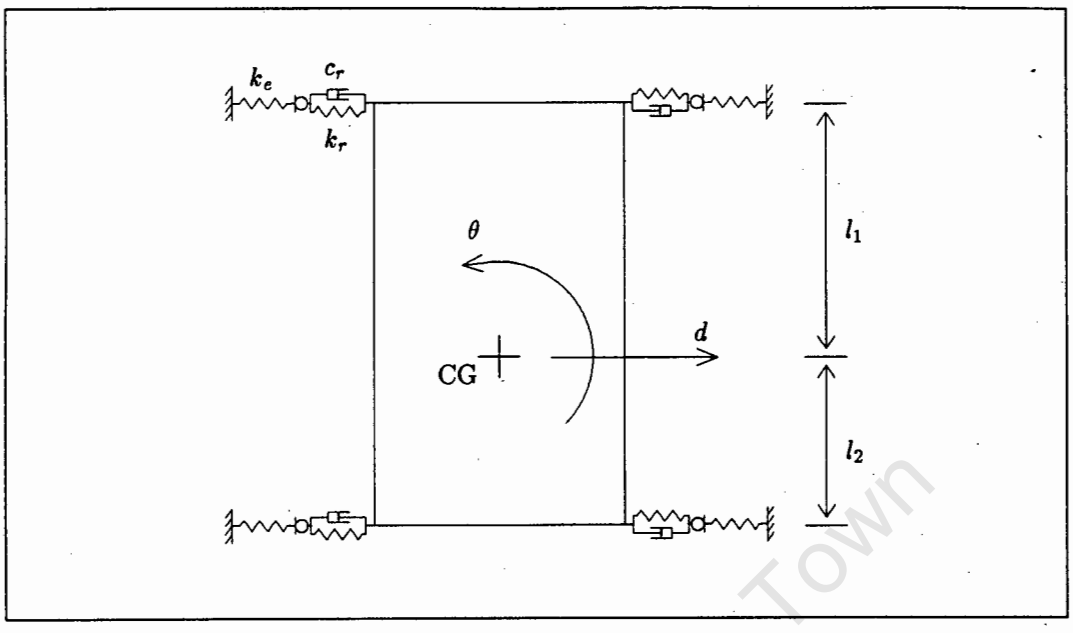

Figure 3.5: Skip Showing Modelling Components at Each Corner

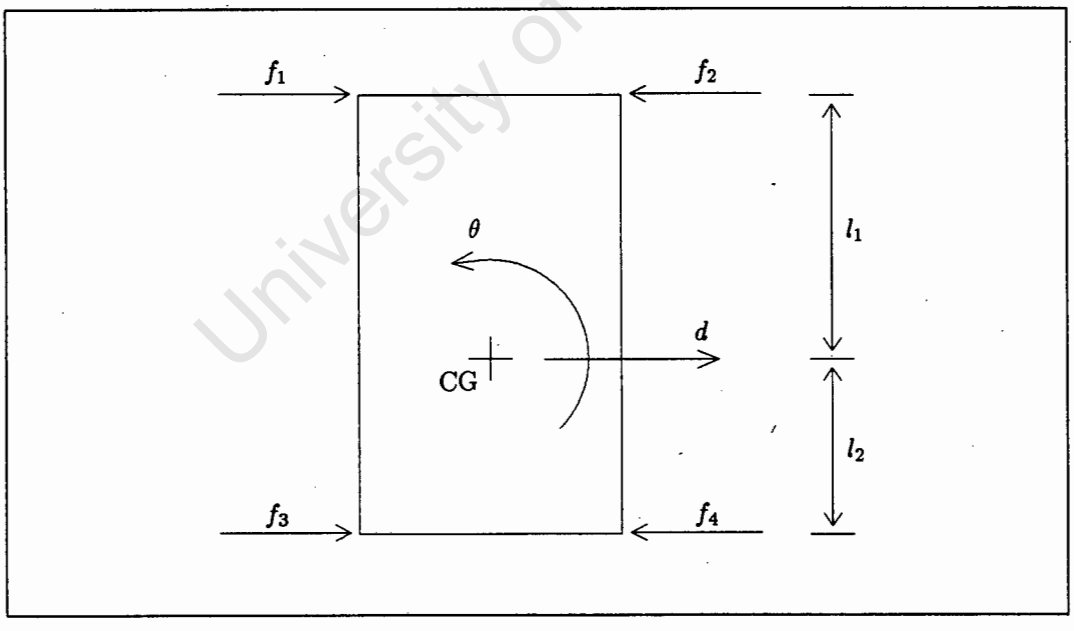

Figure 3.6: System Showing Forces at Each Corner

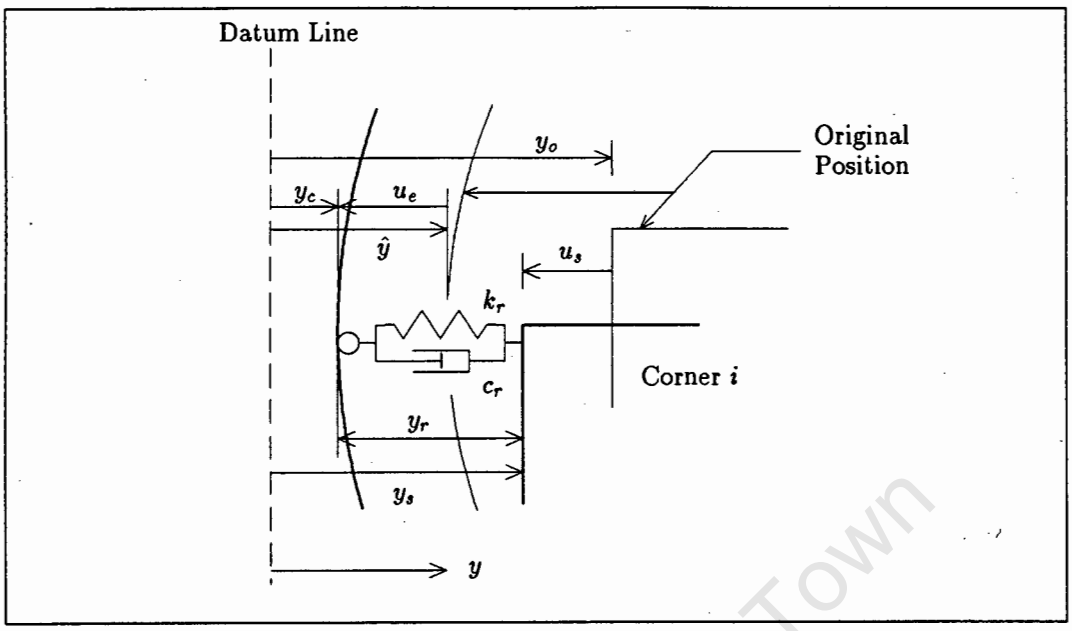

Figure 3.7: Typical Configuration at a Corner

The force in roller i, $f_{r,i}$, is a function of the displacements d and θ, the velocities $\dot{d}$ and $\dot{\theta}$, as well as the coupling effects of skip forces on the same guide. To determine these forces, the actual deflections of the guide at the position of roller i, $u_{e,i}$, have to be determined.

Initially, the case for contact between the roller and the guide will be considered. The configuration for a typical corner (as shown in Figure 3.7) is used to determine the deflection of the guide $u_{e,i}$, at corner i.

$$u_{e,i} = \hat{y}_i - y_{c,i}$$

or

$$y_{c,i} = \hat{y}_i - u_{e,i} \tag{3.3}$$

where $y_{c,i}$ is the 'point of contact' between the roller and the guide
and $\hat{y}_i$ is the original position of the guide before impact.

In order to determine this point of contact $y_{c,i}$, the displacement across the roller i is used. This is defined as:

$$u_{r,i} = y_{r,i}^{\star} - y_{r,i}$$

where the value $y_{r,i}^{\star}$ is introduced as the initial length of the roller, i.e. when the force in the roller is zero. The length of the roller when it is compressed $y_{r,i}$, is subtracted from this initial length to give the displacement $u_{r,i}$ of the roller.

From Figure 3.7, the length of the roller when it is compressed is defined as:

$$y_{r,i} = y_{s,i} - y_{c,i}$$

and the position of corner i of the skip is defined as:

$$y_{s,i} = y_{o,i} - u_{s,i}$$

where $y_{o,i}$ is the original position of corner i from the datum
and $u_{s,i}$ is the displacement of the skip corner i.

The displacements of the corners of the skip can be determined geometrically from the degrees of freedom as follows:

$$\begin{aligned} u_{s,1} &= d - l_1\theta \\ u_{s,2} &= -d + l_1\theta \\ u_{s,3} &= d + l_2\theta \\ u_{s,4} &= -d - l_2\theta \end{aligned} \tag{3.4}$$

where θ is assumed to be small.

Therefore the displacement in roller i is:

$$u_{r,i} = y_{r,i}^{\star} - y_{o,i} + u_{s,i} + y_{c,i} \tag{3.5}$$

Substituting the value of $y_{c,i}$ from equation (3.3) into equation (3.5), yields an expression for the displacement of the roller as follows:

$$u_{r,i} = y_{r,i}^{\star} - y_{o,i} + \hat{y}_i + u_{s,i} - u_{e,i} \tag{3.6}$$

The displacement method was used to obtain the solution of the five span beam. Two two-noded beam elements were used with three degrees of freedom at each node (an axial translation, a lateral translation and a rotation) to model each span of the guide. Each span is divided into two elements so that the roller displacements may always

correspond to a degree of freedom at a node. Therefore, in each span of the guide, there is a 'floating' node which corresponds to the position of the skip corner. The length of these two beam elements are subject to a certain tolerance, since a beam element which is very short, could lead to numerical problems. Therefore, if the position of a floating node is within a specified minimum distance from a bunton, the floating node is relocated at midspan, and the skip corner is deemed to act at the position of the bunton. It should be noted that the floating node is assumed stationary, i.e. the skip is not moving, during a time-step while numerically solving the equations of motions. This is justified since small time-steps are used.

Since the guide misalignment $\hat{y}_i$ has been accounted for in the calculation of the of the roller displacement, see equation (3.6), straight beam sections can be used, hence simplifying the mathematics. Due to the possibility of axial compressive forces occurring in the guides, buckling may occur. These large displacements are accounted for by adding a geometric stiffness matrix to the elastic stiffness matrix [1,3,4].

For each element, there is a 6-by-6 stiffness matrix, and when the global stiffness matrix is assembled, a 33-by-33 system of equations has to be solved, since each guide span is divided into two beam elements, i.e. a total of ten beam elements is used to model the guide. This system of equations can be reduced to a two degree of freedom system using static condensation [2,5]. These two degrees of freedom are chosen to be the lateral displacements of the guide corresponding to the coupled skip forces which need to be calculated. A more detailed description including a formulation of the element stiffness matrices is given in Appendix D. The process of static condensation yields the following coupled set of equations (only the guide with rollers 1 and 3 acting on it is considered for the formulation, the equivalent process is performed on the other guide, i.e. the guide with rollers 2 and 4 acting on it):

$$\begin{bmatrix} k_{11} & k_{13} \\ k_{31} & k_{33} \end{bmatrix} \begin{Bmatrix} u_{e,1} \\ u_{e,3} \end{Bmatrix} = \begin{Bmatrix} f_{r,1} \\ f_{r,3} \end{Bmatrix} \tag{3.7}$$

In equation (3.7), a coupled relationship between the forces in the rollers has been derived in terms of the displacements of the guides. The force in roller i is defined as:

$$f_{r,i} = k_{r,i}\, u_{r,i} \; + \; c_{r,i}\, \dot{u}_{r,i} \tag{3.8}$$

The relative velocity across the roller $\dot{u}_{r,i}$ is expressed in terms of the displacements using a backward difference approximation. The velocity is evaluated in terms of the displacements at the previous and present time-steps, n and $n+1$ respectively, as follows:

$$\dot{u}_{r,i}^{[n+1]} = (u_{r,i}^{[n+1]} - u_{r,i}^{[n]})/\Delta t \tag{3.9}$$

Substituting equations (3.6) and (3.9) into equation (3.8), gives an expression for the roller force at time-step $n+1$:

$$\begin{aligned} f_{r,i}^{[n+1]} &= k_{r,i}\left\{y_{r,i}{}^{*} - y_{o,i} + \hat{y}_i^{[n+1]} + u_{s,i}^{[n+1]} - u_{e,i}^{[n+1]}\right\} \\ &\quad + \frac{c_{r,i}}{\Delta t}\left\{\left(\hat{y}_i^{[n+1]} - \hat{y}_i^{[n]}\right) + \left(u_{s,i}^{[n+1]} - u_{s,i}^{[n]}\right) - \left(u_{e,i}^{[n+1]} - u_{e,i}^{[n]}\right)\right\} \end{aligned}$$

If this relationship is used in equation (3.7), and the guide displacement terms $u_{e,i}^{[n+1]}$ are taken across to the left hand side of the equation, the following set of equations, which can be used to solve for $u_{e,i}^{[n+1]}$, are obtained:

$$\begin{bmatrix} k_{11}{}^{*} & k_{13} \\ k_{31} & k_{33}{}^{*} \end{bmatrix} \begin{Bmatrix} u_{e,1}^{[n+1]} \\ u_{e,3}^{[n+1]} \end{Bmatrix} = \begin{Bmatrix} k_{r,1}u_{k,1} + \frac{c_{r,1}}{\Delta t}u_{c,1} \\ k_{r,3}u_{k,3} + \frac{c_{r,3}}{\Delta t}u_{c,3} \end{Bmatrix} \tag{3.10}$$

where $k_{ii}{}^{*} = k_{ii} + k_{r,i} + \frac{c_{r,i}}{\Delta t}$,

$$u_{k,i} = y_{r,i}{}^{*} - y_{o,i} + \hat{y}_i^{[n+1]} + u_{s,i}^{[n+1]}$$

and $$u_{c,i} = \left(\hat{y}_i^{[n+1]} - \hat{y}_i^{[n]}\right) + \left(u_{s,i}^{[n+1]} - u_{s,i}^{[n]}\right) + u_{e,i}^{[n]}$$

These values of $u_{e,1}^{[n+1]}$ and $u_{e,3}^{[n+1]}$ are substituted back into equation (3.7) to obtain the coupled forces in the rollers.

The above procedure is only valid for the case when there is contact between the roller and the guide, and the rollers have not bottomed out.

For the case when there is no contact between the roller and the guide, the forces in the roller spring and dashpot are zero, i.e. when:

$$\left\{y_{r,i}{}^{*} - y_{o,i} + \hat{y}_i^{[n+1]} + u_{s,i}^{[n+1]} - u_{e,i}^{[n+1]}\right\} < 0$$

and for the case when the relative velocity in the dashpot is non-positive, the force in the roller dashpot is zero, i.e. when:

$$\frac{1}{\Delta t}\left\{\left(\hat{y}_i^{[n+1]} - \hat{y}_i^{[n]}\right) + \left(u_{s,i}^{[n+1]} - u_{s,i}^{[n]}\right) - \left(u_{e,i}^{[n+1]} - u_{e,i}^{[n]}\right)\right\} < 0$$

Finally, for the case when the roller bottoms out, there is a rigid impact, i.e. the spring has an 'infinite' stiffness. This occurs when:

$$\left\{y_{o,i} - \hat{y}_i^{[n+1]} - u_{s,i}^{[n+1]} + u_{e,i}^{[n+1]}\right\} < 0$$

The forces $f_{r,1}^{[n+1]}$ and $f_{r,3}^{[n+1]}$ are substituted back into the equations of motion (equations (3.1) and (3.2)), to obtain the displacements, velocities and accelerations of the degrees of freedom d and θ at time-step $n+1$.

3.3 Numerical Implementation

A discussion of the time-stepping scheme employed is presented, and summarised in a tabular form. The calculation of the critical time-step for the explicit time integration is presented, as well as the implementation of the model into a computer program.

3.3.1 Predictor-Corrector Method

The forces $f_{r,i}^{[n+1]}$ are used to calculate the degrees of freedom d and θ from the equations of motion (equations (3.1) and (3.2)). These degrees of freedom are required in the calculation of the displacements $u_{s,i}^{[n+1]}$ in equation (3.4), which are in turn used to calculate the forces $f_{r,i}^{[n+1]}$. Therefore, the degrees of freedom are in fact functions of themselves. A time integration algorithm as suggested by Hughes [13] is employed, where a predictor-corrector method is used, allowing an 'explicit' solution to be performed. This predictor-corrector method allows the stiffness and damping terms to be written in terms of explicit predictors. The solution is trivial if the mass matrix is diagonal, and hence the solution is simplified extensively. It is computationally desirable to use an explicit method, since no iteration within a time-step is required to achieve equilibrium. Another reason for the choice of this specific method, is that it is simple to convert it to a fully implicit time integration scheme if so required.

The equations of motion (equations (3.1) and (3.2)) are written in matrix form for clarity:

$$\boldsymbol{M}\ddot{\boldsymbol{d}} + \boldsymbol{p}(\boldsymbol{d}, \dot{\boldsymbol{d}}) = \boldsymbol{f} \tag{3.11}$$

where $\boldsymbol{M}$ is the mass matrix of the system which is symmetric, diagonal and positive-definite:

$$\boldsymbol{M} = \begin{bmatrix} m & 0 \\ 0 & I_G \end{bmatrix}$$

$\boldsymbol{p}$ is the internal force vector of the system due to displacements and velocities:

$$\boldsymbol{p} = \begin{Bmatrix} p_1 \\ p_2 \end{Bmatrix}$$

$\boldsymbol{f}$ is the external force vector of the system due to externally applied loading (which do not exist in the model presented in this thesis):

$$\boldsymbol{f} = \begin{Bmatrix} f_d \\ f_\theta \end{Bmatrix}$$

$\ddot{\boldsymbol{d}}$ is the acceleration vector of the system:

$$\ddot{\boldsymbol{d}} = \left\{ \begin{array}{c} \ddot{d} \\ \ddot{\theta} \end{array} \right\}$$

$\dot{\boldsymbol{d}}$ is the velocity vector of the system:

$$\dot{\boldsymbol{d}} = \left\{ \begin{array}{c} \dot{d} \\ \dot{\theta} \end{array} \right\}$$

and $\boldsymbol{d}$ is the displacement vector of the system:

$$\boldsymbol{d} = \left\{ \begin{array}{c} d \\ \theta \end{array} \right\}$$

The initial value problem for equation (3.11) involves finding the displacements $\boldsymbol{d} = \boldsymbol{d}(t^{[n]})$, satisfying both the equations of motion (equation (3.11)) and the given initial data:

$$\boldsymbol{d}(0) = \boldsymbol{d}^{[0]}, \quad \dot{\boldsymbol{d}}(0) = \boldsymbol{v}^{[0]}$$

The Newmark family [19] of time integration schemes are widely used and will be used here for the solution of the equations of motion, equation (3.11). The Newmark method consists of the following difference equations:

$$\boldsymbol{M}\boldsymbol{a}^{[n+1]} + \boldsymbol{p}(\boldsymbol{d}^{[n+1]}, \boldsymbol{v}^{[n+1]}) = \boldsymbol{f}^{[n+1]} \tag{3.12}$$

$$\boldsymbol{d}^{[n+1]} = \boldsymbol{d}^{[n]} + \Delta t \boldsymbol{v}^{[n]} + \frac{\Delta t^2}{2}\{(1-2\beta)\boldsymbol{a}^{[n]} + 2\beta \boldsymbol{a}^{[n+1]}\} \tag{3.13}$$

and

$$\boldsymbol{v}^{[n+1]} = \boldsymbol{v}^{[n]} + \Delta t\{(1-\gamma)\boldsymbol{a}^{[n]} + \gamma \boldsymbol{a}^{[n+1]}\} \tag{3.14}$$

where $\boldsymbol{d}^{[n]}$, $\boldsymbol{v}^{[n]}$ and $\boldsymbol{a}^{[n]}$ are the approximations of $\boldsymbol{d}(t^{[n]})$, $\dot{\boldsymbol{d}}(t^{[n]})$ and $\ddot{\boldsymbol{d}}(t^{[n]})$ respectively, and equation (3.12) is the equation of motion in terms of the approximate solution at time $t^{[n+1]}$. The Newmark parameters β and γ determine the stability and accuracy of the algorithm.

The mass matrix $\boldsymbol{M}$ is diagonal and an explicit Newmark algorithm suggested by Hughes [13] is used. A reason for the choice of this method is that it is simple to implement, and can easily be adapted to a full implicit scheme if need be. The method is expressed in the form of a predictor-corrector algorithm, and the calculation is now explicit since predicted values are used from information given in the previous time step. Therefore equation (3.12) can be rewritten as:

$$\boldsymbol{M}\boldsymbol{a}^{[n+1]} + \boldsymbol{p}(\tilde{\boldsymbol{d}}^{[n+1]}, \tilde{\boldsymbol{v}}^{[n+1]}) = \boldsymbol{f}^{[n+1]} \tag{3.15}$$

where $\tilde{\boldsymbol{d}}^{[n+1]}$ and $\tilde{\boldsymbol{v}}^{[n+1]}$ are predicted values of the approximations $\boldsymbol{d}^{[n+1]}$ and $\boldsymbol{v}^{[n+1]}$ respectively. The predicted values are defined as:

$$\boldsymbol{d}^{[n+1],0} = \tilde{\boldsymbol{d}}^{[n+1]} = \boldsymbol{d}^{[n]} + \Delta t \boldsymbol{v}^{[n]} + \frac{\Delta t^2}{2}(1-2\beta)\boldsymbol{a}^{[n]} \tag{3.16}$$

$$\boldsymbol{v}^{[n+1],0} = \tilde{\boldsymbol{v}}^{[n+1]} = \boldsymbol{v}^{[n]} + \Delta t(1-\gamma)\boldsymbol{a}^{[n]} \tag{3.17}$$

and

$$\boldsymbol{a}^{[n+1],0} = \boldsymbol{0} \tag{3.18}$$

Equations (3.13) and (3.14) can then be rewritten as:

$$\boldsymbol{d}^{[n+1],1} = \tilde{\boldsymbol{d}}^{[n+1]} + \Delta t^2 \beta \boldsymbol{a}^{[n+1]} \tag{3.19}$$

and

$$\boldsymbol{v}^{[n+1],1} = \tilde{\boldsymbol{v}}^{[n+1]} + \Delta t \gamma \boldsymbol{a}^{[n+1]} \tag{3.20}$$

To start the time integration algorithm, $\boldsymbol{a}^{[0]}$ is calculated from:

$$\boldsymbol{M}\boldsymbol{a}^{[0]} = \boldsymbol{f} - \boldsymbol{p}(\boldsymbol{d}^{[0]}, \boldsymbol{v}^{[0]}) \tag{3.21}$$

or it may be specified directly *a priori*.

The predictor values are calculated (equations (3.16) to (3.18)) and and are used to form the vector of internal forces $\boldsymbol{p}$ from equation (3.7) in Chapter 3.2. The 'residual' force vector $\boldsymbol{\psi}^{[n+1],0}$ as follows is then calculated as follows:

$$\boldsymbol{\psi}^{[n+1],0} = \boldsymbol{f}^{[n+1]} - \boldsymbol{p}(\boldsymbol{d}^{[n+1],0}, \boldsymbol{v}^{[n+1],0}) \tag{3.22}$$

and the system to be solved is:

$$\boldsymbol{M}\boldsymbol{a}^{[n+1]} = \boldsymbol{\psi}^{[n+1],0} \tag{3.23}$$

Equation (3.19) can be rewritten as:

$$\boldsymbol{a}^{[n+1]} = \frac{\Delta \boldsymbol{d}^{[n+1],0}}{\Delta t^2 \beta} \tag{3.24}$$

where:

$$\Delta \boldsymbol{d}^{[n+1],0} = \boldsymbol{d}^{[n+1],1} - \tilde{\boldsymbol{d}}^{[n+1]}$$

Therefore, from equations (3.24) and (3.23), the following set of linear equations are obtained:

$$\frac{\boldsymbol{M}}{\Delta t^2 \beta} \Delta \boldsymbol{d}^{[n+1],0} = \boldsymbol{\psi}^{[n+1],0} \tag{3.25}$$

The original problem has now been reduced to an 'effective' static problem, and an 'effective stiffness' term $\boldsymbol{K}^*$ is identified as follows:

$$\boldsymbol{K}^* \Delta \boldsymbol{d}^{[n+1],0} = \boldsymbol{\psi}^{[n+1],0} \tag{3.26}$$

where:

$$\boldsymbol{K}^* = \frac{\boldsymbol{M}}{\Delta t^2 \beta}$$

Since the mass matrix $\boldsymbol{M}$ does not change, $\boldsymbol{K}^*$ only needs to be formed once, and can therefore be done prior to the commencement of the time integration.

The system of equations in the 'effective static problem' (equation (3.26)) can now be solved, and since the mass matrix $\boldsymbol{M}$ is diagonal, the system of equations is uncoupled, and hence the solution is trivial. The solution yields a vector of incremental displacements $\Delta \boldsymbol{d}^{[n+1],0}$ which are used to correct the initial predictions of the response of the system. In this corrector phase, the following values are set:

$$\boldsymbol{d}^{[n+1],1} = \boldsymbol{d}^{[n+1],0} + \Delta \boldsymbol{d}^{[n+1],0} \tag{3.27}$$

$$\boldsymbol{a}^{[n+1],1} = \left[\boldsymbol{d}^{[n+1],1} - \boldsymbol{d}^{[n+1],0}\right] / (\Delta t^2 \beta) \tag{3.28}$$

and

$$\boldsymbol{v}^{[n+1],1} = \boldsymbol{v}^{[n+1],0} + \Delta t \gamma \boldsymbol{a}^{[n+1],1} \tag{3.29}$$

Finally, the values at time-step $n+1$ are set equal to the corrector values that were calculated in equations (3.27) to (3.29):

$$\boldsymbol{d}^{[n+1]} = \boldsymbol{d}^{[n+1],1} \tag{3.30}$$

$$\boldsymbol{v}^{[n+1]} = \boldsymbol{v}^{[n+1],1} \tag{3.31}$$

and

$$\boldsymbol{a}^{[n+1]} = \boldsymbol{a}^{[n+1],1} \tag{3.32}$$

These values of the response, $\boldsymbol{d}^{[n+1]}$, $\boldsymbol{v}^{[n+1]}$ and $\boldsymbol{a}^{[n+1]}$, are then used to predict the response at the next time-step. Set $n = n+1$, form the new internal force vector $\boldsymbol{p}$ and begin the next time-step. A summary of the predictor-corrector time integration algorithm is given in Table 3.1 [20].

Table 3.1: Explicit Predictor-Corrector Algorithm

1 Begin predictor phase by setting

$$\boldsymbol{d}^{[n+1],0} = \tilde{\boldsymbol{d}}^{[n+1]} = \boldsymbol{d}^{[n]} + \Delta t \boldsymbol{v}^{[n]} + \tfrac{\Delta t^2}{2}(1-2\beta)\boldsymbol{a}^{[n]} \quad \text{(i)}$$

$$\boldsymbol{v}^{[n+1],0} = \tilde{\boldsymbol{v}}^{[n+1]} = \boldsymbol{v}^{[n]} + \Delta t(1-\gamma)\boldsymbol{a}^{[n]} \quad \text{(ii)}$$

$$\boldsymbol{a}^{[n+1],0} = \boldsymbol{0}. \quad \text{(iii)}$$

2 Evaluate the residual forces using the equation

$$\boldsymbol{\psi}^{[n+1],0} = \boldsymbol{f}^{[n+1]} - \boldsymbol{p}(\boldsymbol{d}^{[n+1],0}, \boldsymbol{v}^{[n+1],0}). \quad \text{(iv)}$$

3 If required, form the 'effective' stiffness matrix using the expression

$$\boldsymbol{K}^{\star} = \boldsymbol{M}/(\Delta t^2 \beta). \quad \text{(v)}$$

Note that as the mass matrix $\boldsymbol{M}$ does not change $\boldsymbol{K}^{\star}$ will be formed once only.

4 Solve the following set of equations (trivial if $\boldsymbol{M}$ is diagonal)

$$\boldsymbol{K}^{\star}\Delta\boldsymbol{d}^{[n+1],0} = \boldsymbol{\psi}^{[n+1],0}. \quad \text{(vi)}$$

5 Enter the corrector phase and set

$$\boldsymbol{d}^{[n+1],1} = \boldsymbol{d}^{[n+1],0} + \Delta\boldsymbol{d}^{[n+1],0} \quad \text{(vii)}$$

$$\boldsymbol{a}^{[n+1],1} = \left[\boldsymbol{d}^{[n+1],1} - \boldsymbol{d}^{[n+1],0}\right]/(\Delta t^2 \beta) \quad \text{(viii)}$$

$$\boldsymbol{v}^{[n+1],1} = \boldsymbol{v}^{[n+1],0} + \Delta t \gamma \boldsymbol{a}^{[n+1],1}. \quad \text{(ix)}$$

6 Set

$$\boldsymbol{d}^{[n+1]} = \boldsymbol{d}^{[n+1],1} \quad \text{(x)}$$

$$\boldsymbol{v}^{[n+1]} = \boldsymbol{v}^{[n+1],1} \quad \text{(xi)}$$

$$\boldsymbol{a}^{[n+1]} = \boldsymbol{a}^{[n+1],1}. \quad \text{(xii)}$$

7 Calculate $\boldsymbol{p}$ for use in the next time step. Set $n = n + 1$ and goto step 1.

3.3.2 Critical Time-Step

Since the predictor-corrector time-stepping scheme employed to perform the transient analyses is explicit, a condition is placed on the size of time-step chosen in order to achieve stability, i.e. it is conditionally stable. For the case where $\gamma = \frac{1}{2}$, the critical time-step may be written as:

$$\Delta t_{\text{crit}} = 2/\omega_{\text{max}}$$

where ω_{max} is the maximum frequency of the system.

Since it is difficult to accurately determine all of the frequencies of a system, it has been shown [2] that the highest frequency of any element of the system, considered individually, is an upper bound to the frequencies of the system. Hence, taking a bunton stiffness of $k_b = 26330$ kN/m, a skip length of $h = 12.192$ m, a mass moment of inertia of $I_G = 386 \times 10^3$ kg·m^2, the highest natural frequency of the system is:

$$\begin{aligned} \omega_{\text{max}} &= \sqrt{\frac{k_b(h/2)^2}{I_G/4}} \\ &\approx 100.695 \text{ 1/s} \end{aligned}$$

This yields a critical time-step of:

$$\Delta t_{\text{crit}} \approx 0.02 \text{ s}$$

Therefore, for the chosen time-stepping algorithm, a time-step of less than 0.02 s is required to achieve stability in the algorithm for the above system.

3.3.3 Program SKIPDYN

A computer program called **SKIPDYN** [22] was developed in order to perform the analysis described in Chapter 3.2. The program was written in FORTRAN 77, and implemented on a DEC MicroVAX II.

3.4 Results of Numerical Modelling

3.4.1 Introduction

Two types of results are presented, namely bump tests where straight guides with uniform bumps are used to excite the model are used to verify the model, and results for an actual mine shaft. The bump tests are included in order to compare results with those obtained by SDRC [26], for the case of zero axial compressive loads. These simple bump tests permit an otherwise complex problem to be simplified in order to understand the basic mechanics and responses of the system, whereas results using actual mine shaft guide misalignment data give a feel of the magnitudes of the various responses of the system. Results are presented graphically, where the responses of the skip are plotted against time. The responses that are presented are the translation and rotation of the centre of gravity of the skip, as well as the forces at the four corners of the skip. Only the translation of the centre of gravity of the skip and the forces at a corner of the skip are discussed here, while all of the results are presented in Appendix E. Two cases of the axial compressive forces on the guides being zero and equal to half the critical (Euler) buckling loads of a simply supported beam with the same properties are investigated to illustrate the effects of the axial compressive loads.

3.4.2 Bump Tests

The response of the skip as it travels over a single bump (or two bumps), with guide misalignments as illustrated in Figures 3.8 and 3.9, is presented. The purpose of the bump tests is to achieve confidence with the model in order to analyse more complex situations. The following parameters are chosen in order to compare the response to the results obtained by SDRC [26] (data from President Steyn Gold Mine No. 4 Shaft):

Parameter	Value
Roller Stiffness	483 kN/m
Roller Damping	5% of Critical Damping
Skip Mass (m)	28.9 t
Skip Mass Moment of Inertia (I_G)	386×10^3 kg·m^2
Skip Velocity (v_s)	15.2 m/s
Young's Modulus (E)	200 GPa
Guide Section Moment of Inertia (I)	10.1×10^{-6} m^4
Guide Cross-sectional Area (A)	7.213×10^{-3} m^2
Bunton Spacing (l)	6.10 m
Bunton Stiffness (k_b)	26.33 MN/m

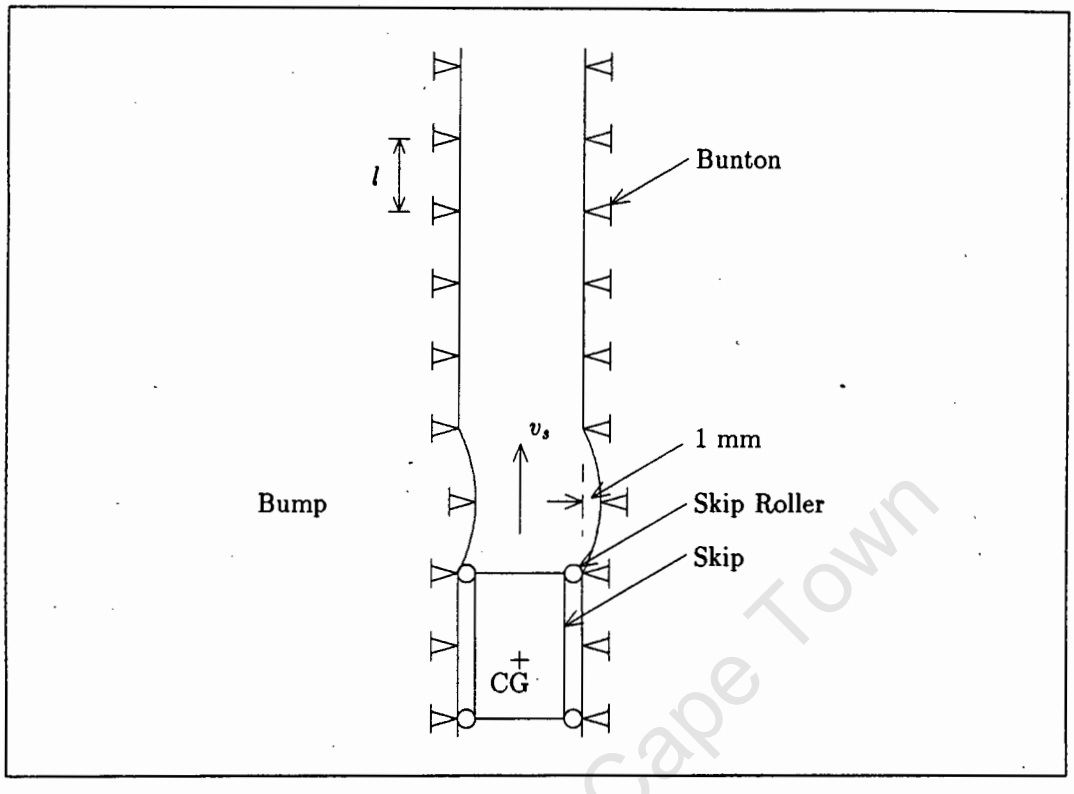

Figure 3.8: Guide Misalignment for Single Bump Test

Skip Length (h)	12.192 m
Distance to Skip Centre of Gravity	0.6 h
Skip to Guide Clearance	12 mm

The results for zero axial compressive forces in the guides compare reasonably well with those in the SDRC report [26], where the general shape of the curves conform to those obtained by the SDRC, and the maxima are of the same order. Differences in the results can be accredited to the fact that neither the exact nature of the SDRC model, nor the exact input data, was known. Due to the damping in the rollers, the responses of the skip tend to attenuate.

The inclusion of axial compressive forces in the guides cause the guides to soften, hence affecting the responses of the skip. For the the bump tests, there are no significant differences for the results between zero axial compressive loads and those for half of the critical buckling loads of the guides. Generally, the responses are of the same magnitude, so that the inclusion of axial compressive loads does not appear to affect the response

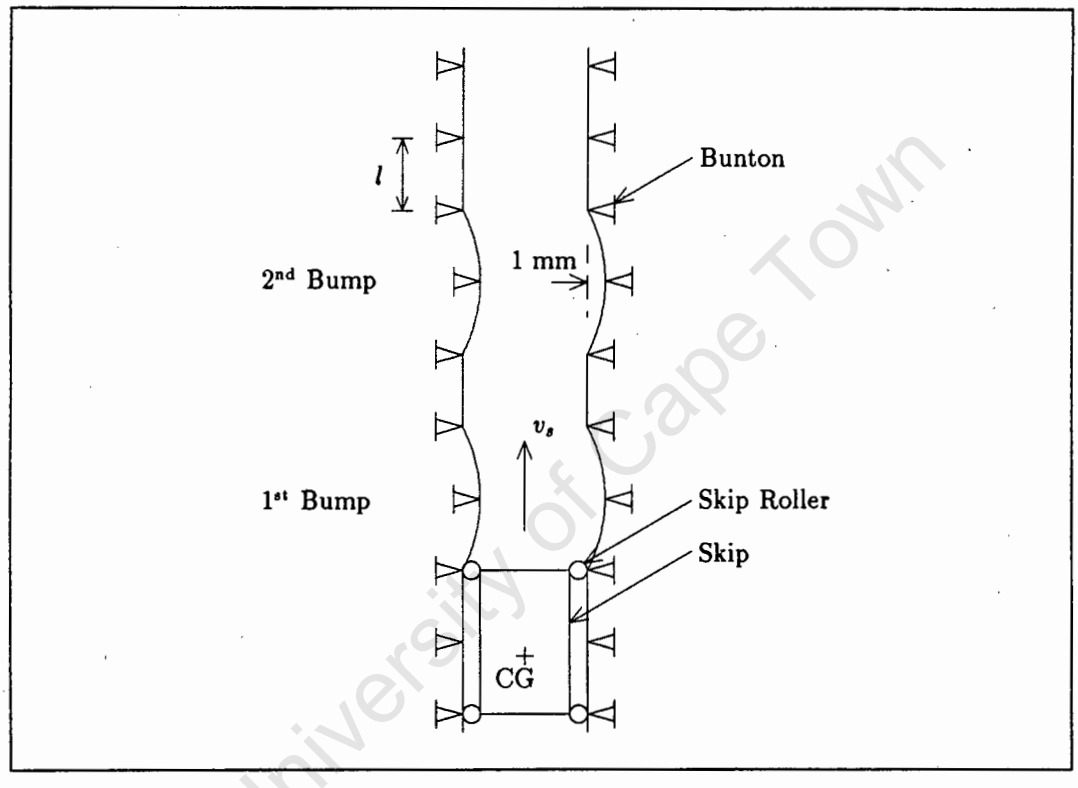

Figure 3.9: Guide Misalignment for Double Bump Test

of the system significantly. It must be pointed out, however, that the results are for a limited set of examples only, and a complete spectrum of different shaft steelwork configurations should be evaluated in order to make proper conclusions. However, this does not fall within the bounds of the objectives of this thesis.

To check the magnitudes of the response, the design curves in the SDRC Design Guidelines [27] were used. Using the data from the President Steyn No. 4 Shaft, with a guide misalignment of 1 mm, a roller force of 0.89 kN and a skip displacement of 1.85 mm were calculated. The maxima obtained in the double bump tests, see Figures 3.12 and 3.13, are 0.98 kN and 1.61 mm respectively. The discrepencies are 10.1% and 13.0% for the roller forces and the skip displacements respectively. Based upon these observations, the stage has been reached where the model may be used with confidence in predicting the response of a skip to guide misalignments for actual mine shaft data.

The results presented in Figures 3.10 to 3.13 show the response of the skip versus time. As stated previously, only the results for the translation of the centre of gravity of the skip and the force at a corner of the skip have been presented here, and the rest of the results are given in Appendix E.

Single Bump Test

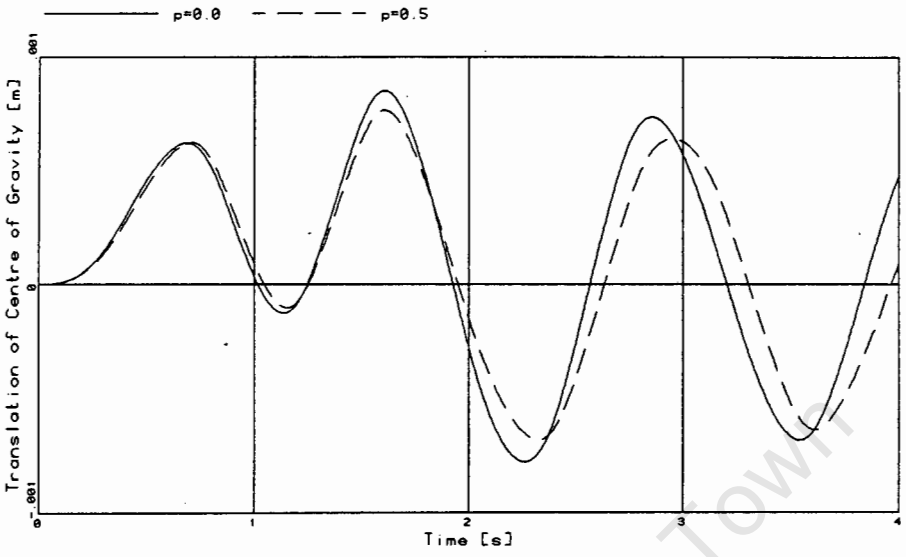

Figure 3.10: Plot of Displacement versus Time

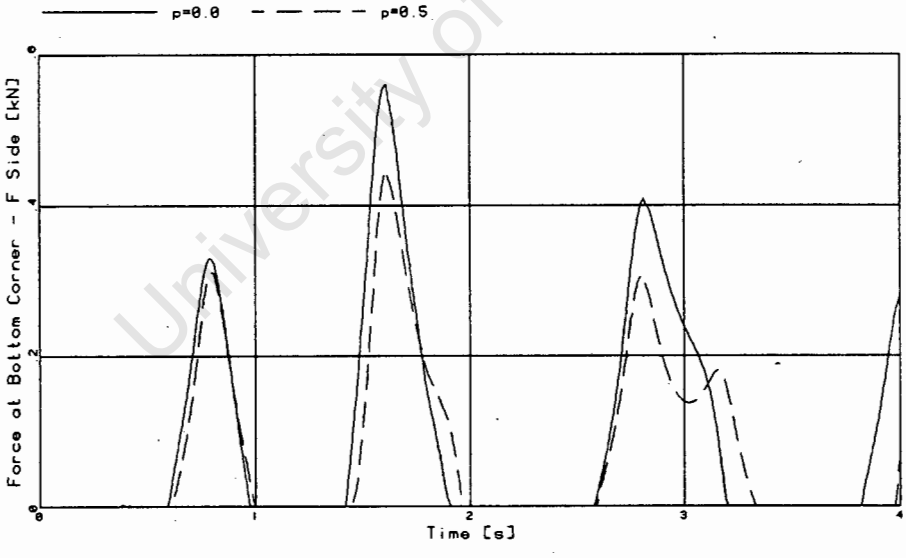

Figure 3.11: Plot of Corner Force versus Time

Double Bump Test

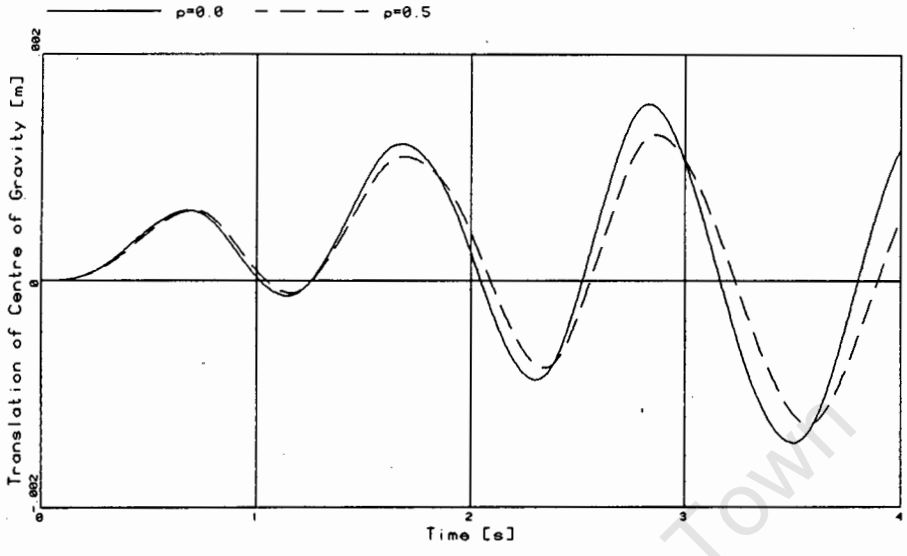

Figure 3.12: Plot of Displacement versus Time

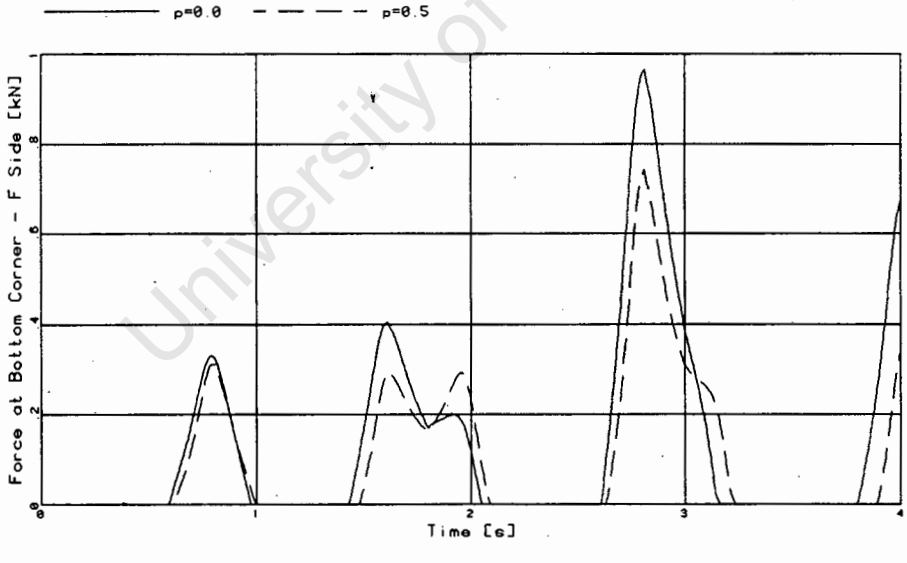

Figure 3.13: Plot of Corner Force versus Time

3.4.3 General Tests

The response of the skip to a general set of misalignment data is now presented, where data from the President Steyn No. 4 Shaft was used [17]. The following parameters are used in the calculation of the response of the skip:

Parameter	Value
Roller Stiffness	483 kN/m
Roller Damping	5% of Critical Damping
Skip Mass (m)	28.9 t
Skip Mass Moment of Inertia (I_G)	386×10^3 kg·m^2
Skip Velocity (v_s)	15.2 m/s
Young's Modulus (E)	200 GPa
Guide Section Moment of Inertia (I)	10.1×10^{-6} m^4
Guide Cross-sectional Area (A)	7.213×10^{-3} m^2
Bunton Spacing (l)	6.10 m
Bunton Stiffness (k_b)	26.33 MN/m
Skip Length (h)	10.668 m
Distance to Skip Centre of Gravity	0.6 h
Skip to Guide Clearance	12 mm
Skip Roller Preload	100 N

Due to the length of the shaft, it is not possible to show a complete set of results. Instead, 7.2 s (18 guide spans) of the skip moving in the shaft has been presented, which represents 18 guide spans or approximately 110 m of the shaft. It is also difficult to make a direct comparison of the results with any previously obtained results [11,26], since the response is sensitive to starting conditions and actual misalignment data, and the way in which the misalignment data is interpretted. The magnitudes of the results give a good idea of the forces and displacements taking place under operating conditions.

The design curves in the SDRC Design Guidelines Report [27] are used as a check of the validity of the results. Using the data from the President Steyn No. 4 Shaft, and initially assuming the shaft to be a category B (average) shaft, a roller force of 13.4 kN and a skip displacement of 11 mm were calculated. Since the shaft under consideration is known to be a problem shaft, the same analysis is performed using the criteria for a category C shaft. The corresponding values are 26.8 kN and 22 mm.

The following results were obtained numerically. A maximum skip displacement of approximately 18 mm was obtained for the case when $p = 0.0$. This value falls within the range of the two values calculated using the design guidelines, namely 11 and 22 mm.

The force at the top corners of the skip fall into two categories. Either they are approximately 14 kN, or they are about 30 kN. These two forces agree with the values calculated using the design guidelines. The skip displacements are illustrated in Figure 3.14, while the forces at the top left corner of the skip (E side) are illustrated in Figure 3.15. The bunton are located at the tick marks on the time scales, and the misalignment for the left guide, i.e. the E side guide according to the SDRC [26] report, is illustrated in Figure E.23. It should be noted that the maximum force in a roller is governed by the skip to guide clearance, i.e. 12 mm, and therefore the maximum force is 5.796 kN. Any forces in excess of this value, are forces that are due to the slipper plates being in contact with the guide. A complete set of results for the President Steyn Gold Mine No. 4 Shaft is presented in Appendix E.

The displacements and the forces at the corners of the skip appear to behave periodically. The period is approximately two guide spans, and since the skip has a vertical speed of 15.2 m/s and the guide span is 6.1 m, the time period is approximately 0.8 s. This converts to a frequency of 1.25 peaks per second. The bunton passing frequency is 2.5 buntons per second, which is twice the frequency of the skip response. This scenario was identified by the SDRC [25,26] as a resonance state, hence the magnitudes of the forces and displacements are expected to be large.

The inclusion of axial compressive forces in the guides cause the guides to soften, hence affecting the responses of the skip. For these specific examples, there are no significant differences for the translations and the rotations of the centre of gravity of the skip for axial compressive loads of zero and half of the critical buckling loads of the guides. There is an amplification of forces at the corners of the skip of approximately 17%. Therefore, the inclusion of axial compressive loads does not appear to affect the displacements of the system significantly, but there is a significant increase in the magnitudes of the skip corner forces. It must be pointed out again, however, that the results are for one case only and for only 150 m of the shaft, and a complete spectrum of different shaft steelwork configurations should be analysed in order to make meaningful conclusions.

President Steyn Gold Mine No. 4 Shaft

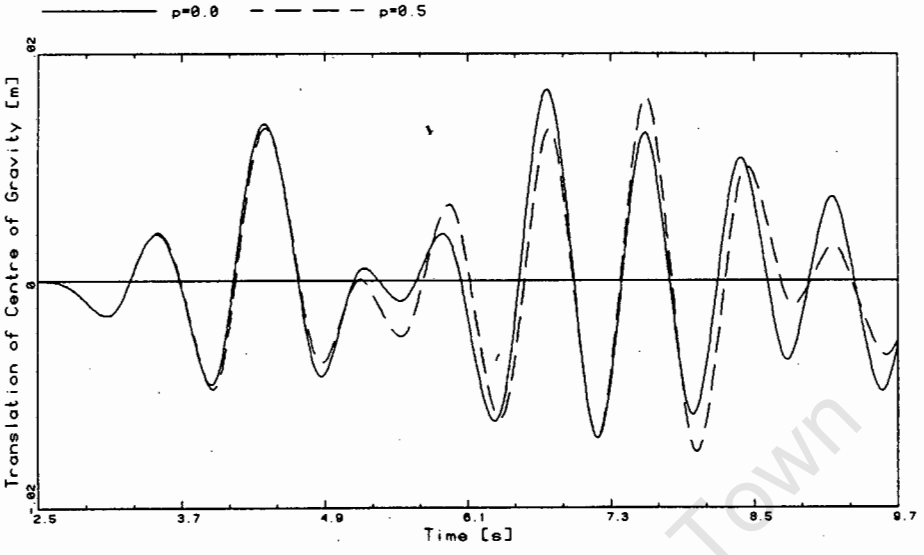

Figure 3.14: Plot of Displacement versus Time

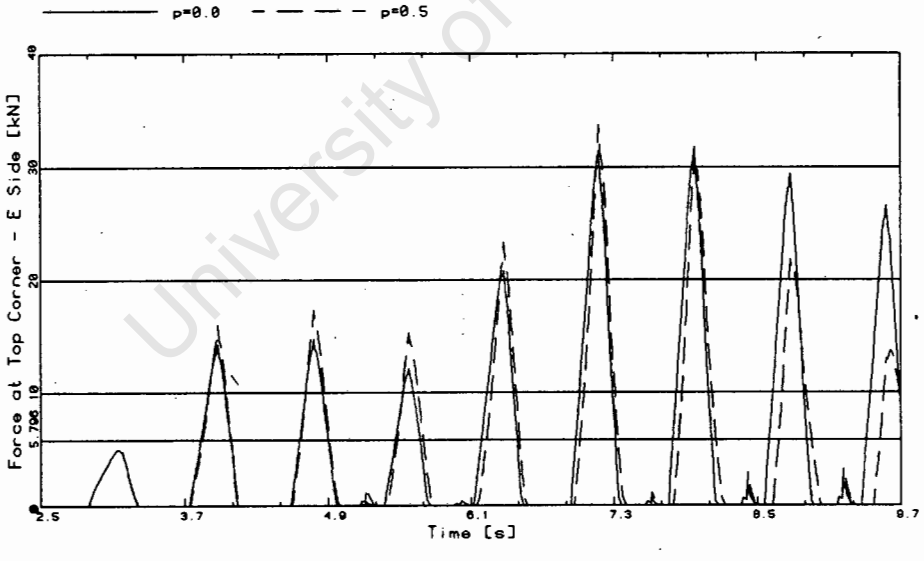

Figure 3.15: Plot of Corner Force versus Time

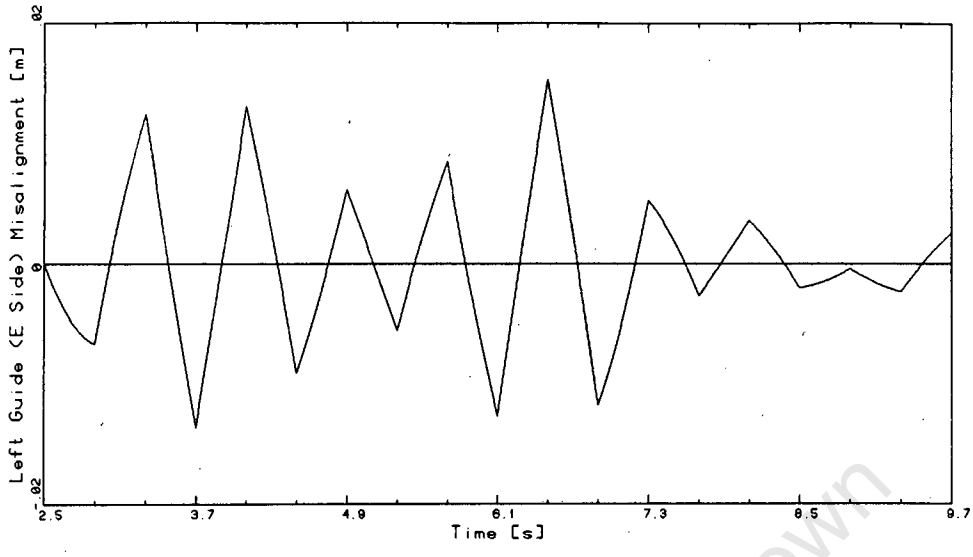

Figure 3.16: Plot of Guide Misalignment versus Time

3.5 Conclusions

A model has been presented to simulate the response of a mine skip to lateral excitation due to misalignments of the guides while skip rollers are active, but the capability of allowing the skip rollers to bottom out has been included. The effects of axial loading have been accounted for in the model by including a geometric stiffness matrix which is a function of the axial load in the formulation. Bump tests were performed in order to verify the model and to achieve confidence in the results. An example using data from an actual mine shaft (President Steyn Gold Mine No. 4 Shaft) is presented to show the effects of the axial load under practical conditions.

From the results of the model, discussed in Chapter 3.4, it is evident that the axial compressive forces in the guides, induced by the shaft wall strains, do not have a large effect on the response of the skip. In the bump test examples, the response is actually reduced, while for the practical example, the results for the maximum forces at the corners of the skip are slightly amplified when this axial compressive force is present. While it appears that axial compressive loads do not significantly influence the response of the skip, it must be born in mind that the range of these test examples is limited, and therefore a wider range of tests needs to be performed in order to state what the effects of axial loads are on the response of the skip.

4 Summary

4.1 Introduction

Two models have been presented in the thesis to model the response of a mine skip as it is laterally excited by misaligned guides while moving vertically in the shaft. The lateral position of the skip in the shaft is generally maintained by flexible rollers acting on the guides. For some reason or other these rollers may not be present and previous researchers identified a phenomenon called slamming, which occurs when a corner of the skip impacts a guide. The two scenarios which have been modelled are the slamming event and the case where the rollers are operational, with the capability of allowing the bottoming out of the skip rollers. This section summarises the two models presented and gives conclusions and recommendations for further work. Possible future reasearch areas are suggested, which include second order stiffening effects.

4.2 Conclusions and Recommendations

It is evident that the axial compressive forces in the guides, induced by the shaft wall strains, do reduce the lateral stiffness of the guides. The results for the maximum forces, bending moments, displacements and velocities, in the slamming case, are amplified when this axial compressive force is present. The results for the rollers operational case are also affected when these axial compressive forces are present, but the effects are not as prominent as in the slamming case. A wider range of tests needs to be performed in order to state what the effects of axial loads are on the response of the skip with the rollers operational. Since slamming is a severe event, and in terms of shaft steelwork design it is the governing case for determining loading on the steelwork, the effects of the axial compressive loads on the steelwork are emphasised. Therefore, in future designs of shaft steelwork, cognisance should be made of the effects of these axial compressive loads.

An exploratory study of the effects of second order stiffening was carried out. Results showed that for low values of p, the ratio of the axial compressive load to the critical buckling load of the guide, the second order effects did not appear to have a marked effect on the response of the skip. However, for high values of p, the response of the skip is clearly reduced and it appears that the inclusion of these second order effects could yield a less conservative response of the skip for the slamming analyses. The inclusion of the second order effects in the formulation of the mathematical model is not trivial. However, since the models presented in this thesis appear to yield results which are too conservative, more rigorous studies of these effects are justified. A better judgement of whether these second order effects should be included in future models can then be made.

4.3 Scope for Future Work

Due to the severity of the slamming event, and the fact that it has been observed and recorded in operating mine shafts, it is of prime importance that a thorough understanding of the event be acquired. The scope of this thesis was to include the axial compressive loads in the formulation of a model for a single slamming event. In practice, however, a series of slamming events has been observed during a single hoist of the skip in the shaft. This sustained slamming can lead to increased rebound velocities and hence increased impact velocities in successive slamming events, causing responses that cannot be predicted using the present models. An extension to the work presented in this thesis should include the capability of analysing this phenomenon called sustained slamming, although in principle, the present model should be able to analyse sustained slamming.

Second order stiffening effects were briefly discussed in Chapter 2.6, but only for the slamming event. Since the study of these effects was only performed using a specific example, as well as simplifying the problem extensively, a more rigorous approach might be adopted in future analyses to verify the need for these secondary effects to be included in the formulation of the slamming model. These second order effects should also be investigated for the case when the skip rollers are active.

Another aspect which was not included in this thesis, are the effects of fish or splice plates in the guides. Plastic deformations of these fish plates have been observed, and in one shaft, most of the fish plates had yielded. Areas which could be investigated are a study of the sensitivity of the locations of these guide joints, as well as the possibility of other, more effective, types of guide joints.

Finally, more examples, which could include analyses of a large spectrum for different shaft configurations and skip types, should be performed using the models presented in this thesis. These analyses should be performed using data from shafts with extensive test data in order to calibrate the model further. As stated in the discussions of the results in Chapters 2.4 and 3.4, the tests were only performed for particular examples. Further tests would enable a better understanding of the mechanics of skip vibrations, as well as permitting more extensive conclusions to be made.

References

[1] ALLEN, H.G. and BULSON, P.S., **BACKGROUND TO BUCKLING**, McGraw-Hill Book Company (U.K.) Limited, Maidenhead, Berkshire, England, pp 273-277, (1980).

[2] BATHE, K.-J. and WILSON, E.L., **NUMERICAL METHODS IN FINITE ELEMENT ANALYSIS**, Prentice-Hall Inc., Englewood Cliffs, New Jersey, U.S.A., pp 259-263, (1976).

[3] COOK, R.D., **CONCEPTS AND APPLICATIONS OF FINITE ELEMENT ANALYSIS**, 2nd Edition, John Wiley & Sons, New York, U.S.A., pp 331-337, (1981).

[4] DAWE, D.J., **MATRIX AND FINITE ELEMENT ANALYSIS OF STRUCTURES**, Clarendon Press, Oxford, U.K., pp 504-513, (1984).

[5] GALLAGHER, R.H. and PADLOG, J., "Discrete Element Approach to Structural Instability Analysis", *AIAA Journal*, **1**, pp 1437-1439, (1963).

[6] GALLOWAY, L.G. and TILEY, P.M., *"The Performance of Fixed Guidance Systems in Mine Shafts"*, CIM Bulletin, pp 54-60, November 1982.

[7] GREENWAY, M.E., *"Analysis of Skip Slamming"*, Mechanical Engineering Department, Anglo American Corporation of South Africa, Johannesburg, 8 August 1985.

[8] GREENWAY, M.E., Communication with SDRC on the COM Steelwork Programme, Mechanical Engineering Department, Anglo American Corporation of South Africa, Johannesburg.

[9] GREENWAY, M.E., Private Communication on Compressive Deformation and Buckling of Shaft Steelwork, Mechanical Engineering Department, Anglo American Corporation of South Africa, Johannesburg, 7 August 1988.

[10] GREENWAY, M.E., *"Further Test Data on Skip and Shaft Steelwork Dynamic Behaviour — Free State Geduld No. 5 Shaft"*, Mechanical Engineering Department, Anglo American Corporation of South Africa, Johannesburg, Submitted to the Chamber of Mines, February 1986.

[11] GREENWAY, M.E., *"Future Trends in the Design of Shaft Steelwork and Conveyances"*, Mechanical Engineering Department, Anglo American Corporation of South Africa, Johannesburg.

[12] HIBBITT, KARLSSON & SORENSON Inc., "ABAQUS User's Manual", Providence, R.I., U.S.A., (1988).

[13] HUGHES, T.J.R. and LIU, W.K., "Implicit-Explicit Finite Elements in Transient Analysis: Implementation and Numerical Examples", *J. Appl. Mech. ASCE*, **45**, pp 375-378, (1978).

[14] HUTTON, F.C.L., JAMES, C.L. and SCHWARTZ, C.R., *"Design of Shaft Systems at Depth"*, Rock Mechanics, South Div., Western Deep Levels, Ltd, Anglo American Corporation of South Africa, Johannesburg.

[15] JOYCE, P. and HALBAUER, S., Private Communication on Shaft Steelwork Analyses, Mechanical Engineering Department, Anglo American Corporation of South Africa, Johannesburg, 20 September 1988.

[16] KREYSZIG, E., **ADVANCED ENGINEERING MATHEMATICS**, 4th Edition, John Wiley & Sons, New York, U.S.A., pp 471-489, (1979).

[17] LINDEGGER, R., Private Communication on Shaft Steelwork Misalignment Data, Mechanical Engineering Department, Anglo American Corporation of South Africa, Johannesburg, October 1988.

[18] MARTIN, J.B., *"Displacement Bounds for Dynamically Loaded Elastic Structures"*. J. Mech. Eng. Sc. 1968 **10**, 3.

[19] NEWMARK, N.M., "A Method of Computation for Structural Dynamics", *J. Eng. Mech. ASCE*, pp 67-94, (1959).

[20] OWEN, D.J.R. and HINTON, E., **FINITE ELEMENTS IN PLASTICITY: Theory and Practice**, Pineridge Press Limited, Swansea, U.K., pp 432-434, (1980).

[21] PRETORIUS, T.S., MERCER, C.D. and MARTIN, J.B., "SLAMMING ANALYSIS OF MINE SKIPS — The Effects of Compressive Force in the Guides", *AMRU Tech. Rep.* 123, UCT/CSIR Applied Mechanics Research Unit, University of Cape Town, South Africa, (1988).

[22] PRETORIUS, T.S., MERCER, C.D. and MARTIN, J.B., Incomplete Report on Vibration Analyses of Mine Skips, FRD/UCT Centre for Research in Computational and Applied Mechanics, University of Cape Town, South Africa, (1989).

[23] REDPATH, J.S. and SHAVER, W.M., *"Towards a Better Understanding of Mine Shaft Guides"*, CIM Bulletin, pp 90-100, September 1977.

[24] SCHMIDT, G. and TONDL, A., **NON-LINEAR VIBRATIONS**, Cambridge University Press, Cambridge, U.K., pp 270-277, (1986).

[25] STRUCTURAL DYNAMICS RESEARCH CORPORATION Final Report No. 11251, *"An Investigation into Shaft Steelwork and Skip Dynamics, Phase I — Experimental Programme"*, Submitted to the Chamber of Mines, June 1983.

[26] STRUCTURAL DYNAMICS RESEARCH CORPORATION Final Report No. 11801, *"An Investigation into Shaft Steelwork and Skip Dynamics, Phase II — Analytical Programme"*, Submitted to the Chamber of Mines, February 1984.

[27] STRUCTURAL DYNAMICS RESEARCH CORPORATION Final Report No. 11964, *"An Investigation into Shaft Steelwork and Skip Dynamics, Phase III — Design Guidelines"*, Submitted to the Chamber of Mines, August 1987.

[28] STRUCTURAL DYNAMICS RESEARCH CORPORATION Final Report No. 11964, *"An Investigation into Shaft Steelwork and Skip Dynamics, Phase IV — Calibration"*, Submitted to the Chamber of Mines, February 1987.

[29] STRUCTURAL DYNAMICS RESEARCH CORPORATION Final Report No. 12207, *"An Investigation into the Slamming Behavior of Flexible Skips"*, Submitted to the Chamber of Mines, May 1985.

A Fourier Series Sensitivity Analysis

Tests were performed to determine the sensitivity of the number of terms chosen in the Fourier series approximation. For the case of one term versus three, the difference in the dimensionless stiffness multipliers is never greater than 1.0%, while for the case of two terms versus three, the difference is always less than 0.25%. Adding further terms did not yield a significant increase in accuracy, and it was decided that two approximation terms are sufficient. Tests were done for the following p ratios, $p = 0.2,\ 0.4,\ 0.6,\ 0.8$, and the results were plotted on graphs of % variance of the dimensionless multiplier $f(\xi)$ (equation (2.21), Chapter 2.2.3) versus position.

The dimensionless stiffness multiplier is therefore taken as:

$$\begin{aligned}
[\, f(\xi)\,]^{-1} \;=\; & \xi^2 + (1-\xi)^2 + 16r\xi^2(1-\xi)^2 \\
& + r\,\frac{96}{\pi^4}\sin^2(\pi\xi)\,\frac{p}{1-p} \\
& - r\left\{\frac{6}{\pi^4}(2\xi-1)\sin^2(2\pi\xi)\right. \\
& \left. + \frac{12}{\pi^3}\xi(1-\xi)\sin(4\pi\xi)\right\}\frac{p}{4-p} \qquad \text{(A.1)}
\end{aligned}$$

The graphs shown in Figures A.1 to A.4, were used to determine the accuracy of the Fourier approximation of the displacement due to the compressive axial loads. The graphs exhibit plots of the approximations using 1 or 2 terms. An approximation using 3 terms was taken as being very accurate, therefore this was used as a datum. The plots are therefore either 1 or 2 terms shown as a percentage of a 3 term approximation.

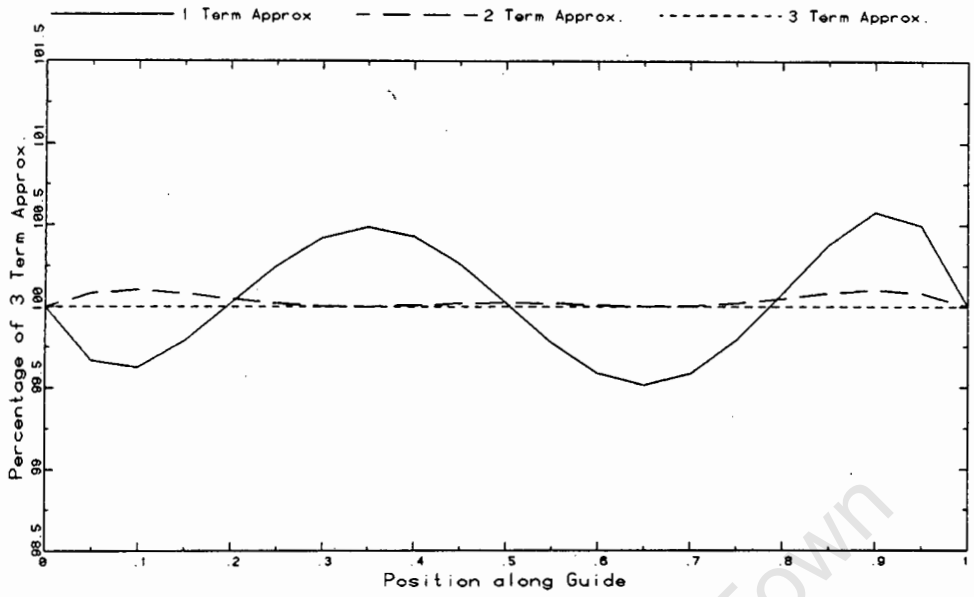

Figure A.1: Sensitivity Analysis with $p = 0.2$

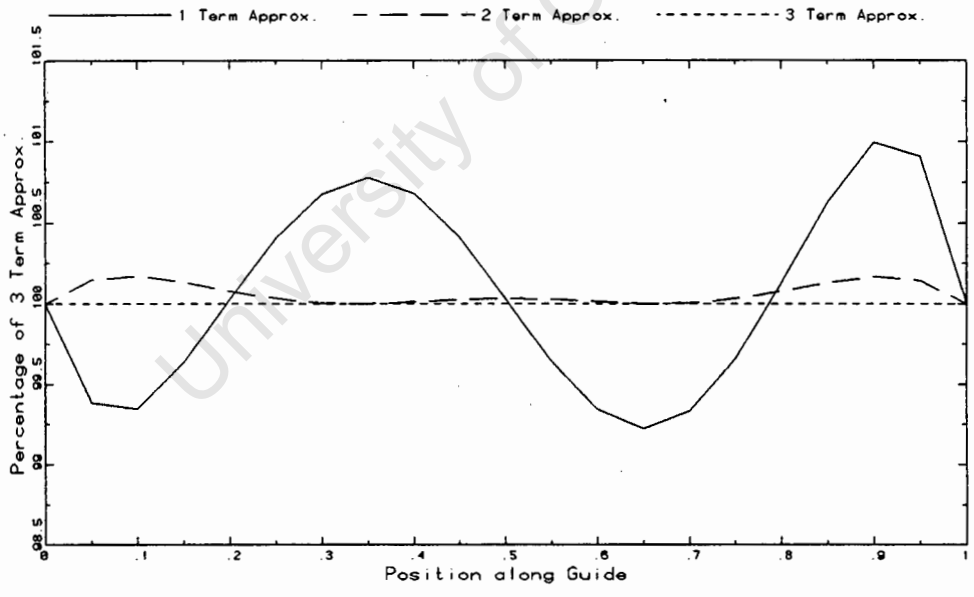

Figure A.2: Sensitivity Analysis with $p = 0.4$

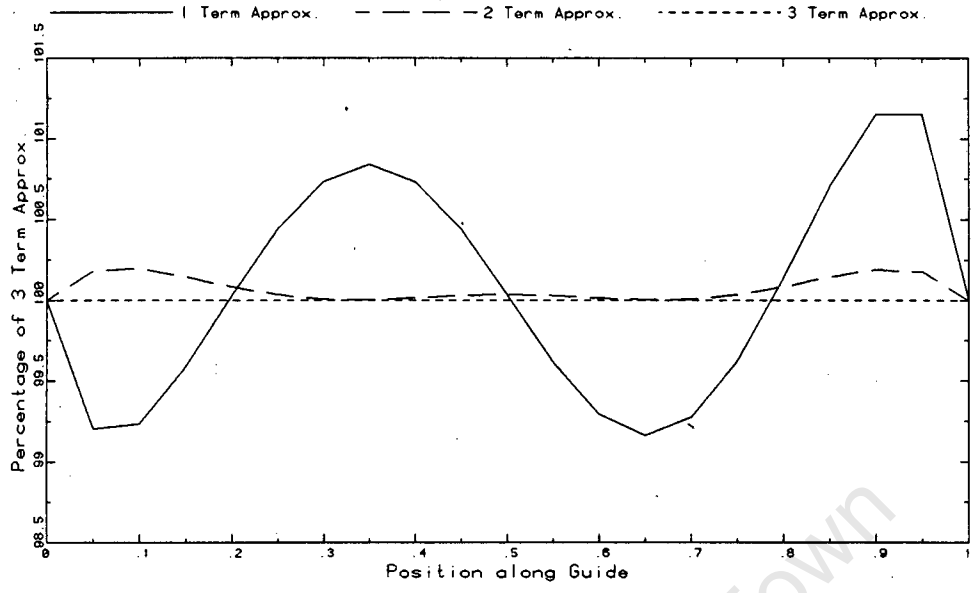

Figure A.3: Sensitivity Analysis with $p = 0.6$

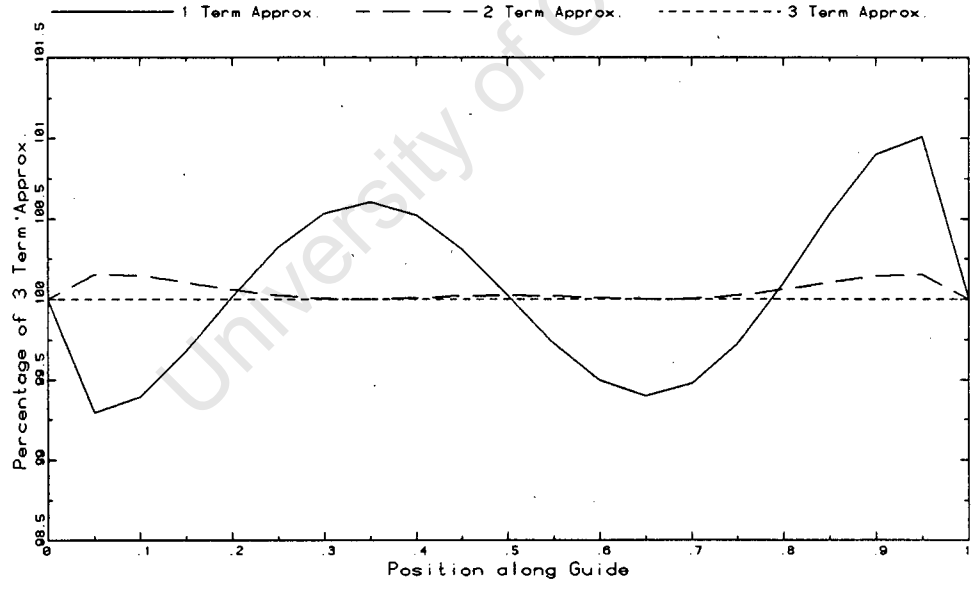

Figure A.4: Sensitivity Analysis with $p = 0.8$

B Bending Moments due to Bunton Displacements

The justification of ignoring the bending moments induced by the displacements of the buntons and the axial compressive loads is discussed. Assume that the skip is not moving vertically in the shaft, since the displacement at a bunton is to be determined, and hence the difference between the bunton displacements will be a maximum. The kinetic energy of the skip just before impact is:

$$\text{K.E.} = \tfrac{1}{2} m_e \dot{u}_0$$

and the strain energy of the maximum displacement of the bunton is:

$$\text{S.E.} = \tfrac{1}{2} k_e(\xi = 0) y$$

Using the dimensionless parameters introduced in Chapter 2.2.4, the maximum non-dimensional displacement is $Y = 1.0$. From equation (2.27) in Chapter 2.2.6, the corresponding bending moment is therefore:

$$\text{B.M.} = \frac{\pi^2 p}{48 r}$$

For the same example as the one used to obtain the results in Chapter 2.4, this bending moment does not amount to more than 4% of the bending moments illustrated in Figure 2.13, for the various values of p. Therefore, the exclusion of these bending moments in the formulation of the dimensionless guide stiffness is justified.

C Results of Alternative Slamming Formulation

The complete set of results for the proposal suggested by Greenway [9] is presented here. The results are presented in the same way as the initial formulation.

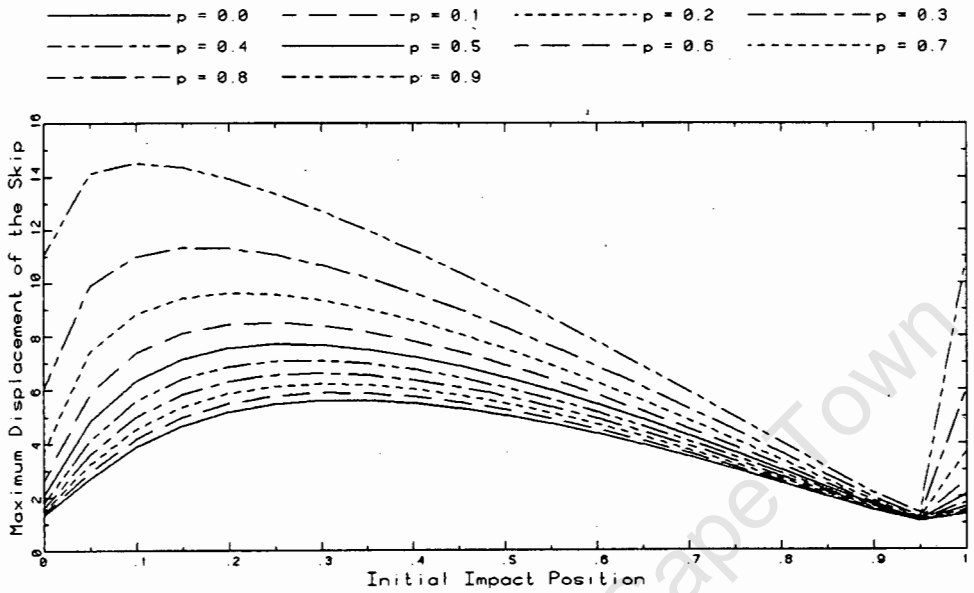

Figure C.1: Maximum Displacement of the Skip Corner

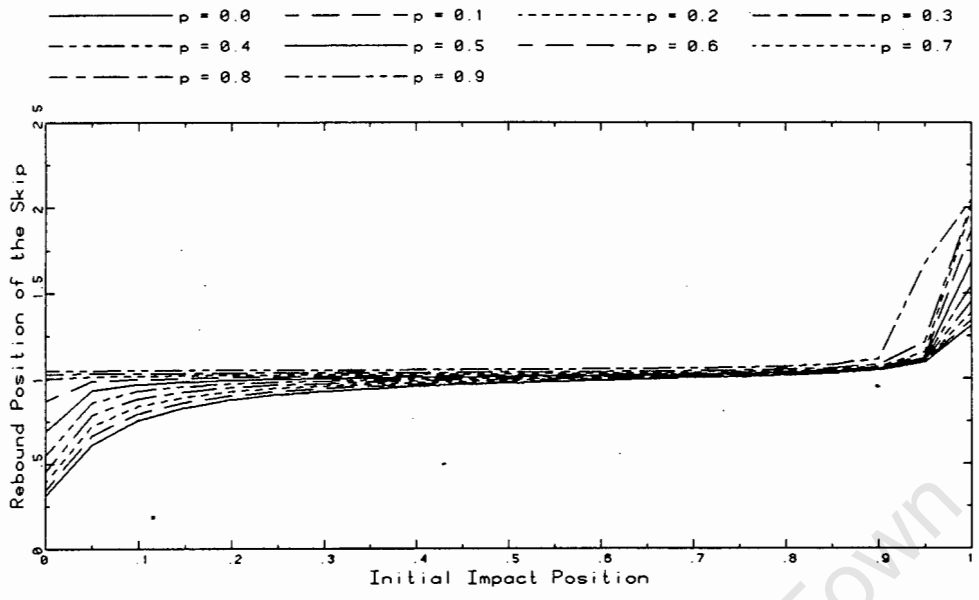

Figure C.2: Position at which the Skip leaves the Guide

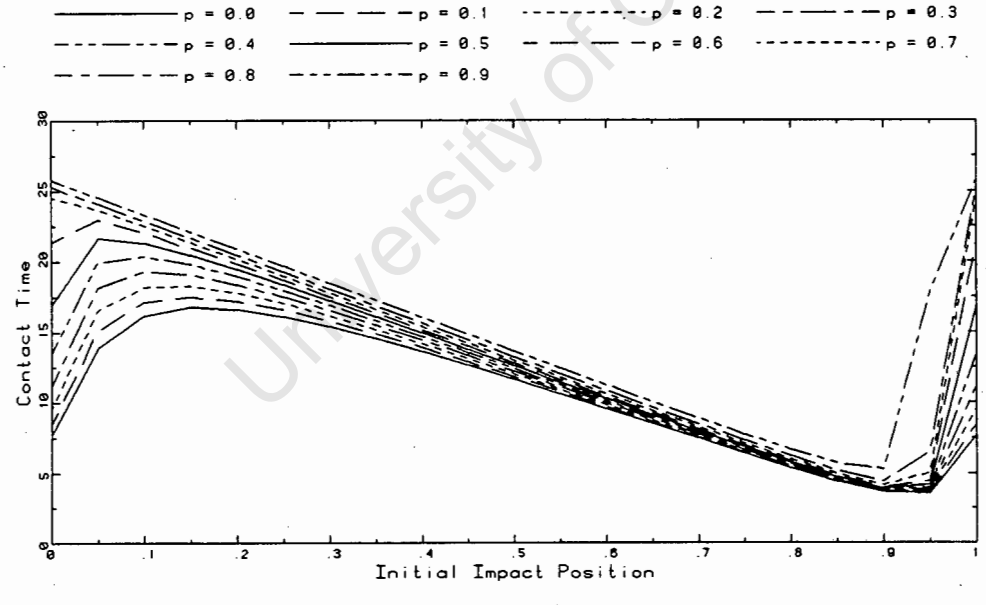

Figure C.3: Time of Contact between the Skip and the Guide

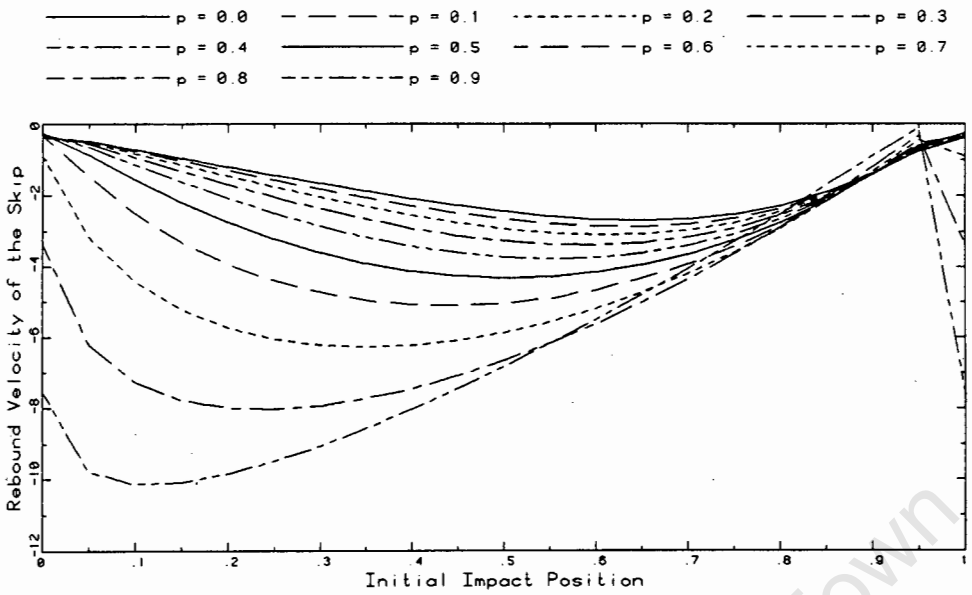

Figure C.4: Velocity at which the Skip leaves the Guide

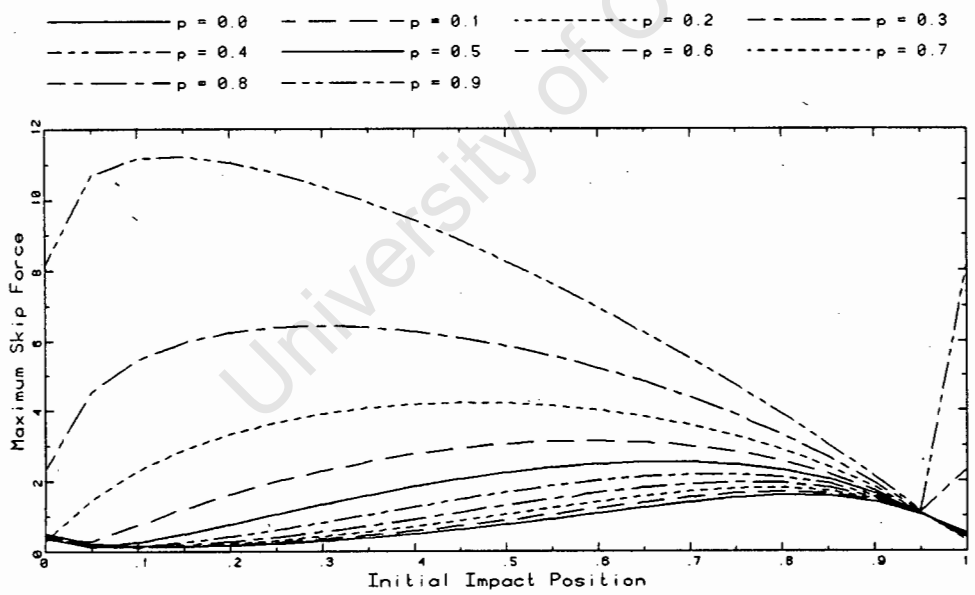

Figure C.5: Maximum Force in the Slipper Plate of the Skip

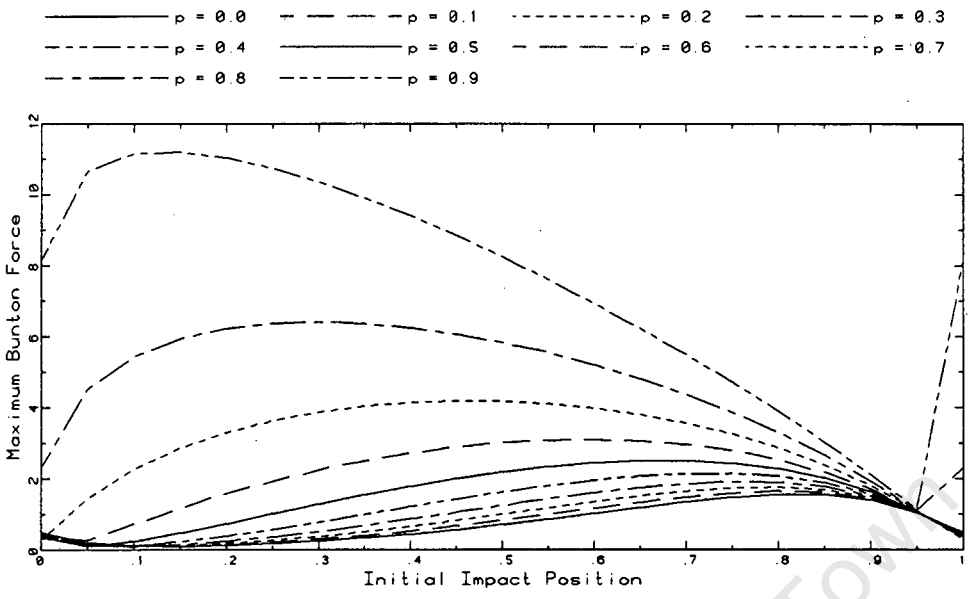

Figure C.6: Maximum Force in the Bunton

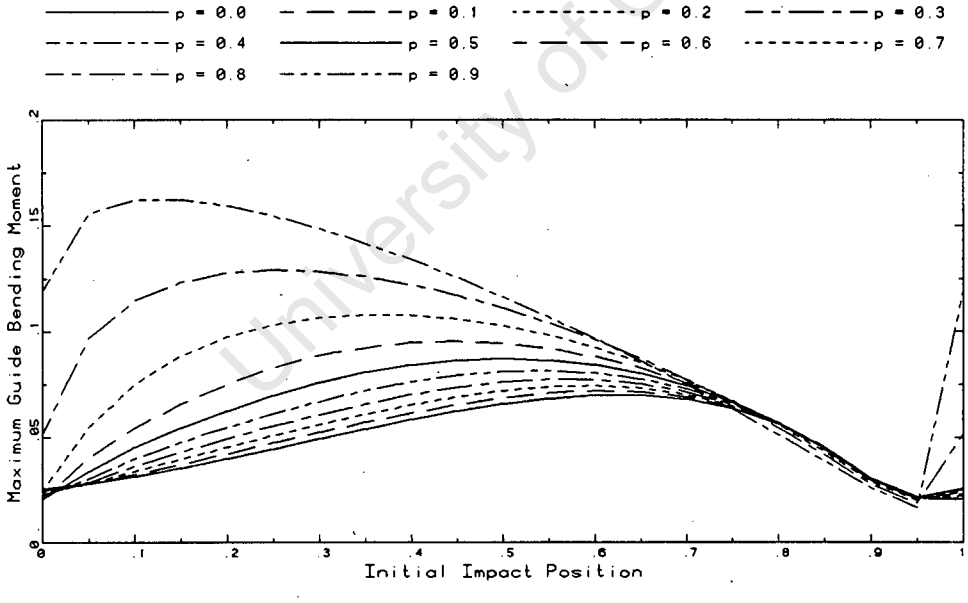

Figure C.7: Maximum Bending Moment in the Guide

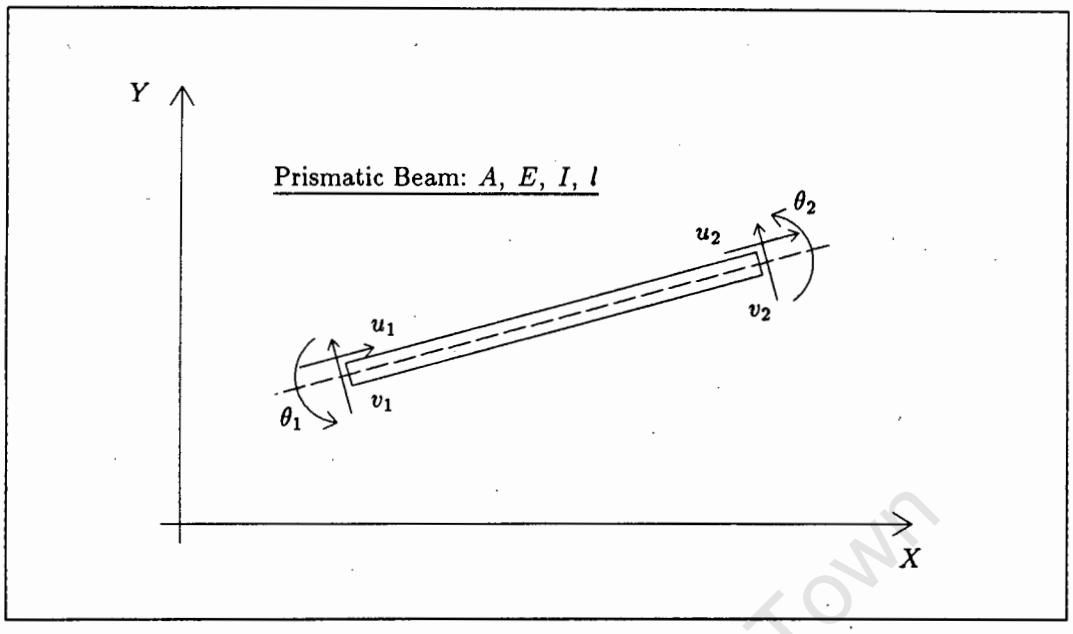

Figure D.1: Standard Two Node Beam Element

D Five Span Beam Model

The elastic and geometric element stiffness matrices for a standard two node beam element are given. The order of the matrices is 6×6 and the degrees of freedom are:

$$\{\boldsymbol{d}\} = \left\{ \begin{array}{cccccc} u_1 & v_1 & \theta_1 & u_2 & v_2 & \theta_2 \end{array} \right\}^T$$

The degrees of freedom are defined in Figure D.1.

D.1 Element Elastic Stiffness Matrix

The standard Euler-Bernoulli beam element is used and has the following elastic stiffness matrix:

$$[k] = \begin{bmatrix} \frac{EA}{l} & 0 & 0 & -\frac{EA}{l} & 0 & 0 \\ 0 & \frac{12EI}{l^3} & \frac{6EI}{l^2} & 0 & -\frac{12EI}{l^3} & \frac{6EI}{l^2} \\ 0 & \frac{6EI}{l^2} & \frac{4EI}{l} & 0 & -\frac{6EI}{l^2} & \frac{2EI}{l} \\ -\frac{EA}{l} & 0 & 0 & \frac{EA}{l} & 0 & 0 \\ 0 & -\frac{12EI}{l^3} & -\frac{6EI}{l^2} & 0 & \frac{12EI}{l^3} & -\frac{6EI}{l^2} \\ 0 & \frac{6EI}{l^2} & \frac{2EI}{l} & 0 & -\frac{6EI}{l^2} & \frac{4EI}{l} \end{bmatrix}$$

where E is the modulus of elasticity of the beam element,
A is the cross-sectional area of the beam element,
I is the second moment of area of the beam element
and l is the length of the beam element.

D.2 Geometric Element Stiffness Matrix

The derivation of the geometric element stiffness matrix, which is used to include the bending effects due to an axial compressive load, is presented below. Tensile axial loads are considered positive. Consider the element illustrated in Figure D.2, and assume that it can deform axially but is infinitely stiff in bending. The axial strain for small displacements is:

$$\epsilon_x = \epsilon_u + \epsilon_v \tag{D.1}$$

where:

$$\epsilon_u = \frac{u_2 - u_1}{l} \quad \text{and} \quad \epsilon_v = \frac{1}{2}\left(\frac{v_2 - v_1}{l}\right)^2$$

The strain ϵ_v is a truncation to the first two terms of the Maclaurin secant series ($\sec\theta = 1 + \theta^2/2! + \cdots$). Specifically, $\epsilon_v = \Delta l/l$, where Δl is the lengthening associated with rotation of the element through a *small* angle θ without x-direction motion of any point (Figure D.2). Therefore:

$$\Delta l = \frac{l}{\cos\theta} - l = l(\sec\theta - 1) \approx l\frac{\theta^2}{2} \approx \frac{l}{2}\left(\frac{v_2 - v_1}{l}\right)^2 \tag{D.2}$$

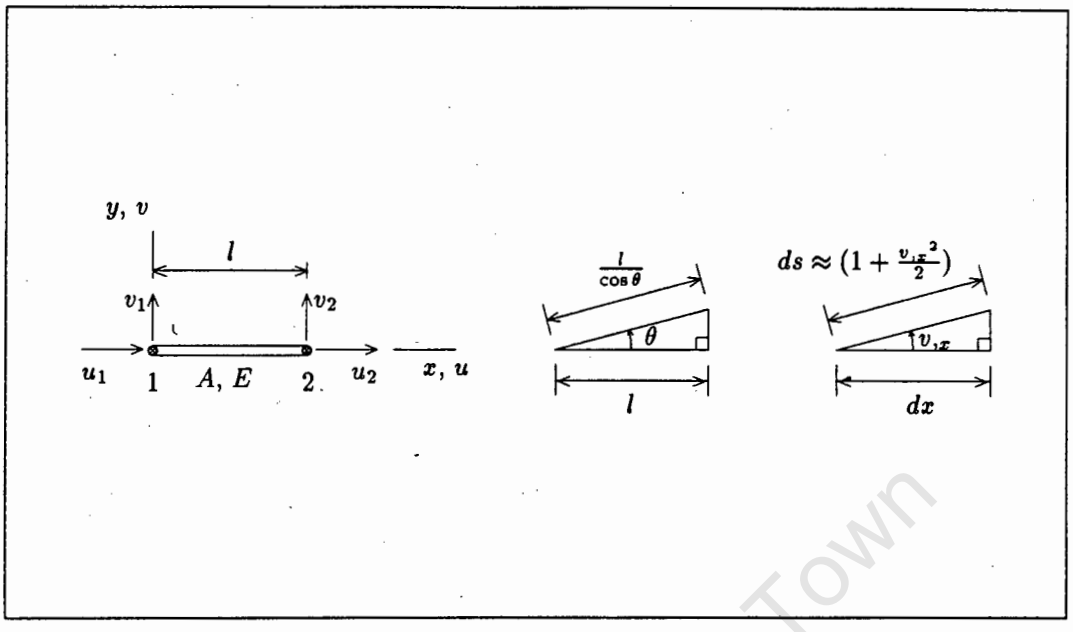

Figure D.2: Truss Element with Geometric Relationships

The strain energy in the bar is $U = AEl{\epsilon_x}^2/2$. Thus:

$$U = AEl\left(\frac{{\epsilon_u}^2}{2} + \epsilon_u\epsilon_v + \frac{{\epsilon_v}^2}{2}\right) = \frac{AEl}{2}\left({\epsilon_u}^2 + {\epsilon_v}^2\right) + Pl\epsilon_v \tag{D.3}$$

where $AE\epsilon_u$ has been identified as an axial force P, positive in tension. With displacements interpolated linearly from nodal values, the following expressions for the strain terms are obtained:

$$\epsilon_u = \frac{1}{l}\left\{ \begin{array}{cc} -1 & 1 \end{array} \right\}\left\{ \begin{array}{cc} u_1 & u_2 \end{array} \right\}^T \tag{D.4}$$

$$\epsilon_v = \frac{1}{2l^2}\left\{ \begin{array}{c} v_1 \\ v_2 \end{array} \right\}^T \left\{ \begin{array}{cc} -1 & 1 \end{array} \right\}^T \left\{ \begin{array}{cc} -1 & 1 \end{array} \right\} \left\{ \begin{array}{c} v_1 \\ v_2 \end{array} \right\} \tag{D.5}$$

The terms ${\epsilon_u}^2$ and ϵ_v in equation (D.3) are quadratic in nodal degrees of freedom, but ${\epsilon_v}^2$ is quartic, so it may be discarded as negligible in comparison with ${\epsilon_u}^2$. Thus equation (D.3) yields, with $\{\boldsymbol{d}\} = \left\{ \begin{array}{cccc} u_1 & v_1 & u_2 & v_2 \end{array} \right\}^T$:

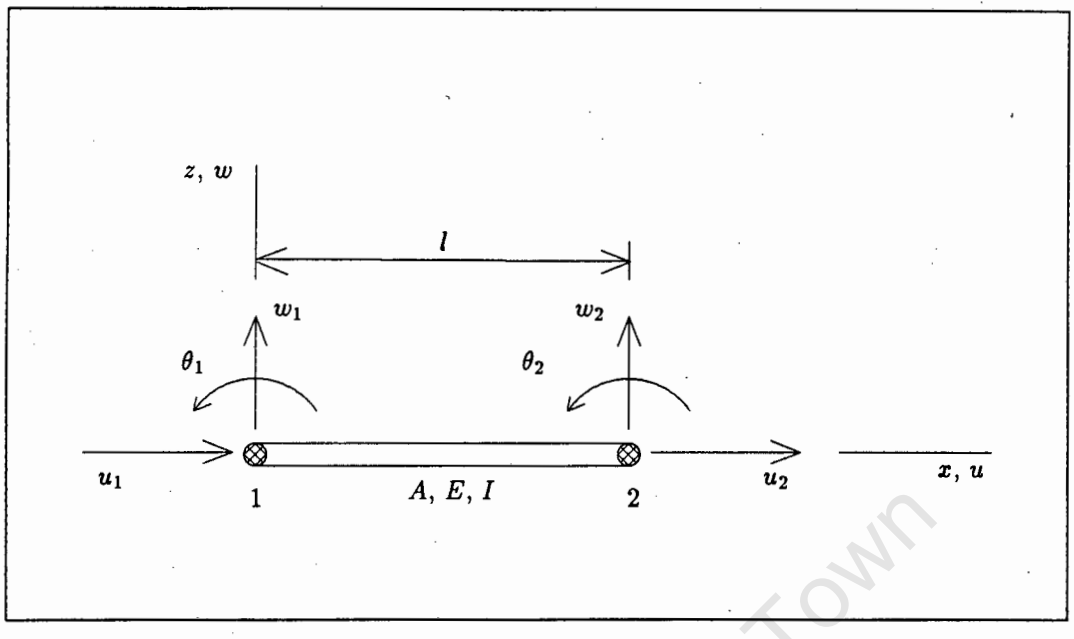

Figure D.3: Beam Element

$$U = \frac{1}{2}\{\boldsymbol{d}\}^T \left(\frac{AE}{l} \begin{bmatrix} 1 & 0 & -1 & 0 \\ 0 & 0 & 0 & 0 \\ -1 & 0 & 1 & 0 \\ 0 & 0 & 0 & 0 \end{bmatrix} + \frac{P}{l} \begin{bmatrix} 0 & 0 & 0 & 0 \\ 0 & 1 & 0 & -1 \\ 0 & 0 & 0 & 0 \\ 0 & -1 & 0 & 1 \end{bmatrix} \right) \{\boldsymbol{d}\} \qquad \text{(D.6)}$$

The first 4×4 matrix, with the coefficient AE/l, can be identified as the conventional stiffness matrix $[\boldsymbol{k}]$ for a plane truss element. The second 4×4 matrix, with the coefficient P/l, can be identified as the stress stiffness matrix $[\boldsymbol{k}_\sigma]$ for a plane truss element. Using $[\boldsymbol{k}_\sigma]$, *overall* buckling of a plane truss could be analysed (buckling of individual bars is not accounted for).

Consider a beam element (Figure D.3). A fiber at distance z above the neutral axis of bending has the strain:

$$\epsilon_x = \frac{\partial u}{\partial x} - z\frac{\partial^2 w}{\partial x^2} + \frac{1}{2}\left(\frac{\partial w}{\partial x}\right)^2 \qquad \text{(D.7)}$$

The symbol $u_{,x}$ is now used to represent the partial derivative of u with respect to x, i.e. $\frac{\partial u}{\partial x}$. The following terms can be identified in equation (D.7). $u_{,x}$ represents axial

stretching: $-z\,w_{,xx}$ is the strain produced by the curvature $w_{,xx}$, negative if z and $w_{,xx}$ are of the same sign; and ${w_{,xx}}^2/2$ is ϵ_v in equation (D.1), but written for a differential element of length dx (Figure D.2). With $dV = dA\,dx$, the element strain energy is:

$$U = \int_0^l \int_A \tfrac{1}{2} E\,{\epsilon_x}^2\,dA\,dx \tag{D.8}$$

Noting that:

$$\int dA = A\,, \quad \int z dA = 0\,, \quad \int z^2 dA = I\,, \quad \int E\frac{\partial u}{\partial x} dA = P\,, \tag{D.9}$$

where P is again the axial force, positive in tension, and a term ${w_{,x}}^4$, quartic in nodal degrees of freedom, is discarded, the element strain energy is obtained by substituting equation (D.7) into equation (D.8):

$$U = \int_0^l \frac{AE}{2}\left(\frac{\partial u}{\partial x}\right)^2 dx + \int_0^l \frac{EI}{2}\left(\frac{\partial^2 w}{\partial x^2}\right)^2 dx + \int_0^l \frac{P}{2}\left(\frac{\partial w}{\partial x}\right)^2 dx \tag{D.10}$$

The first integral yields $[\boldsymbol{k}]$ for a truss element, associated with degrees of freedom u_1 and u_2 (see equation (D.6)). The second integral yields $[\boldsymbol{k}]$ for a standard beam element. The third integral sums the work done, and hence the strain energy stored, when differential elements dx are stretched an amount ${w_{,x}}^2\,dx/2$ by tensile force P. This third integral yields $[\boldsymbol{k}_\sigma]$ for a beam element, and it is derived as follows:

Lateral displacement w of the beam, and its first derivative $w_{,x}$ are:

$$w = [\boldsymbol{N}]\,\{\boldsymbol{d}\} \quad \text{and} \quad \frac{\partial w}{\partial x} = [\boldsymbol{G}]\,\{\boldsymbol{d}\} \tag{D.11}$$

where $[\boldsymbol{N}] = \begin{bmatrix} N_1 & N_2 & N_3 & N_4 \end{bmatrix}$ are cubic shape functions. These shape functions are exact since only point loads are being considered, and they are:

$$\begin{aligned} N_1 &= 2\xi^3 - 3\xi^2 + 1 \\ N_2 &= \xi^3 l - 2\xi^2 l + \xi l \\ N_3 &= -2\xi^3 + 3\xi^2 \\ N_4 &= \xi^3 l - \xi^2 l \end{aligned}$$

where $\xi = x/l$.

The four coefficients in $[G]$ are $G_i = N_{i,x}$. Also, $\{ d \} = \left\{ w_1 \quad \theta_1 \quad w_2 \quad \theta_2 \right\}^T$. With ${w,_x}^2 = {w,_x}^T w,_x$, the following relationship is obtained from the third integral in equation (D.10):

$$\tfrac{1}{2} \{d\}^T [K_\sigma] \{d\} = \tfrac{1}{2} \{d\}^T \left[\int_0^l [G]^T P [G] \, dx \right] \{d\} \tag{D.12}$$

Integration yields, for constant P (written out as a 6×6 matrix):

$$[k_\sigma] = \begin{bmatrix} 0 & 0 & 0 & 0 & 0 & 0 \\ 0 & \frac{6P}{5l} & \frac{P}{10} & 0 & -\frac{6P}{5l} & \frac{P}{10} \\ 0 & \frac{P}{10} & \frac{2Pl}{15} & 0 & -\frac{P}{10} & -\frac{Pl}{30} \\ 0 & 0 & 0 & 0 & 0 & 0 \\ 0 & -\frac{6P}{5l} & -\frac{P}{10} & 0 & \frac{6P}{5l} & -\frac{P}{10} \\ 0 & \frac{P}{10} & -\frac{Pl}{30} & 0 & -\frac{P}{10} & \frac{2Pl}{15} \end{bmatrix} \tag{D.13}$$

where P is the axial load applied to the element (tension positive)
and l is the length of the beam element.

Equation (D.13) reduces to the $[k_\sigma]$ of equation (D.6) if bending is suppressed by setting $\theta_1 = \theta_2 = (w_2 - w_1)/l$.

Note that $[k_\sigma]$ is added to the normal element elastic stiffness matrix $[k]$. Therefore an axial tensile force causes the element to be 'stiffened', while an axial compressive force, 'softens' the element. Therefore the total element stiffness matrix is:

$$[k_t] = [k] + [k_\sigma]$$

D.3 Static Condensation

Using a process called static condensation [2,5], the global stiffness matrix K and the global force vector R can be reduced to an equivalent two by two coupled stiffness matrix

and a two component coupled force vector respectively. It is a two by two matrix since only the forces in the rollers which correspond to two degrees of freedom of this five span beam model need to be calculated. Static condensation is done by partitioning the global stiffness matrix $\boldsymbol{K}$ into four partitions as follows:

$$\begin{bmatrix} \boldsymbol{K}_{aa} & \boldsymbol{K}_{ac} \\ \boldsymbol{K}_{ca} & \boldsymbol{K}_{cc} \end{bmatrix} \begin{Bmatrix} \boldsymbol{U}_a \\ \boldsymbol{U}_c \end{Bmatrix} = \begin{Bmatrix} \boldsymbol{R}_a \\ \boldsymbol{R}_c \end{Bmatrix} \tag{D.14}$$

where $\boldsymbol{U}_a$ and $\boldsymbol{U}_c$ are the vectors of displacements to be retained and condensed out, respectively. The matrices $\boldsymbol{K}_{aa}$, $\boldsymbol{K}_{ac}$, $\boldsymbol{K}_{ca}$ and $\boldsymbol{K}_{cc}$, and vectors $\boldsymbol{R}_a$ and $\boldsymbol{R}_c$ correspond to the displacement vectors $\boldsymbol{U}_a$ and $\boldsymbol{U}_c$.

Using the second matrix equation in (D.14), the following relationship for $\boldsymbol{U}_c$ is obtained:

$$\boldsymbol{U}_c = \boldsymbol{K}_{cc}^{-1}(\boldsymbol{R}_c - \boldsymbol{K}_{ca}\boldsymbol{U}_a) \tag{D.15}$$

The relation in (D.15) is used to substitute for $\boldsymbol{U}_c$ into the first matrix equation in (D.14) to obtain the condensed equation:

$$(\boldsymbol{K}_{aa} - \boldsymbol{K}_{ac}\boldsymbol{K}_{cc}^{-1}\boldsymbol{K}_{ca})\boldsymbol{U}_a = \boldsymbol{R}_a - \boldsymbol{K}_{ac}\boldsymbol{K}_{cc}^{-1}\boldsymbol{R}_c \tag{D.16}$$

Therefore, an equivalent stiffness matrix of the form:

$$\boldsymbol{K}_{eq} = (\boldsymbol{K}_{aa} - \boldsymbol{K}_{ac}\boldsymbol{K}_{cc}^{-1}\boldsymbol{K}_{ca}) \tag{D.17}$$

and an equivalent force vector of the form:

$$\boldsymbol{R}_{eq} = \boldsymbol{R}_a - \boldsymbol{K}_{ac}\boldsymbol{K}_{cc}^{-1}\boldsymbol{R}_c \tag{D.18}$$

have been derived, which can be used to solve for the degrees of freedom $\boldsymbol{U}_a$.

E Rollers Operational — All Results

The complete set of results for the bump tests as well as those for the President Steyn Gold Mine, No. 4 Shaft, is presented on the following pages. No discussions are included as the same discussions as those in Chapter 3.4 apply here.

Single Bump Test

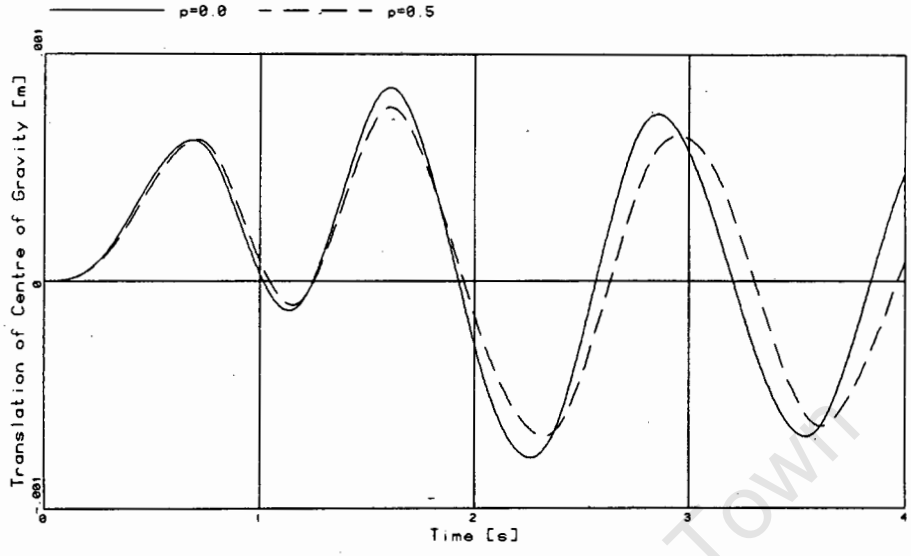

Figure E.1: Plot of Translation versus Time

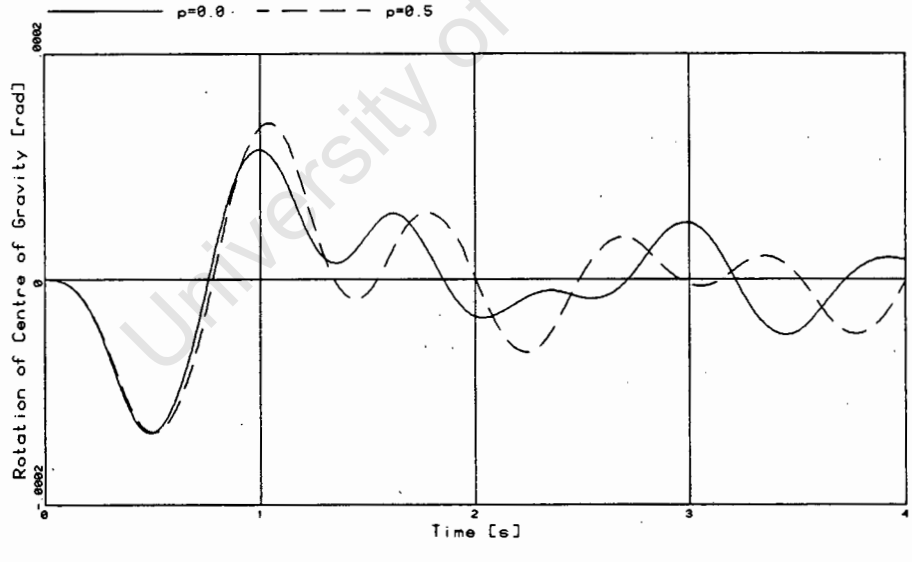

Figure E.2: Plot of Rotation versus Time

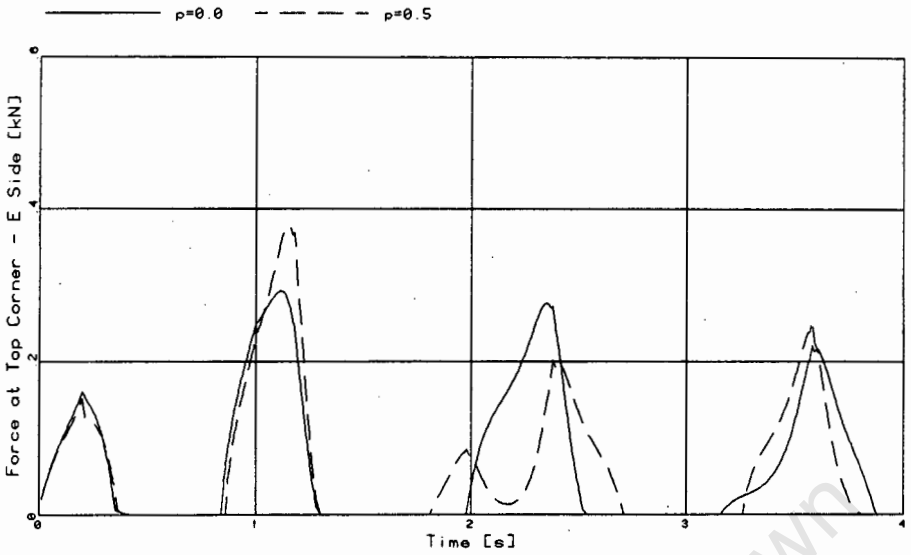

Figure E.3: Plot of Force versus Time

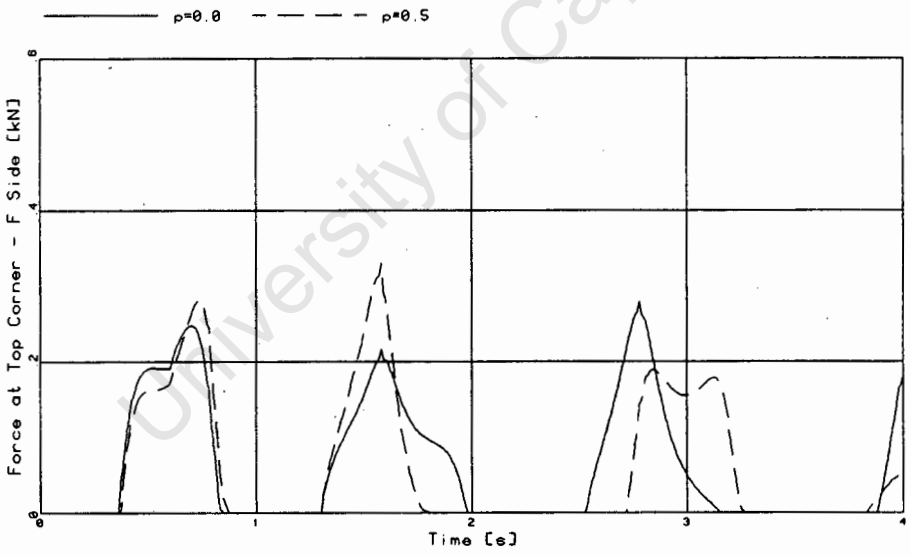

Figure E.4: Plot of Force versus Time

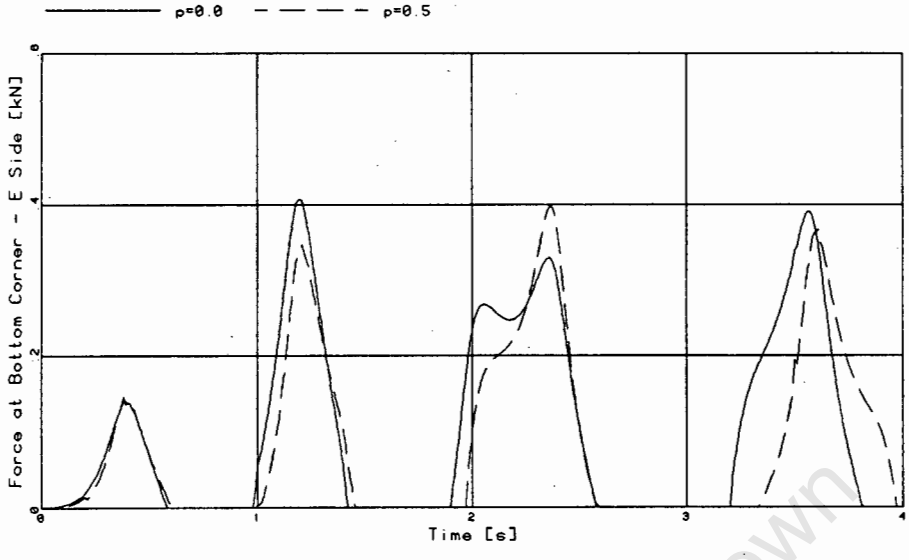

Figure E.5: Plot of Force versus Time

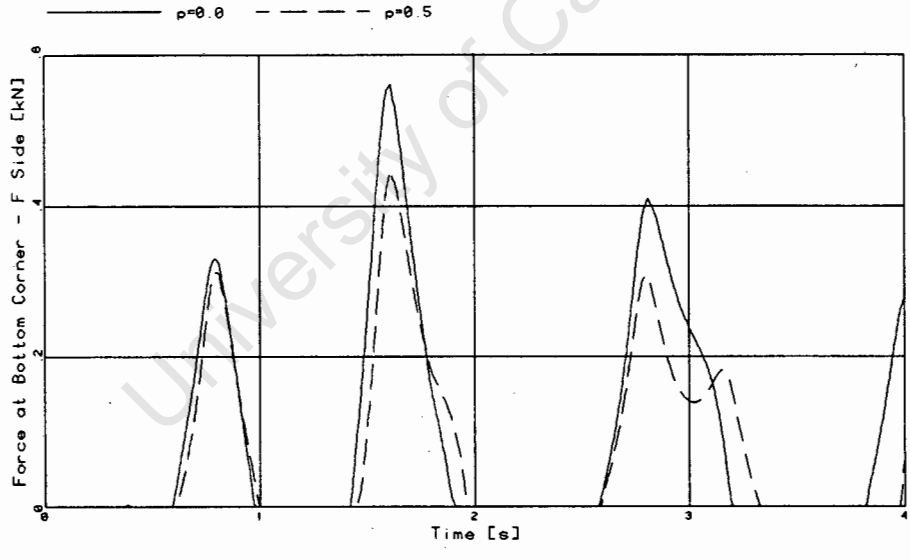

Figure E.6: Plot of Force versus Time

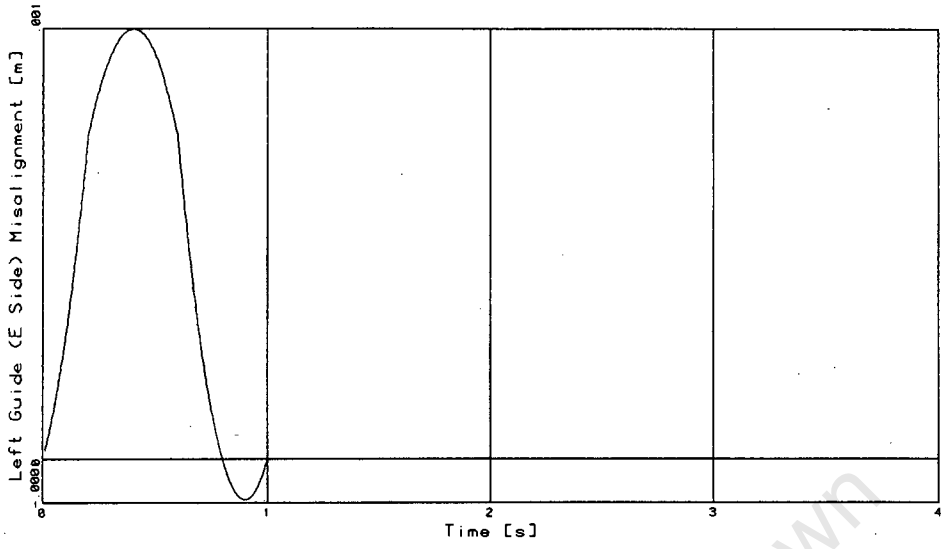

Figure E.7: Plot of Guide Misalignment versus Time

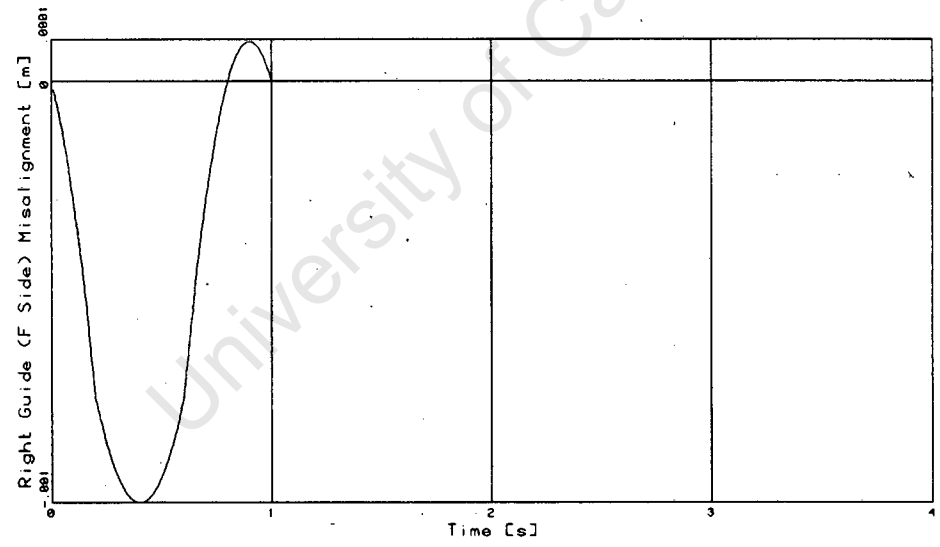

Figure E.8: Plot of Guide Misalignment versus Time

Double Bump Test

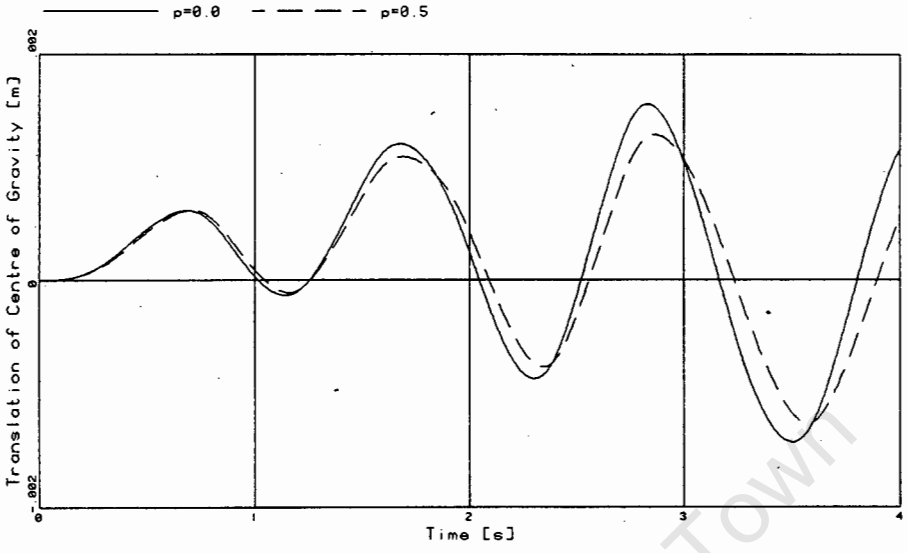

Figure E.9: Plot of Translation versus Time

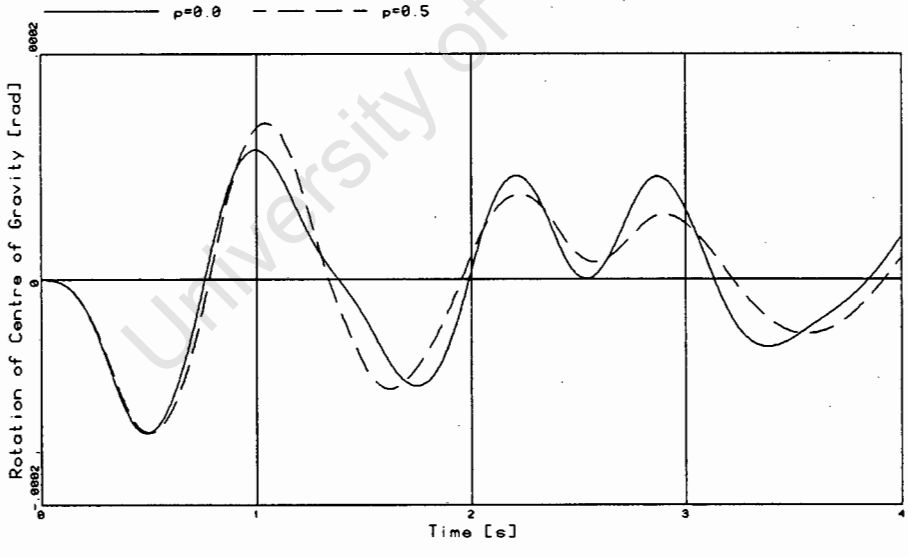

Figure E.10: Plot of Rotation versus Time

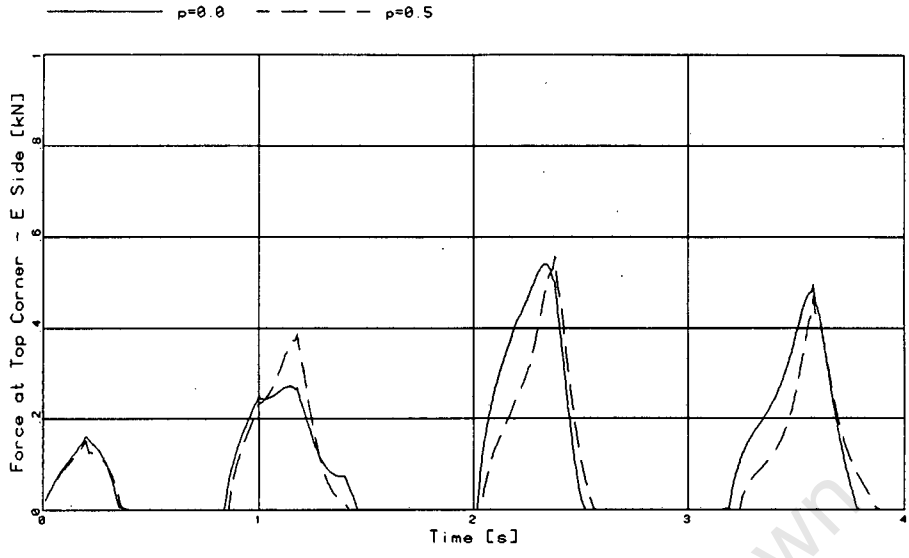

Figure E.11: Plot of Force versus Time

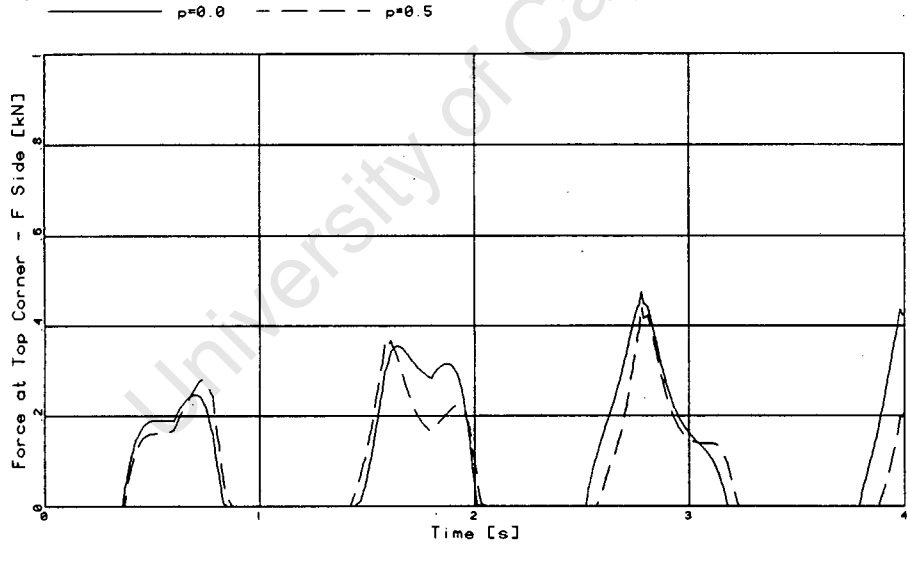

Figure E.12: Plot of Force versus Time

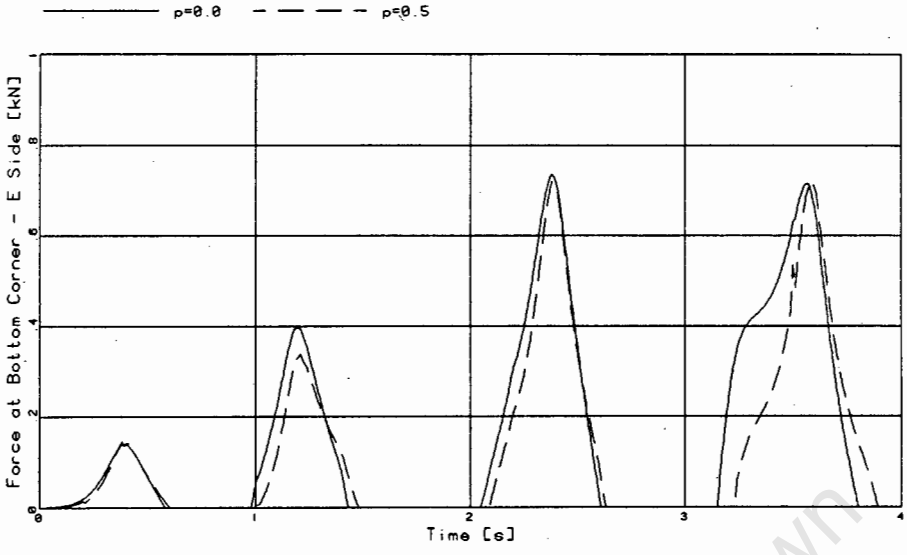

Figure E.13: Plot of Force versus Time

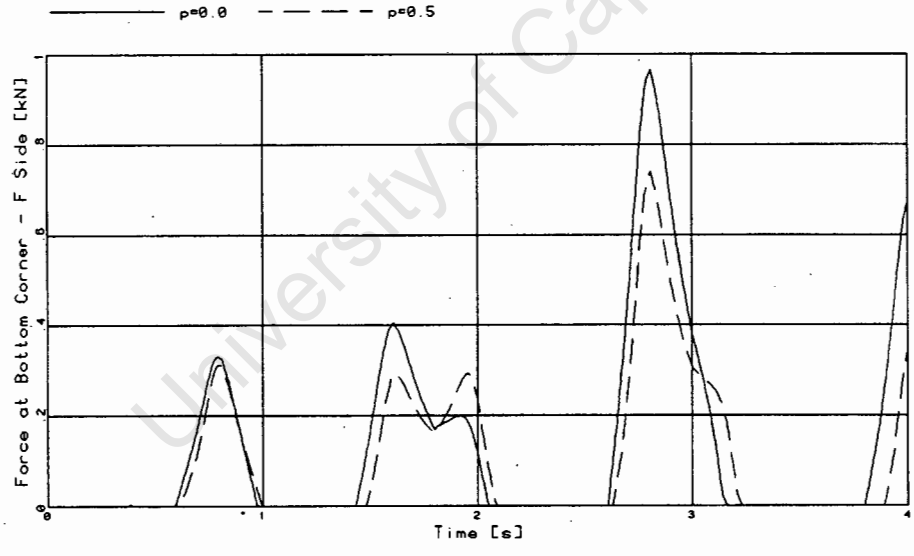

Figure E.14: Plot of Force versus Time

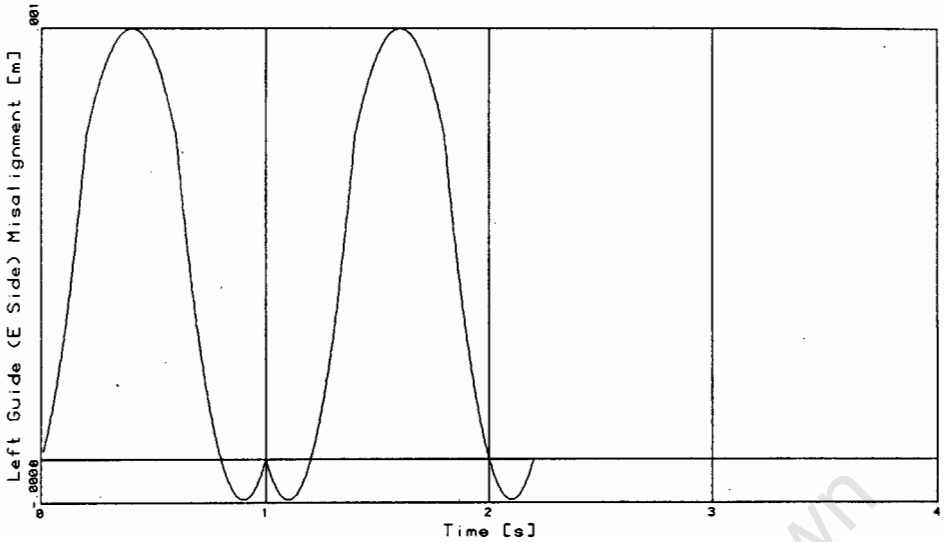

Figure E.15: Plot of Guide Misalignment versus Time

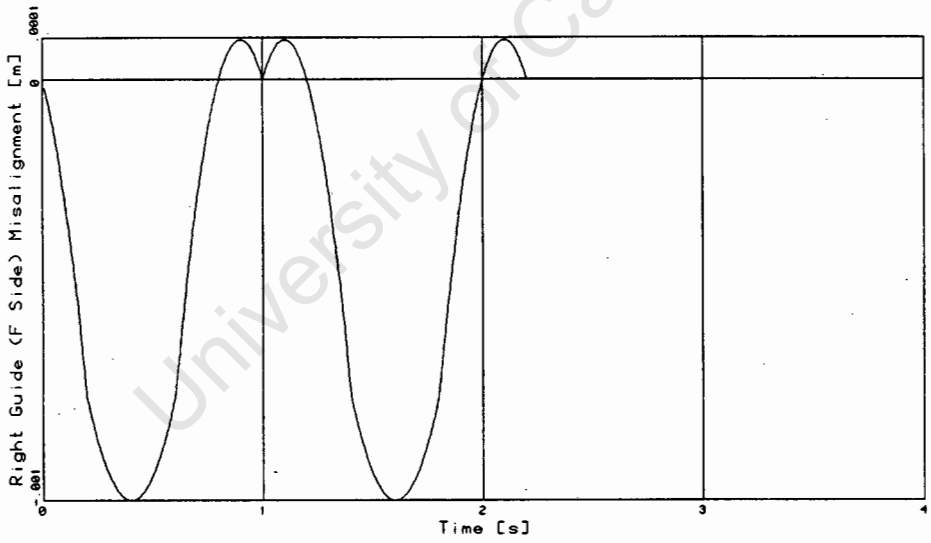

Figure E.16: Plot of Guide Misalignment versus Time

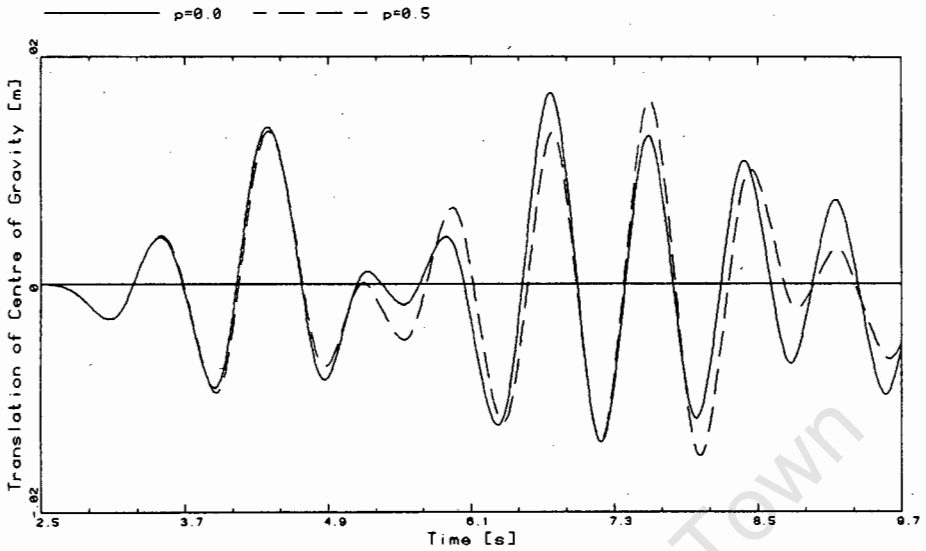

Figure E.17: Plot of Translation versus Time

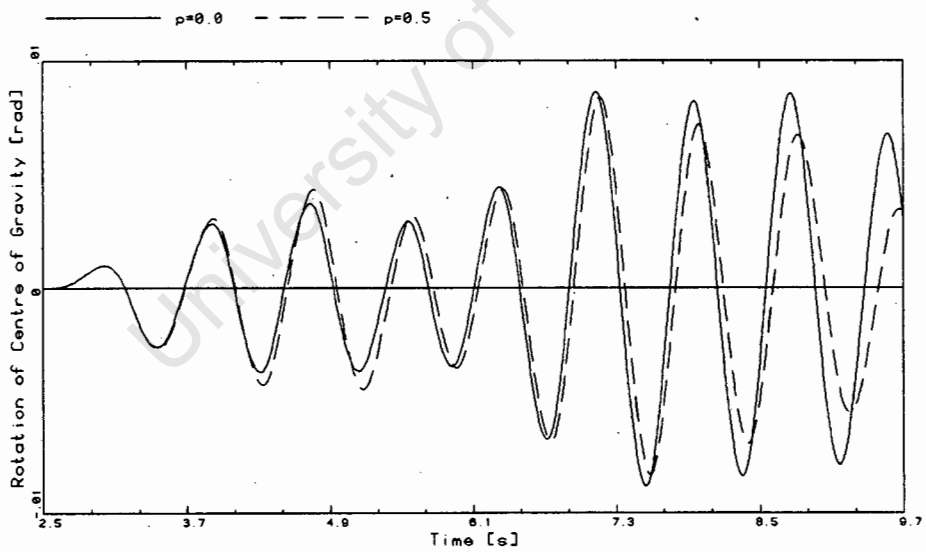

Figure E.18: Plot of Rotation versus Time

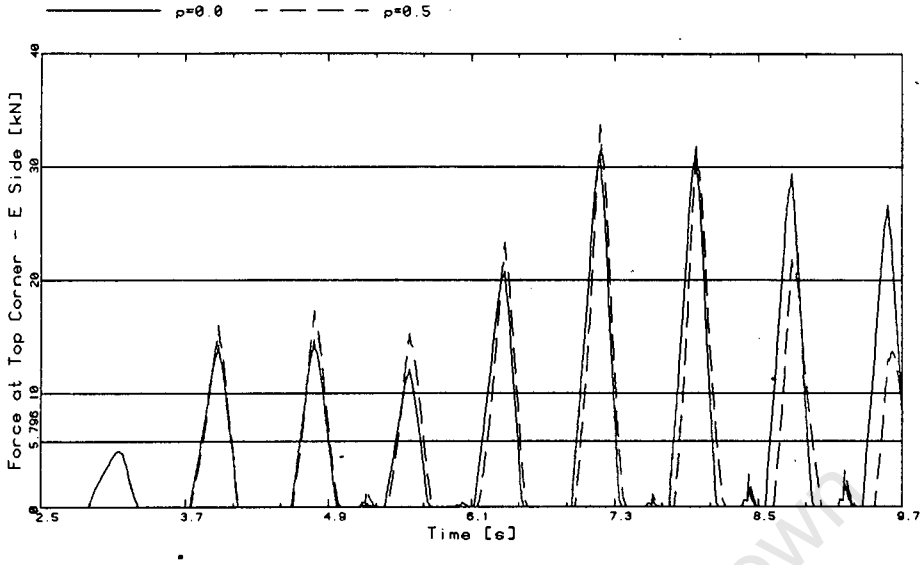

Figure E.19: Plot of Force versus Time

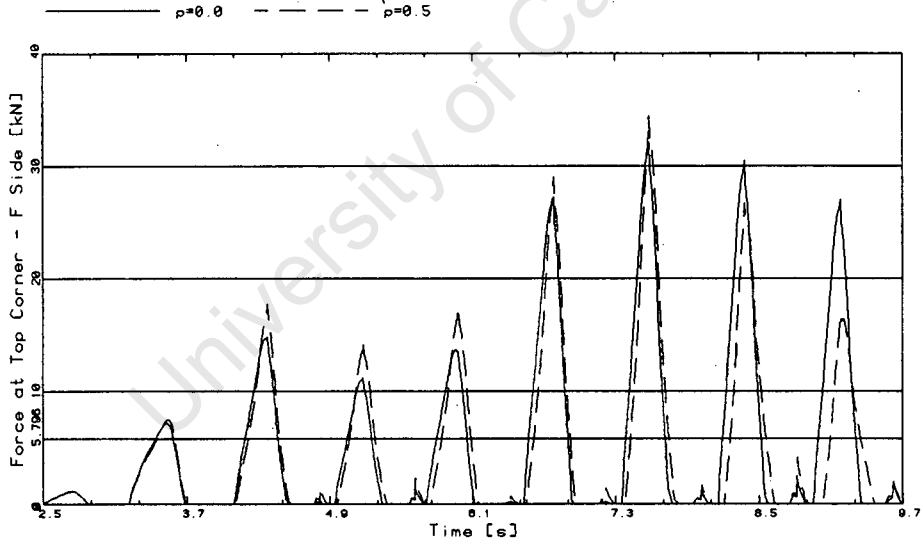

Figure E.20: Plot of Force versus Time

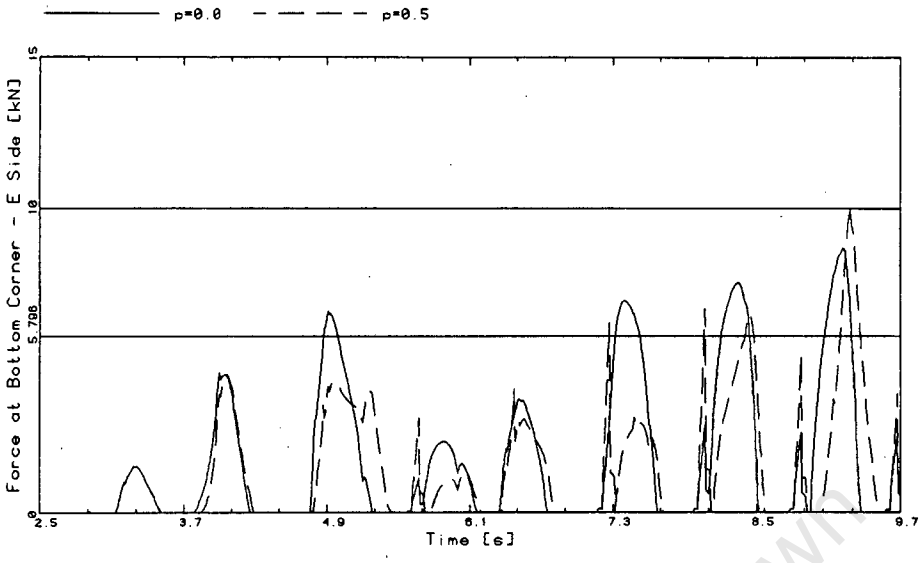

Figure E.21: Plot of Force versus Time

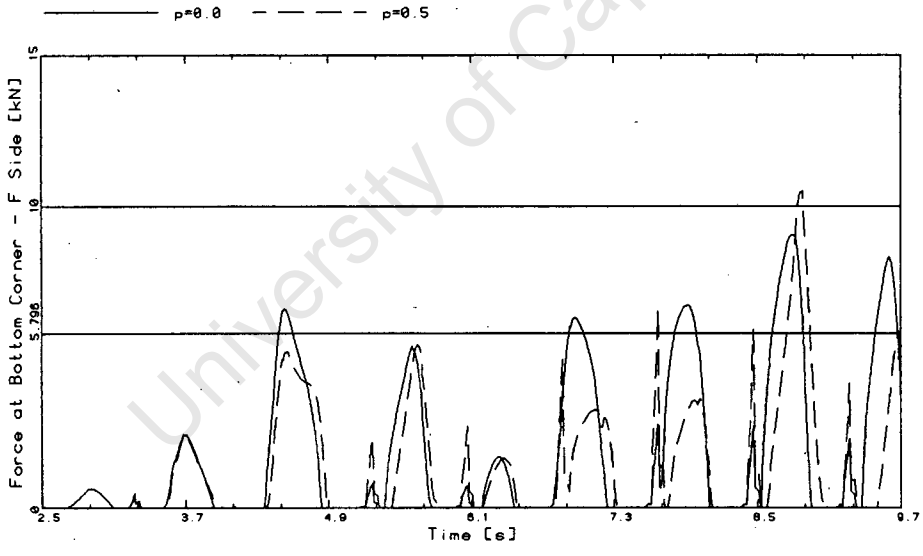

Figure E.22: Plot of Force versus Time

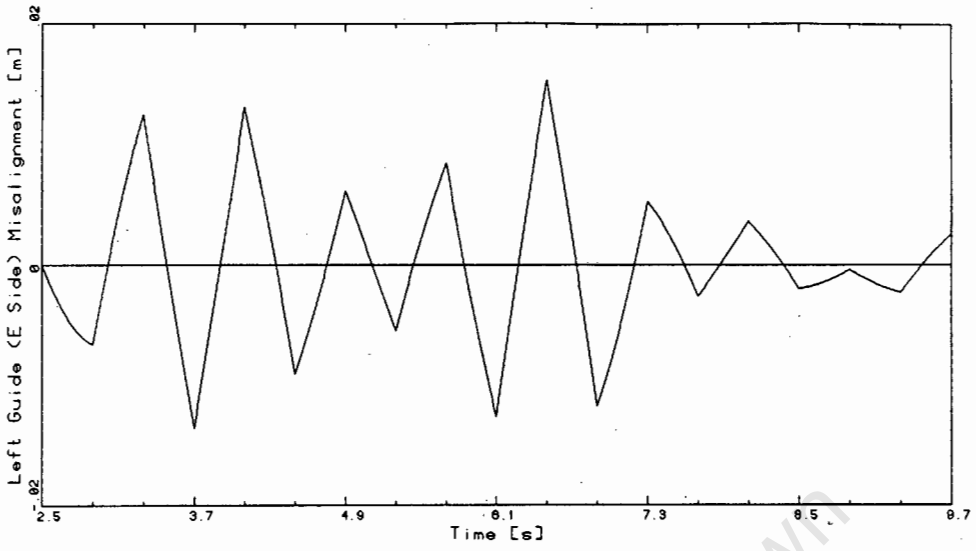

Figure E.23: Plot of Guide Misalignment versus Time

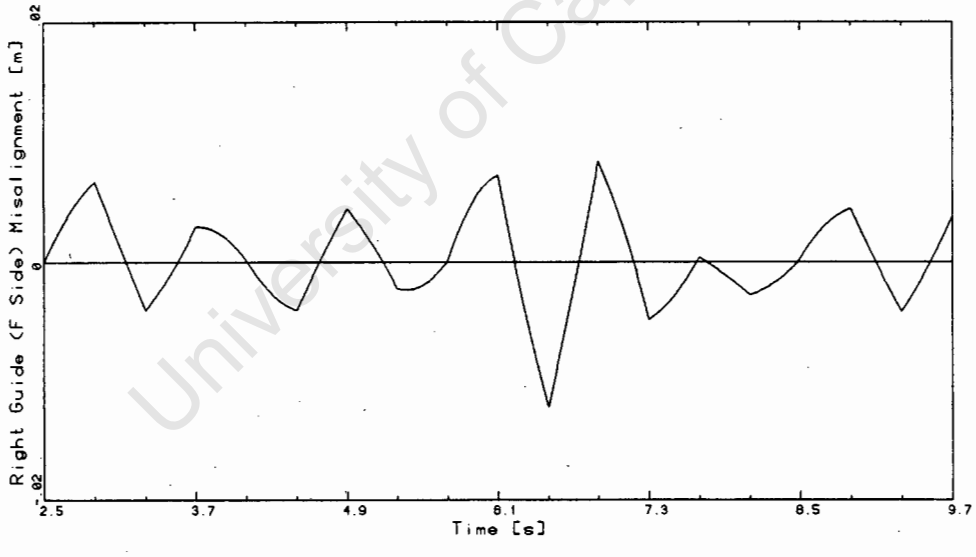

Figure E.24: Plot of Guide Misalignment versus Time

F MSc Coursework

The following courses were completed in partial fulfilment of the degree of Master of Science in Engineering. The degree requirements are 20 credits coursework, and a half thesis.

Course:			Year:	Credits:
CIV	502F	Prestressed Concrete	1986	5
CIV	504S	Structural Dynamics	1986	3
CIV	507B	Introduction to the Theory of Elasticity	1986	2
CIV	508S	Plates and Shells	1986	2
CIV	535S	Finite Element Modelling of Structures	1986	4
CIV	540F	Finite Element Analysis	1986	4
AMA	363F	Numerical Analysis	1986	3
			TOTAL:	23

F.1 Description of Individual Courses

CIV 502F PRESTRESSED CONCRETE

5 credits

Limit state design; partial prestressing; bending, shear, torsion; continuous structures; composite construction and recent development.

CIV 504S STRUCTURAL DYNAMICS

3 credits

Numerical procedures in dynamics including time stepping techniques for transient response and iterative methods for computation of eigen values and eigen vectors. Formulation of the equations of motion in the finite element framework. Applications of vibration theory to the analysis of earthquake and wind loaded structures.

CIV 507B INTRODUCTION TO THE THEORY OF ELASTICITY

2 credits

Stress, strain, equilibrium, strain displacement relationships. Elastic constants. Solutions of simple boundary value problems in plane stress and plane strain.

CIV 508S PLATES AND SHELLS

2 credits

An introduction to the elastic theory of plates and shells. Differential equations of equilibrium. Variational methods in mechanics leading to the Ritz procedure and an introduction to the finite element method. Finite elements for plates and shells.

CIV 535S FINITE ELEMENT MODELLING OF STRUCTURES

4 credits

Simple to complex models, appropriate analysis models, types of finite elements available, which elements to use, numerical integration, assessment of solution errors, use of substructuring. Examples in plane-stress, plane-strain axisymmetric shells, plates and transitional shells and 3-D analysis. Dynamic analysis, vibration analysis, wave propagation analysis.

CIV 540F FINITE ELEMENT ANALYSIS

4 credits

Generalised displacement method of analysis. Elastic energy theorems leading to basic procedures of the finite element method. Approximation and interpolation of functions. Isoparametric formulation of elements. 2-D and 3-D elements of structural mechanics. Equation solving in the computer and the structure of the finite element program. Introduction to finite element packages for practical applications. Some advanced topics in finite element analysis.

AMA 363F NUMERICAL ANALYSIS

3 credits

Aim: To provide an introduction to the theory and practice of numerical approximation.

Interpolation and approximation. Numerical integration. Numerical solution of non-linear equations and of initial value problems. Accuracy of numerical solutions.